Technical University
of Denmark

Asynchronous Media Access Control for Energy Harvesting Wireless Sensor Networks

Madava Dilshan Vithanage
s090912

Master's Thesis, August 2012
IMM-MSC-96

DTU Informatics
Department of Informatics and Mathematical Modelling

Asynchronous Media Access Control for Energy Harvesting Wireless Sensor Networks

Madava Dilshan Vithanage
s090912

Master's Thesis, August 2012
IMM-MSC-96

Asynchronous Media Access Control for Energy Harvesting Wireless Sensor Networks

This report was prepared by

Madava Dilshan Vithanage
s090912@student.dtu.dk

Supervisors

Nicola Dragoni	Xenofon Fafoutis	Claus Bo Andersen	Leonardo Azzinnari
Assoc. Prof.	PhD. Stud.	R&D Mngr.	Sr. RF Eng.
DTU	DTU	Brunata A/S	Brunata A/S
ndra@imm.dtu.dk	xefa@imm.dtu.dk	cla@brunata.dk	laz@brunata.dk

---

Thesis Period:	6 Months
Release Date:	31/08/2012
Category:	2 (Confidential)
Comments:	This report is part of the requirements to achieve the Master of Science in Engineering (M.Sc.Eng.) at the Technical University of Denmark. This report represents 32.5 ECTS points.
Rights:	

DTU Informatics
Department of Informatics and Mathematical Modelling
Technical University of Denmark
Richard Petersens Plads, Building 321,
DK-2800 Kgs. Lyngby
Denmark
Tel: (+45) 4525 3351
Fax: (+45) 4588 2673
E-mail: reception@imm.dtu.dk
Web: http://www.imm.dtu.dk/

IMM-MSC-96

Preface

This thesis was prepared at the Department of Informatics and Mathematical Modelling at the Technical University of Denmark in collaboration with Brunata A/S in Herlev, Denmark as fulfilment of the requirements for acquiring a M.Sc. Eng. in Embedded and Distributed Systems.

The advancement of energy harvesting technologies have opened up the potential to apply them for industrial use. Increasing the applications of energy harvesting systems would help reduce the costs of these technologies. At the same time, companies like Brunata A/S, would benefit from a reduction in installation and maintenance costs while increasing the lifetime of their products.

To this end, this thesis consists of a study conducted to evaluate the feasibility of using energy harvesting in the metering industry.

Kgs. Lyngby, 31/08/2012

Madava Dilshan Vithanage

Abstract

The main purpose of this study is to investigate the performance of on-demand media access control (ODMAC) when used with thermal energy harvesting in automatic metering infrastructure (AMI). AMI systems consist of smart meters and collectors with half-duplex bi-directional communication over the free industrial, scientific, and medical (ISM) band, where the meters are typically fixed and the collectors can be either fixed or mobile. Generally the lifetime of the devices are greater than 10 years, hence reliability is of paramount importance. The system under investigation is a single-hop, unstructured topology where meters and collectors are harvesting thermal and solar energy, hence requiring duty cycling. Another aim of the study is to find out if ODMAC can be generalized for both battery powered and energy harvesting wireless sensor networks (WSN). Finally, improvements such as automatic transmission power control, frequency-hopping spread spectrum (FHSS), direct-sequence spread spectrum (DSSS) will be investigated.

Acknowledgements

I have been extremely lucky to have a personal tutor who gave me the freedom to explore on my own. I would like to extend my sincere gratitude to Nicola Dragoni, and Xenofon Fafoutis for the guidance and counseling to recover when my steps went astray.

I am deeply thankful to Leonardo Azzinnari, who taught me how to question thoughts and express ideas.

Special thanks to Claus Bo Andersen for this exciting opportunity to collaborate and my warmest thanks to all my colleagues in the R&D department at Brunata A/S who helped me with my work.

Thanks to Wladimir Punt from Micropelt GmbH in Freiburg, Germany, Jens Kischkel from Panasonic Industrial Europe GmbH in Haar, Germany, and Tim Cooper from Semtech, Switzerland, for being prompt and helpful throughout the project.

My heart-felt regards to all my teachers for making me who I am today.

Most importantly, none of this would have been possible without patience, love, support and strength over the years from my family. Especially my sister, Shalini, who spent several evenings preparing 3D CAD drawings and my girlfriend, Kawmadi, for tolerating my anxiety.

Contents

Abbreviations

AC	Alternating Current
AC-MAC	Adaptive Coordinated MAC
ACK	Acknowledgement
ADB	Asynchronous Duty cycle Broadcasting protocol
ADC	Analog-to-Digital Convertor
AES	Advanced Encryption Standard
AMI	Advanced Metering Infrastructure
AMR	Automatic Meter Reading
AREA-MAC	Asynchronous Real-time Energy-efficient and Adaptive MAC
ARQ	Automatic Repeat Request
ASK	Amplitude-Shift Keying
ATPM	Adaptive Transmit Power MAC
B-MAC	Berkley MAC
BEB	Binary Exponential Backoff
BER	Bit Error Rates
CAODA	Collision Avoidance with Opportunistic Data Aggregation
CC	Closed-Circuit
CCA	Clear Channel Assessment
CCV	Closed-Circuit Voltage
CDMA	Code-Division Multiple-Access
CMSIS	Cortex Microcontroller Software Interface Standard
CPU	Central Processing Unit
CRC	Cyclic Redundancy Check
CSMA	Carrier-Sense Multiple-Access

CTR	Clear-To-Receive
CTS	Clear-To-Send
DC	Direct Current
DFS	Dynamic Frequency Scaling
DOD	Depth Of Discharge
DPM	Dynamic Power Manager
DSMAC	Dynamic Sensor MAC
DSSS	Direct-Sequence Spread Spectrum
DVS	Dynamic Voltage Scaling
DW-MAC	Demand Wake-up MAC
EE-RI-MAC	Energy-Efficient RI-MAC
EEPROM	Electrically Erasable Programmable Read-Only Memory
EH	Energy Harvesting
EH-HCA	Energy Harvesting Heat Cost Allocator
EH-WSN	Energy Harvesting Wireless Sensor Network
ENO	Energy Neutral Operation
ENO-Max	Energy Neutral Operation with Maximum performance
EVM	Evaluation Model
FDMA	Frequency-Division Multiple-Access
FEC	Forward Error Correction
FHSS	Frequency-Hopping Spread Spectrum
FIFO	First-In First-Out
Firmware	Software written for embedded microcontrollers
FSK	Frequency-Shit Keying
GPIO	General Purpose Input/Output
GPRS	General Packet Radio Service
HCA	Heat Cost Allocators
I2C	Inter-Integrated Circuit
IC	Integrated Circuit
ID	Identifier

IMR+	Inter-Meter Reading +
IOTA	Information Over The Air mote
IR	Infra-Red
ISM	Industrial, Scientific, and Medical
JTAG	Joint Test Action Group
LCD	Liquid Crystal Display
LCP	Liquid Crystalline Polymer
LDO	Low-Dropout
LFSR	Linear Feedback Shift Register
Li	Lithium
LLC	Logical Link Control
LST	Low Surface Temperature
MAC	Medium Access Control
MCU	Microcontroller Unit
MEMS	Micro-Electro-Mechanical Systems
MMRTG	Multi-Mission Radioisotope Thermoelectric Generator
MOSFET	Metal-Oxide-Semiconductor Field-Effect Transistor
Mote	Wireless Sensor Node
MPPT	Maximum Power Point Tracking
NASA	National Aeronautics and Space Administration
NTC	Negative Temperature Coefficient
O-MAC	Staggered On MAC
OC	Open-Circuit
OC-MAC	Opportunistic Cooperation MAC
OCV	Open-Circuit Voltage
ODMAC	On-Demand MAC
OF	Opportunistic Forwarding
OOK	On-Off Keying
OPAMP	Operational Amplifier
OSI	Open Systems Interconnection

OTP	One-Time Programmable
PC	Personal Computer
PCB	Printed Circuit Board
PDA	Personal Digital Assistant
PFM	Pulse-Frequency Modulator
PHY	Physical Layer
PID	Proportional-Integral-Derivative
PW-MAC	Predictive Wake-up MAC
PWM	Pulse-Width Modulator
QoS	Quality of Service
RAM	Random Access Memory
RB	Random Backoff
RCH	RTS/CTS Handshaking
RF	Radio Frequency
RH	Relative Humidity
RI-MAC	Receiver-Initiated MAC
RISC	Reduced Instruction Set Computing
RMAC	Routing Enhanced MAC
RSSI	Received Signal Strength Indicator
RTC	Real-Time Clock
RTR	Ready-To-Receive
RTS	Ready-To-Send
RW-MAC	Receiver Wake-up MAC
S-MAC	Sensor MAC
SAW	Surface Acoustic Wave
SCP-MAC	Scheduled Channel Polling MAC
SMA	Sub-Miniature version A
SORE	State Of Residual Energy
SPI	Serial Peripheral Interface
SYNC	Synchronisation

T-MAC	Timeout MAC
TDMA	Time-Division Multiple-Access
TEG	Thermo-Electric Generator
TGP	Thermo-Generator Package
TRAMA	Traffic Adaptive Medium Access protocol
TRV	Thermostatic Radiator Valve
UART	Universal Asynchronous Receiver Transmitter
UPMA	Unified Power Management Architecture
USA	United States of America
USB	Universal Serial Bus
WiseMAC	Wireless Sensor MAC
WSN	Wireless Sensor Network
X-MAC	Short Preamble MAC

ජීවිතයේ සෑම සන්දිස්ථානයකදීම මා ගැන විශ්වාසයෙන්. මා හට සහයෝගය දුන්. මගේ මව ජානකි සියඹලාපිටිය (1961-2008) ආදර්ශීය මතකයෙන්...

In loving memory of Janaki Siyambalapitiya (1961-2008), mother, teacher, who believed in me even when I didn't...

Chapter 1

Introduction

This chapter explains the necessary background and related work to understand the motivation of the project. It then clearly defines the scope and structure of the thesis.

1.1 Advanced Metering Infrastructure

Automatic Meter Reading (AMR) systems, or systems with smart meters, consists of embedded devices which perform time domain measurements and provide data over a remote connection from a customer [1]. Advanced metering infrastructure (AMI) refers to the entire measurement and collection system, including meters installed on-site, communication networks, data reception and database management systems which provide the information to the utility company and/or customer. An AMI system provides bi-directional communication between the service provider and customer, which reduces operational and maintenance costs. The data from these systems can be used for billing purposes or as feedback into home automation systems [2], such as Z-Wave and ZigBee, for intelligent regulation of energy sources.

1.1.1 Brunata A/S

Brunata is an independent Danish exporter of solutions for individual billing of costs for heating and water. Brunata has more than 85 years of experience within the development and production of metering equipment, shown in figure 1.1, and consumption accounts. The company is headquartered in Denmark but is represented in countries around the world. There are more than 20 million Brunata meters in service.

Brunata meters ensure that costs for heating and water are billed according to metered consumption. The company monitors these meters and can therefore supply accurate and fair billing information according to heat and water consumed by individual offices or dwellings.

Producing over 500k meters annually, Brunata require fast and reliable methods of data extraction and configuration. There are different types of meters developed over the years, which uses methods ranging from protocols over Infra-Red (IR) communication to wireless transmission to extract data.

The advancement in technology has led to the possibility of harvesting ambient energy, such as heat, from radiators, where heat cost allocators are mounted, and hot water pipes in buildings, where water meters are mounted. This, along with changing markets, has

(a) Futura+ heat cost allocator

(b) Gate receiver

Figure 1.1: Main products of Brunata

shifted the business focus towards behavioural analytics using the data gathered from meters [3]. The objective is to encourage building dwellers to be more energy aware, thereby change their behaviour at a fundamental level. This has shown to be a very efficient driver in cutting down on wasted energy [4].

1.2 Wireless Sensor Networks

Wireless Sensor Networks (WSNs) are a class of distributed systems associated with pervasive computing which is highly embedded within the environment in which they are placed. A fundamental feature common to all WSNs is that they extract information about the physical world in which they inhabit, where as computer network systems primarily deal with user generated data [5]. Sensors can be used to detect parameters such as temperature, humidity, motion, light, chemicals, proximity, etc. and even provide feedback to actuators which can control devices such as servo motors.

WSNs consists of collections of nodes that are several orders of magnitude higher than in computer networks and are densely deployed. Each individual node operates autonomously within a limited range and collaborate as a group to cover a large area. This scalability can address issues involved in observing the environment at a granular level providing the potential to industry and research to expose previously unobservable phenomena.

Due to the diversity of the applications and constraints on nodes, a WSN typically consists of a tiered architecture. The highest tier is typically connected to the internet while the lower end consists of nodes with limited resources. Such an architecture is composed of various platforms where each platform is optimized toward a certain requirement like computation capability, wireless range, energy consumption, financial cost, and physical size.

The tendency of technology to follow Moore's Law [6] has led high-end computational capability from a couple of decades ago to be available in today's smallest processors. Furthermore, the industry and research community has come to the realization that in order to keep up with Moore's Law, low power and distributed computing techniques has to be developed further. All this culminates in the presence of low-cost low-power devices with

good processing capability in the industry today.

These advancements lead to the need of efficient communication models. WSNs primarily focus on the communication between nodes. This is because, unlike in computer networks, users do not micro-manage the flow of information as in the internet or cellular phone networks. The interest of the end user of a WSN is on the high level results. In fact, this is not simply out of convenience, but rather a design principle to conserve the most precious resource in a WSN: energy.

Since the data from sensor nodes tend to be real-time temporal data streams, traditional databases built to insert bulk data in an incremental fashion are not suitable [7]. Hence real-time databases that can cope with variable inter-arrival times and delivery rates from individual nodes are vital within an AMI focused toward behavioural analytics [8].

1.2.1 Applications

WSNs can be generally separated into monitoring applications or tracking applications, or a mixture of both, e.g., in control applications [9]. In monitoring applications the traffic tends to be predictable and continuous, while in tracking applications traffic tends to be unpredictable and event-driven, e.g., the opening of a window by an inhabitant of a home triggers the thermostat to control the radiator, although ultra-low duty cycled periodic data might be necessary to inform the network that it is still alive.

The application spectrum of WSN is very broad, where possible applications are in military command, control, communications, computers, intelligence, surveillance, reconnaissance and tracking applications for offensive and defensive warfare [10], monitoring environment conditions for agriculture to increase the yield of crops, prediction of natural phenomena, such as earthquakes, habitat monitoring to track movements of fauna, metering applications for individual apartment billing, automation for smart homes and office buildings, support for logistics such as tracking of packages on a manufacturing floor and monitoring the quality of products during transportation, etc.

1.2.2 Network Architecture

The logical structure of WSNs are important when designing the underlying components of the system. An example of a WSN and in particular an AMI system is shown in figure 1.2. The diagram shows a three-tiered architecture, where each tier is focused at optimizing a certain cost parameter. The sources of data are the nodes that sense the environment, and the sinks are the databases to which data is delivered.

Tier-1 is subdivided into clusters of nodes. The nodes within each cluster are quasi-structured, meaning that once installed the location of the nodes are static with a recognizable structure, but the structure between two clusters could potentially be different. This reflects a typical scenario in the metering industry, where the location of meters, while unknown prior to installation, forms a repetitive pattern in apartments and blocks after installation. Other applications such as environment monitoring could be unstructured, where the nodes are dispersed via aircraft and the location of the nodes are random. Furthermore, each cluster is formed as a multi-hop mesh topology, where the nodes not only disseminate their own data, but also relay data received from other nodes. This could occur over several wireless links between nodes before it reaches the gateway node [11]. The hardware platform of nodes are primarily focused toward low-cost low-power devices with a long service life.

communication model of a conventional network and WSN. Typically a node in a WSN implements only the first two or three layers of the Open Systems Interconnection (OSI) model [12].

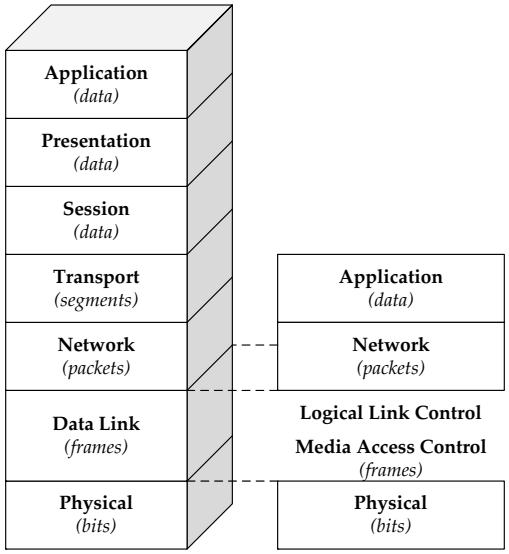

conventional networks, such as IEEE 802.11 [13], where the payload size can be a couple of order of magnitudes larger [14]. It is even desirable to retain a small payload due to the higher Bit Error Rates (BER) present in wireless links, which increases the probability that a received packet will be corrupted.

Nonetheless, there are several similarities in the patterns of communication. Common communication patterns can be grouped into broadcast, unicast, multicast, and gossip [15, 16]. Typically a broadcast pattern is used by the sinks in occasions such as when a firmware update has to be performed on all the nodes on the network. When nodes have data to send to a particular sink, such as a gateway node, a unicast pattern is used. In a multicast pattern, data from sources have to reach multiple sinks, such as between gateways nodes. And finally, in a gossip pattern, nodes communicate locally amongst neighbours to share data.

1.2.3.2 Data Link Layer

In WSNs, the establishment of communication links and regulating access to the shared media in an energy efficient way is a core requirement to setup a self-organized network infrastructure for data transfer. The MAC layer in WSNs must have power management strategies and failure recovery mechanisms built-in. This makes the MAC layer an important consideration when designing WSNs. Figure 1.4 shows a classification of MAC schemes, where they are roughly generalized into two groups, contention-free and contention-based techniques [17, 18].

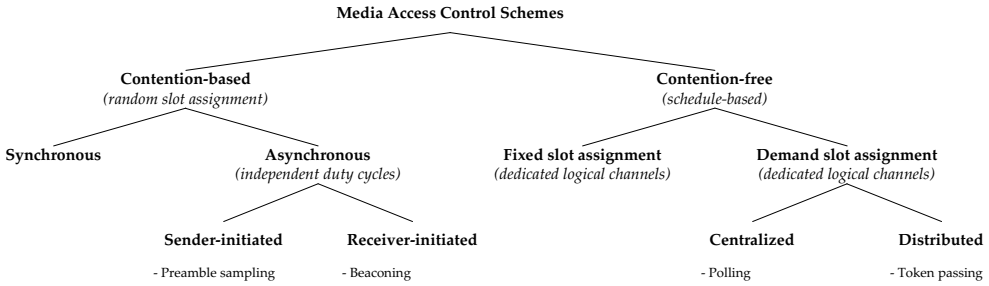

Figure 1.4: Taxonomy of MAC schemes

Contention-free approaches uses static or dynamic schedules to allocate resources to nodes in slots. Fixed resource assignment schemes such as Time-Division Multiple-Access (TDMA) [19], Frequency-Division Multiple-Access (FDMA) , and Code-Division Multiple-Access (CDMA) have been used in cellular networks for a long period of time [20]. Dynamic slot assignment schemes do not allocate dedicated channel capacity to idle nodes, but rather use a demand based approach, where nodes that are ready to communicate are given higher priority. A centralized demand assignment scheme in use is polling, where a base station queries each node in its network in a round-robin fashion about whether it is ready to communicate and allocates the channel. In a distributed demand assignment scheme such as token passing, the nodes pass each other a token so that only the node with the token is allowed to use the channel [21].

Contention-based approaches do not assume any control of the communication medium and therefore no scheduling is performed allowing nodes to duty cycle. Each node contends for access of the transmission channel and is randomly assigned. This inevitably leads to collisions when several nodes transmit at the same time. To deal with this problem, collision detection mechanisms are used such as in Carrier-Sense Multiple-Access (CSMA) [22] schemes. There are two general techniques used in contention-based MACs: synchronous, where nodes in a cluster converge to a synchronized sleep and active state using control packets; or asynchronous, where the sleep and active states of each node remain independent of each other. Another important classification is between receiver-initiated and sender-initiated operation [23]. In the traditional sender-initiated procedure, a node that has data to send transmits a preamble which the receiving node listens for and allows the data to be received, where as in a receiver-initiated procedure, the node that has data to send listens for a beacon that is transmitted by the receiving node before initiating communication.

1.3 Energy Harvesting

Physical phenomena produce some form of energy as a by-product. The concept of Energy Harvesting (EH) is related to using this small-scale ambient energy to power embedded devices, thus averting the need for energy storage. This differs from renewable energy such as from wind farms and solar-array grids since EH is not able to supply household power. But in the context of WSNs, EH systems are very attractive for applications where changing batteries is impractical, e.g., when nodes are densely deployed in a forest, or even impossible, e.g., when embedded within structures such as bridges or buildings. While batteries have a limited amount of energy, energy harvesting can potentially produce an infinite amount of energy as shown in figure 1.5. Furthermore, Energy Harvesting Wireless Sensor Networks (EH-WSNs) reduce the cost involved in installation and maintenance, and provides long lifetimes, which is, from an energy perspective, infinite, although devices are still prone to hardware and firmware failures.

Most of the WSN applications discussed are exposed to some form of ambient energy that can be scavenged. Recent advancements in technologies such as thin-film, thick-film and Micro-Electro-Mechanical Systems (MEMS) have paved the way to make EH systems a reality. Although industrial deployments of such technology is rare, EH remains at the forefront of research in many institutions.

Figure 1.6 shows a general overview of an EH system. It is important to note that the total efficiency, η_{total}, of such a cascaded n-stage system depends on the individual efficiencies of each stage as shown by equation (1.1).

$$\eta_{total} = \eta_{stage_1} * \eta_{stage_2} * ... \eta_{stage_n} \tag{1.1}$$

1.3.1 Sources and Harvesting Technologies

Sources of energy refer to types of ambient energy which can be potential scavenged from the environment. It can be more or less categorized as shown in table 1.1.

Depending on the environment and circumstances in which an energy source is present, two properties can be associated with it, predictability and controllability [25]. An energy source is said to be predictable if suitable models can define its behaviour over a period of time, e.g., solar energy following diurnal and seasonal cycles. An energy source is said to

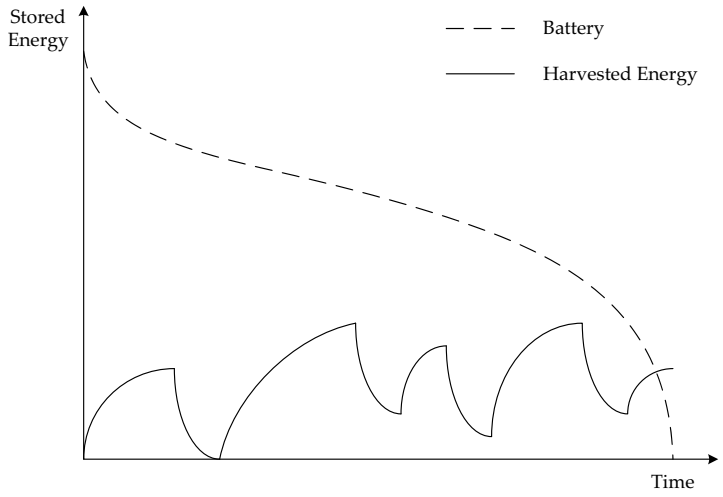

Figure 1.5: Energy from a battery and harvesting source

Table 1.1: Types of ambient energy sources suitable for energy harvesting [24]

Thermal Energy	Radiant Energy	Mechanical Energy
Body Heat	Solar Energy	Body Motion
Industrial Heat	RF Energy	Vibrations
-	-	Air Flow
-	-	Liquid Flow

be controllable if it can be activated when desired, e.g., the rotation of the tire in a bicycle can be used to generate power when cycling.

There are several technologies available for harvesting various types of energy. A non exhaustive list of harvesting technologies and potential power densities that can be extracted are shown in table 1.2.

1.3.2 Power Conditioning

Conditioning the output of the energy harvester is a non-trivial and important stage, if not the most important. Typically the efficiency of the power conditioning dictates the feasibility of a practical EH application. A power converter is used to transform the low positive Direct Current (DC) voltage output produced into a higher DC voltage used by the load. As shown in figure 1.7, thermal and vibration energy sources could produce an Alternating Current (AC) voltage output, where power can be extracted in both polarities, e.g., the output voltage from a thermo-electric generator is linear to the temperature difference across the device, irrespective of the polarity. For EH applications where it is desirable to harvest energy in both polarities, an AC-DC converter is used before the DC-DC converter.

Three main challenges exist for power conditioning circuits. Some energy harvesters

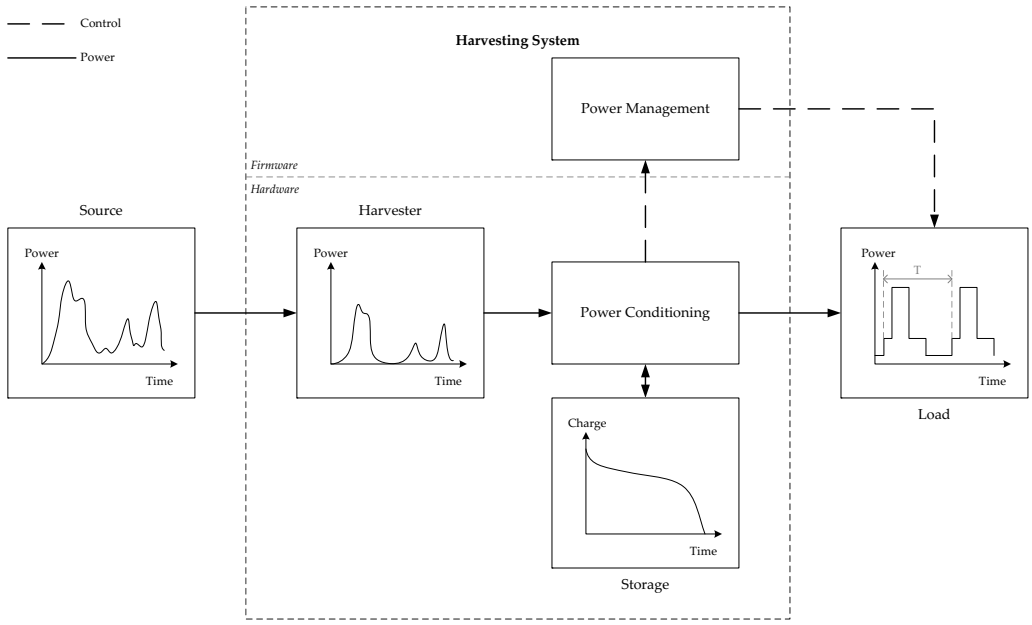

Figure 1.6: General representation of EH system

have a very low output voltage, in the order of millivolts, that could be very close to the noise floor. Boosting it to a usable level, while self-powering the converter circuit, is a significant challenge. Once this is subdued, it is then a challenge to maintain a constant high efficiency over a large dynamic voltage range. The efficiency is a nonlinear function of the input voltage to the power conditioner. Converters most often use Maximum Power Point Tracking (MPPT) techniques to automatically adjust the load on the energy harvester, to get close to the theoretical maximum power that can be extracted. Finally, it is a challenge to maintain an ultra-low quiescent power level of the converter, although modern ultra-low leakage semiconductor processes are helping to improve these levels.

1.3.3 Storage

Portable energy storage can be generally categorized into primary and secondary devices. Primary storage is used in applications that do not have the capability of recharging. Secondary storage devices are rechargeable, and hence of interest to EH-WSNs . Figure 1.8 provides an overview of both types of technologies, with a plot of the peak power that can be drawn by a load against the energy density.

Normally stored energy suitable for EH-WSNs take two forms: energy stored in electric fields, such as in capacitors; and electrochemical energy, such as in batteries. Batteries have been the dominant form of portable energy storage used for the past several decades. Presently, there are electrochemical based lithium film batteries and supercapacitors that is helping to make many applications of EH-WSNs a reality.

Nonetheless, even though the advance in technology has helped to improve the limits, there still exist several issues yet to be resolved. For example, stability over a broad temperature range, self-discharge rate, internal impedance, and cycle life are important

Table 1.2: Power densities of energy sources and harvesting technologies [26–31]

Energy Source		**Harvesting Technology**	
Type	***Power Density*** $(\frac{\mu W}{cm^2})$	***Type***	***Power Density*** $(\frac{\mu W}{cm^2})$
Solar (Indoors)	100@20%	Photovoltaic Cells	10
Solar (Outdoors)	100000@20%		10000
Electromagnetic	0.3	Antenna	0.1
Body Heat	20000	Thermo-Electric	60@5K
Industrial Heat	100000		3500@30K
Body Motion	500@1Hz	Piezo-Electric	4
Vibrations	1000@5Hz		100
Air Flow (Indoors)	-	Turbine	$35@ < 1\frac{m}{s}$
Air Flow (Outdoors)	-		$3500@8.4\frac{m}{s}$

parameters that have to be considered apart from the actual capacity, financial cost and physical size.

1.3.4 Power Management

The power management system, typically an algorithm executing in the microcontroller, is responsible for maintaining a sustainable energy consumption rate of the load. Using the concept of an active and sleep state, as shown in figure 1.9, the load can be duty cycled to vary its average power consumption. During the active state, the node is operational performing required measurements and computations, and then it powers on the radio for communication. Once the communication is completed, the node shuts down the radio and goes into a sleep state until it wakes up again to repeat the cycle. The duty cycle can be define as the percentage of time in which a node is active with respect to its period, shown in equation (1.2).

$$\mathcal{D} = \frac{\tau}{T} * 100 \qquad \text{where} \begin{cases} \mathcal{D} & \text{is the duty cycle, in \%} \\ \tau & \text{is the time in the active state, in seconds} \\ T & \text{is the total time period, in seconds} \end{cases} \tag{1.2}$$

The concept of Energy Neutral Operation (ENO) for EH-WSNs [25], as shown in figure 1.10, describes a state where the amount of energy consumed is less than or equal to the energy that is harvested. This new paradigm aims to maximize the performance (ENO-Max) of a node while maintaining an ENO state. The use of independent adaptive duty cycling allows a node to achieve this sustainable ENO-Max state.

1.4 Project Description

The feasibility of using thermal energy harvesting for Heat Cost Allocators (HCA) with radio communication to function as a WSN node in an AMI system is investigated. HCAs are mandatorily mounted on radiators in Denmark and in an increasing number of countries worldwide, and thus the heat produced by the radiator is an ideal source of power for the HCA. To make efficient use of this energy source, MAC scheme specially designed for EH-WSNs should be identified.

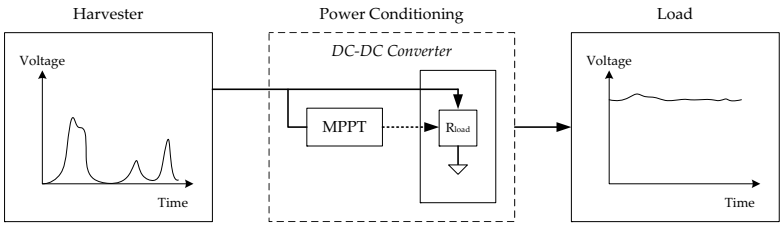

(a) DC input voltage

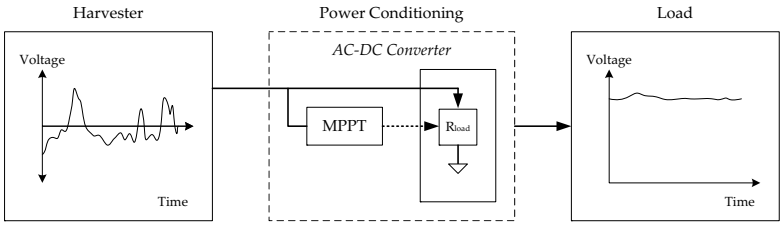

(b) AC input voltage

Figure 1.7: Simplified illustration of power conditioning

This interdisciplinary project explores the benefits and limitations of contention-based MAC schemes when implemented in HCAs, with an emphasis on receiver-initiated schemes such as On-Demand MAC (ODMAC) [32]. A prototype of an EH-HCA is designed and constructed using the Micropelt thin film thermoelectric generator [33] to measure the millivolt output voltage it produces. A suitable power conditioning integrated circuit (IC) that is currently available in the market is assessed to convert the output from the harvester into a usable power level for the HCA. A characteristic model of this harvesting system is then estimated. A wireless sensor node, *ıota*, is designed to be used as a testbed for implementing the MAC schemes and to determine the performance of the EH-WSN designed using EH-HCAs for AMI systems.

1.4.1 Problem Definition

The aim of this project is to verify whether receiver-initiated schemes such as ODMAC is a better choice instead of the basic ALOHA scheme used by Brunata, while assessing whether the technology available today can be feasibly used in an EH application by the industry.

The key milestones to achieve this goal are:

- Design and analysis of thermal energy harvesting system
- Design of the *ıota* wireless sensor node for the testbed

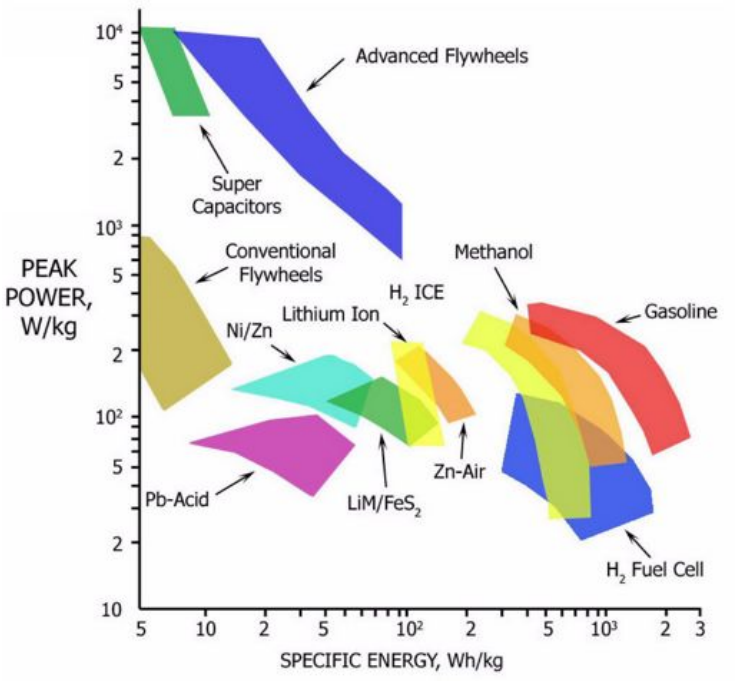

Figure 1.8: Ragone plot of energy storage technologies [24]

- Survey of MAC schemes
- Implementation and evaluation of a suitable MAC scheme for an EH system

1.4.2 Rationale

The main motivation of this project is the lack of state-of-the-art applications of EH used in the metering industry. Although many studies have been carried out by academia, few focus on concrete applications using readily available technology. As such, Brunata is interested in gaining this knowledge to lead the market by deploying a feasible EH-WSN in an AMI system. The increase in the number of EH applications will, inevitably, reduce the manufacturing costs of the technologies required for EH, greatly increasing the potential use of the technology by new entrepreneurs.

Another motivation is the required paradigm shift in designing MAC schemes for EH applications and the exploration of its cross-layer impact.

1.4.3 Application Requirements

[R1] A gateway node, or collector, shall support a maximum of 1000 nodes.

[R2] Each node shall guarantee delivery of at least one measurement per day to the collector.

[R3] Occasional loss of data transmitted by a node, more often than once per day, can be tolerated. i.e., a node performing more than [R2].

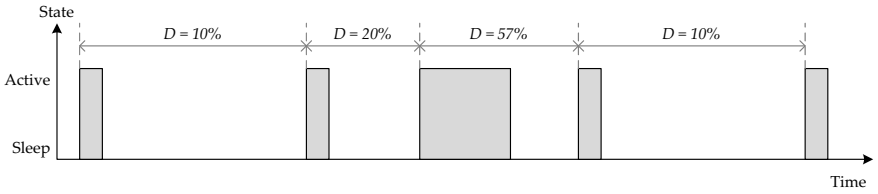

Figure 1.9: Dynamic duty cycling of a node in a WSN

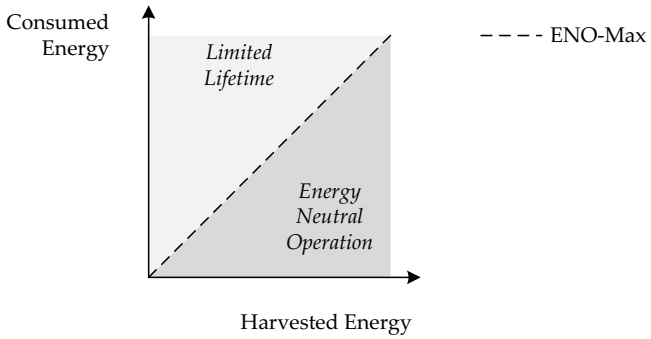

Figure 1.10: The state of ENO and ENO-Max [32]

[R4] Nodes shall have a service life of at least 10 years.

[R5] Excluding the power consumption of the GPRS connection, gateway nodes shall have a service life of at least 5 years.

[R6] The EH-HCA should retain the industrial design of its predecessor, the Futura+.

1.4.4 Project Scope and Limitations

Although AMI includes the entire measurement and collection system, the focus of this thesis is only at the data-link layer of tier-1 level. The case of gateway nodes with two or more radios is beyond the scope and not considered. The application is very specifically designed for HCAs produced by Brunata, mounted on typical radiators found in apartments in Denmark, an example of which is shown in figure 1.11. It is a monitoring application where the traffic is mostly predictable and continuous with a unicast communication pattern.

The harvesting system works with a non-ideal energy storage and a load with a non-zero power consumption. Only a single-channel scenario is considered and hence the scope of this study covers single-channel contention-based MAC schemes, in particular ODMAC.

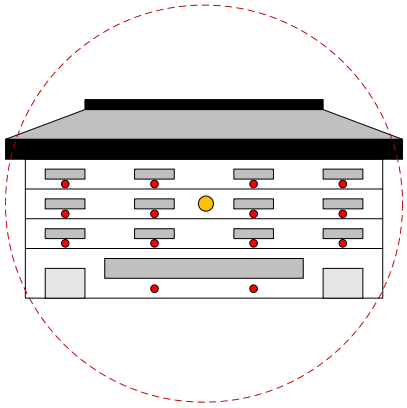

Figure 1.11: Deployed site

Even though ODMAC is designed for multi-hop networks, this project is limited to a single-hop topology, as shown in figure 1.12. Specifically, to a single cluster with several nodes and a gateway node, where all are duty cycling. The scalability and optimal size of a cluster is a non-trivial problem that is not examined in this study. The design of the EH system is focused on using ICs and technologies available in the market at the time of this study.

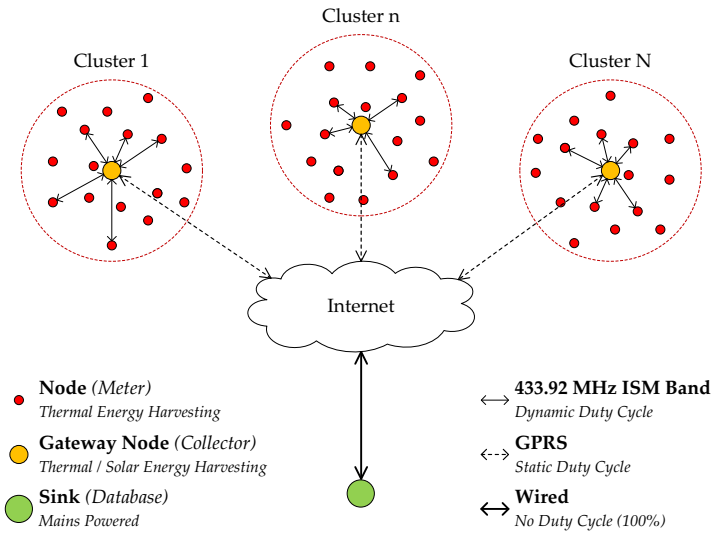

Figure 1.12: The network topology analysed in this study

1.4.4.1 Assumptions

[A1] The free ISM spectrum is shared by products from other manufacturers making it difficult to predict the usage of the spectrum.

[A2] The spatiotemporal distribution of energy available for harvesting is not uniform across all radiators.

[A3] The energy source is unpredictable and uncontrollable to a network administrator.

[A4] A unique address is assigned to each node during production at Brunata.

[A5] Prior to approval for usage in production, energy storage such as batteries are thoroughly characterised by the manufacturer or Brunata.

[A6] The deployed nodes in the WSN are homogenous in terms of hardware and firmware.

[A7] In a battery powered WSN, the battery depletion rate is not homogenous for all nodes due to variations in environmental conditions, such as temperature and humidity.

1.4.5 Key Contributions

- A prototype for a thermal energy harvesting HCA was designed and mathematically modelled to analyse the feasibility of its implementation.
- Then the prototype was manufactured as a practical EH-HCA which could be deployed.
- An experiment was designed to investigate the amount of power that could be harvested from the heat energy of a radiator.
- An empirical model was developed to estimate the amount of power that can be practically harvested.
- A state-of-the-art wireless sensor node was designed and manufactured as a platform to be used in a testbed, while also providing realistic power consumption measurements.
- A literature survey of MAC schemes for WSNs was performed to establish the state-of-the-art. and qualitatively identify MAC schemes suitable for EH-WSNs.
- The MAC scheme used by Brunata, along with a state-of-the-art scheme designed for EH-WSNs were mathematically modelled.
- Then both the MAC schemes were analytically compared with respect to a given power budget and network density.

1.5 Thesis Structure

The first chapter is a self contained introduction to advanced metering infrastructure, wireless sensor networks, and energy harvesting with a discussion of the motivation for the project, ending with defining the problem that will be studied.

The solution to the problem is explained in the chapters 2 to 4, covering an analysis of the mechanical and electronic design of the EH-HCA prototype, the hardware design and implementation of the *ιota* wireless sensor node, and finally a survey of asynchronous MAC schemes.

The chapters 6 to 9 deal with the carried out experiments and the obtained results, concluding with a summary and further investigations.

Chapter 1: Provides the background of the study, introducing the concepts of EH-WSN and its applications in the metering industry.

Chapter 2: Covers the mechanical design of the prototype HCA with the thermoelectric generator and the electronics of the harvesting system. Performs a theoretical analysis of the power output from the thermal energy harvester. Defines a controlled setup and experiments to verify the analysis, and compares the results obtained from practical measurements using the prototype with the analytical model.

Chapter 3: Describes the hardware design and implementation of the *ıota* wireless sensor node that is used for the testbed and provides a theoretical power consumption profile of the mote.

Chapter 4: Contains a survey of asynchronous contention-based MAC schemes, which is then evaluated qualitatively. A MAC scheme suitable for EH systems, along with the MAC scheme used by Brunata is modelled and analysed.

Chapter 5: Unifies the work from chapter 2, 3, and 4. Explains an overview of how the work for the previous chapters can be used in the future, along with important considerations for the firmware implementation of ODMAC on *ıota*. Discusses the significance of the study.

Chapter 6: Concludes the project with a summary of the contributions and possible work for the future.

Chapter 2

Thermal Energy Harvesting

This chapter describes a investigation into thermal energy harvesting from radiators for powering HCAs, which operate as nodes in a WSN. An illustration of the new design of the EH-HCA using novel materials, to accommodate the thermo-electric generator is provided, along with a simple analytical model. This is followed by an overview of power conditioning solutions currently available. The chapter concludes with a discussion of the experiment setup and an evaluation of the results obtained along with a proposed empirical model of the harvested power.

2.1 Background

Granting long operating lifetimes or better performance for a given energy budget is a design objective in WSNs. In this context, scavenging freely available ambient energy is a promising power source for EH-WSNs, as an alternative or supplement to batteries, leading toward the development of energy-autonomous sensing nodes.

HCAs mounted on radiators in apartment dwellings, have access to thermal energy during the winter season, where suitable temperature gradients across the radiator surface and the room in which it is placed exists. During the heating season, the temperature gradient tends to be slowly varying or continuous in time. Conversely, during the summer season, the temperature gradients drop significantly and are either discontinuous or often non-existent. As a consequence, the energy harvested during the winter season should not only power the system, but also stored to be used during the summer season. Energy storage devices typically have varying levels of leakage, hence the EH system required for a HCA is classified as a harvesting system with a non-ideal energy buffer, and a non-zero power consumption rate by the system.

The most promising thermal energy harvester for this low temperature application is the solid-state power generation device known as a thin-film Thermo-Electric Generator (TEG) . TEGs [34, 35] produce a voltage difference when a temperature gradient exists across it, which can then be converted into useful power for a system. TEGs also have the benefits from the lack of mechanical vibrations, long operating lifetimes of over 100,000 hours [36, 37], and low maintenance costs.

TEGs have been around since the late 1950's, but mostly used as high temperature generators for space applications. The National Aeronautics and Space Administration (NASA) of the United States of America (USA) , deployed power generators that coupled TEGs with a nuclear heat source in over 25 missions [38], the most recent being the

Multi-Mission Radioisotope Thermoelectric Generator (MMRTG) [39] used on the Curiosity rover [40] in a mission to Mars. This initial investment into material research have enabled TEGs to be used in industrial and consumer applications, where the most widely researched applications [41–45] today are in the area of low temperature thermal energy scavenging.

A previous study [46] presents a low temperature thermal EH system, which extracts a maximum of 150mW of power from the heat of a radiator to operate ZigBee based electronics. The prototypes described, which are intended for radiator valve regulation, are highly impractical for the metering industry, and hence less likely that it will be adopted. In contrast to this study, it does not consider a device placed as a conventional HCA. Instead, large heat sinks are used with good insulation, where the prototype is placed in an ideal position on top of the radiator, which results in a very large temperature gradient that is not feasible to obtain in a practical implementation.

This study uses an off-the-shelf thermo-electric generator to design a new EH-HCA, which can be manufactured using traditional methods. The novelty lies in the design of a solution with minor modifications to the existing HCA to transform it into a practical EH-HCA product. A new brass nut is designed to fasten the HCA to the radiator, while a new plastic cover is moulded with thermo-plastic material to act as both, a lid for the HCA, and a heat sink for the thermal energy harvester. An analytical thermal model of this new construction is described, to evaluate whether a sufficient temperature gradient can be obtained across the thermo-electric generator in a practical deployment. Furthermore, an experiment that uses an off-the-shelf power conditioner, is designed to characterise the amount of power that can be harvested from the heat energy. The results obtained from the experiment are used to define an empirical model for the power scavenged by this specific EH-HCA design. This empirical model can then be used for future research, such as, network feasibility testing, analysis of EH communication protocols, or simulation/emulation of thermal energy harvesting.

2.1.1 Theory

Thermo-electric power generation is based on the Seebeck effect, discovered by Thomas Johann Seebeck in 1821. As shown in figure 2.1, when a temperature difference is established between the hot and cold ends of a thermoelectric material, a voltage known as the Seebeck voltage is generated. An electric field is created when electrons and holes thermally diffuse from the hot side to the cold side and carry their charge with them.

The Seebeck coefficient is the ratio of the voltage difference, ΔV, created by the electric field and the temperature gradient. The temperature gradient, ΔT_{HC}, across the TEG is the difference between the temperature of the hot side, T_{H}, and the cold side, T_{C}. In solid-state TEGs, the p-type semiconductor has a positive Seebeck coefficient , α_p, where as the n-type semiconductor has a negative Seebeck coefficient, α_n, giving an overall positive Seebeck coefficient, α. Therefore the voltage generated by the TEG, V_{TEG}, can be expressed by the linear equation (2.1).

$$\Delta T_{\mathrm{HC}} = (T_{\mathrm{H}} - T_{\mathrm{C}}) \qquad \text{where} \begin{cases} \Delta T_{\mathrm{HC}} & \text{is in kelvin} \\ T_{\mathrm{H}} & \text{is in kelvin} \\ T_{\mathrm{C}} & \text{is in kelvin} \end{cases}$$

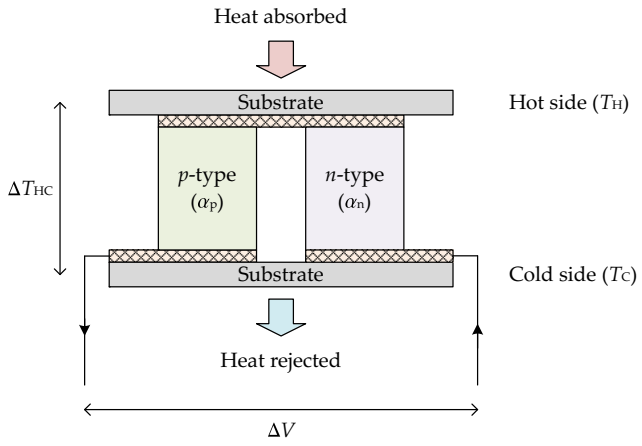

Figure 2.1: Basic structure of a semiconductor thermo-electric couple [47]

$$\alpha = \alpha_p - \alpha_n = \frac{\Delta V}{\Delta T_{\mathrm{HC}}} \qquad \text{where} \begin{cases} \alpha & \text{is in volt per kelvin} \\ \Delta V & \text{is in volt} \end{cases}$$

$$\Delta V = \alpha \cdot \Delta T_{\mathrm{HC}}$$

$$V_{\mathrm{TEG}} = \alpha \cdot (T_{\mathrm{H}} - T_{\mathrm{C}}) \tag{2.1}$$

The Seebeck effect is actually the inverse of the Peltier effect, independently discovered by Jean Charles Athanase Peltier in 1834. Since the Seebeck and Peltier effects are thermodynamically reversible, a voltage across a thermo-electric couple can also convert electricity into a temperature difference.

The maximum efficiency, η_{Carnot}, that any heat engine can obtain is defined by the Carnot limit, described in equation (2.2).

$$\eta_{\mathrm{Carnot}} = \frac{(T_{\mathrm{H}} - T_{\mathrm{C}})}{T_{\mathrm{H}}} \tag{2.2}$$

Furthermore, the ability of thermo-electric materials to convert heat energy into electricity is approximately described by the figure of merit, Z, where λ is the thermal conductivity, and ρ is the electrical resistivity.

$$Z = \frac{\alpha^2}{\lambda \cdot \rho} \qquad \text{where} \begin{cases} \lambda & \text{is in watt per meter kelvin} \\ \rho & \text{is in ohm meter} \end{cases}$$

A performance metric is obtained by multiplying Z with the average temperature, $\bar{T}$, which is the dimensionless figure of merit normalized to temperature, ZT, as described by equation (2.3).

$$\bar{T} = \frac{T_{\mathrm{H}} + T_{\mathrm{C}}}{2}$$

$$ZT = \frac{\alpha^2 \cdot \bar{T}}{\lambda \cdot \rho} \tag{2.3}$$

The figure of merit of materials available today is around $ZT \approx 1$. Given the latest developments in material research, it is plausible to assume that materials with $ZT \approx 2$ would become a reality in the near future.

The theoretical maximum conversion efficiency, η_{TEG}, of a TEG is related to the Carnot limit and the intrinsic performance of the TEG, and can thus be described by equation (2.4).

$$\eta_{\mathrm{TEG}} = \eta_{\mathrm{Carnot}} \cdot \frac{\sqrt{1+ZT}-1}{\sqrt{1+ZT}+\frac{T_{\mathrm{C}}}{T_{\mathrm{H}}}}$$

$$\eta_{\mathrm{TEG}} = \frac{(T_{\mathrm{H}} - T_{\mathrm{C}})}{T_{\mathrm{H}}} \cdot \frac{\sqrt{1+ZT}-1}{\sqrt{1+ZT}+\frac{T_{\mathrm{C}}}{T_{\mathrm{H}}}} \tag{2.4}$$

Figure 2.2 shows the effect of ZT on the power conversion efficiency of the TEG, where $ZT \rightarrow \infty$ is the maximum theoretical limit. When the temperature gradient is low, the conversion efficiency is affected very little by a change in ZT. For this reason, efficiency is not a primary concern in low temperature TEGs. In high temperature applications, the efficiency is affected considerably by ZT, and therefore becomes an important evaluation parameter. Heat engines with much better efficiency already exists for applications with a very high temperature gradient, and TEGs become feasible only if reliable, scalable, silent, and small generators are required, e.g., in military and space applications.

2.2 Design

The EH system used in this study consists of a thermo-electric energy harvester, power conditioner, and an energy storage, as shown in figure 2.3. The TGP-751 [48] from Micropelt GmbH, is used as the thermo-electric harvester, the BQ25504 [49] boost charger for nano power energy harvesting from Texas Instruments is used as the power conditioner. An electrolytic capacitor is used to store the harvested power in the experiment setup due to the ability to easily model the device, but a Lithium (Li) based battery is proposed for long term use in an application.

2.2.1 Harvester

This study uses the TGP-751 Thermo-Generator Package (TGP) , shown in figure 2.4, which is a solid-state thin-film TEG enclosed in a standard package.

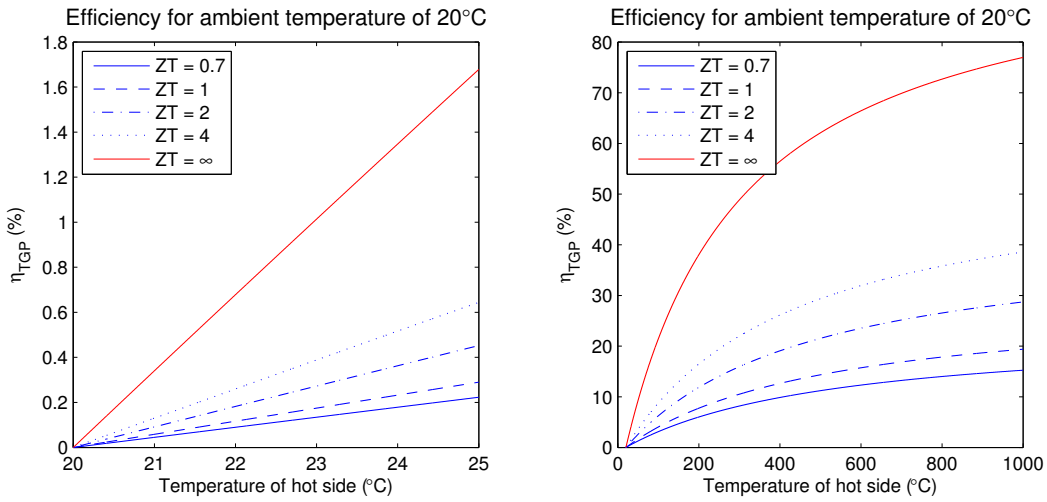

(a) Low temperature

(b) High temperature

Figure 2.2: Assessing the impact of ZT on Carnot efficiency

The manufacturing technology [51] of the TEG shown in figure 2.4b, relies on microelectronic techniques that uses a two-wafer concept, in which standard Silicon Dioxide (SiO_2) wafers are used as the substrate. One wafer is coated with n-type and the other with p-type thermo-electric Bismuth-Telluride (Bi_2Te_3) related materials, and then micro-structured for energy harvesting. While ZT for the TGP-715 is not disclosed, Bi_2Te_3 materials have a figure of merit that is typically around $ZT \approx 0.7$ [52]. As shown in figure 2.4a, up to 100 leg pairs are etched per mm^2 from the thin-film coating, in a single production step. The n-type and p-type wafers or wafer segments are finally bonded together with their exactly mating structure of thermo-electric legs and cut into single functional thermo-electric devices.

The voltage generated, V_{TGP}, by the TGP-751 with a Seebeck coefficient, α_{TGP}, is described by equation (2.5), while the thermal energy conversion efficiency, η_{TGP}, of the standard package is given by equation (2.6).

$$V_{\text{TGP}} = \alpha_{\text{TGP}} \cdot (T_{\text{H}} - T_{\text{C}}) \tag{2.5}$$

$$\eta_{\text{TGP}} = \frac{(T_{\text{H}} - T_{\text{C}})}{T_{\text{H}}} \cdot \frac{\sqrt{1+ZT}-1}{\sqrt{1+ZT}+\frac{T_{\text{C}}}{T_{\text{H}}}} \qquad \text{where } ZT \approx 0.7 \tag{2.6}$$

The existing HCA is mounted on a radiator by welding a copper-plated steel bolt onto the radiator surface. An aluminium back part is used in between the plastic housing and the radiator as a stable support. Various designs of this back part exist to suit different types of radiators. This study considers the most widely used model of the back part. The plastic housing is then fastened onto the radiator with a brass nut. The necessary electronics is placed inside the housing and the plastic lid is snapped into place. Figure 2.5a shows the construction of the HCA when it is mounted on a radiator, while figure 2.5 shows the individual components used.

A novel application of materials is required because the mechanical design of the housing and installation procedure from the existing HCA should be retained as defined by

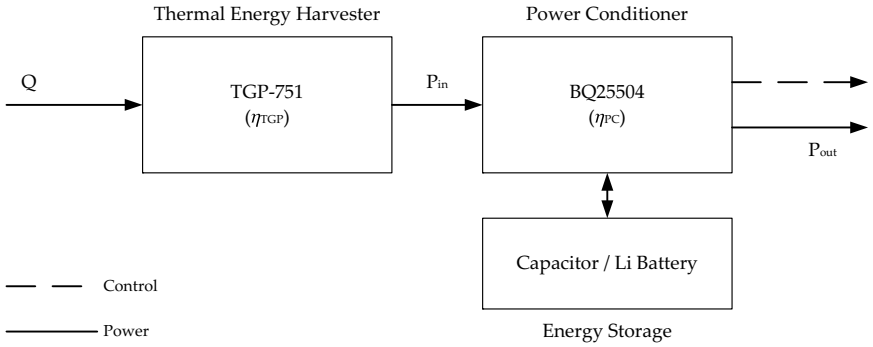

Figure 2.3: The EH system considered in this study

[R6]. Since thermal conduction is the primary means of transferring heat energy from the radiator to the hot side of the TGP, a new brass nut was designed to replace the existing brass nut. In contrast to the existing brass nut, this new brass nut not only fastens the plastic housing to the radiator, but also forms a secure casing for the cylindrical aluminium part of the TGP. The SARCON XR-m [53] thermal gap filler from Fuji Polymer Industries was used to create a tight fit between the TGP and the new brass nut, while the tool shown in figure 2.6d was used to screw it into place.. Furthermore, the need for a lid in the HCA was exploited to form the heat sink for the cold side of the TGP. A thermo-plastic material called CoolPoly D5506 Thermally Conductive Liquid Crystalline Polymer (LCP) [54] from Cool Polymers was used to mould the new lid, such that, the thermo-plastic lid plays dual roles of acting as a heat sink for the TGP and a secure cover for the plastic housing of the HCA. The Sarcon D-Tac 9A [55] thermally conductive double-sided adhesive silicone tape from Fuji Polymer Industries was used to fasten the thermo-plastic lid to the TGP. The new construction setup for the EH-HCA prototype is shown in figure 2.6a, while the new components are shown in figure 2.6.

If the EH application does not have any restrictions on the dimensions of the EH system, a general harvesting module can be used. The TE-gNODE shown in figure 2.7a is a general thermal energy harvesting module from Micropelt which can be used to harvest a larger amount of power. This module is ideally suited to harvest power for collectors, that can be installed on hot water pipes in buildings. The temperature of hot water inside the pipes are kept above 50°C to prevent bacterial growth, and hence provides a large temperature gradient between the surface of the hot water pipe and its ambient environment. The amount of power harvested by the TE-gNODE is shown in figure 2.7b, which shows that a temperature gradient of 25°C can at least supply 3mW of power.

2.2.2 Power Conditioner

The power conditioner is responsible for providing a stable operating voltage to the system, and thus is an important component. In thermal energy harvesting applications, the voltage generated by the TEG, tends to be rather small due to the low temperature gradient. This requires the power conditioner to be very efficient at low input voltages. The electrical

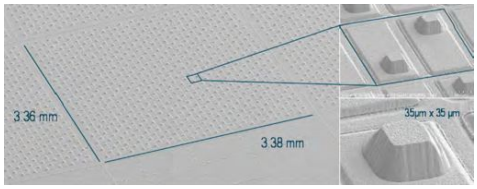

(a) Thermo-electric leg pairs on wafer substrate

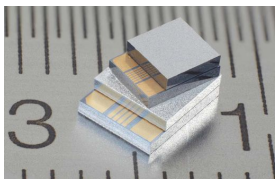

(b) Thin-film TEG [50]

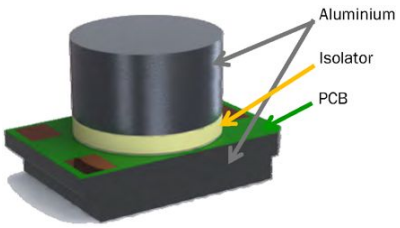

(c) Mechanical construction of standard package

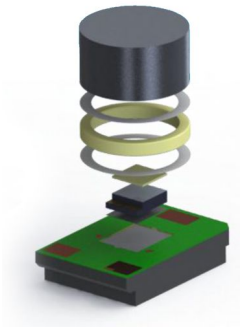

(d) Exploded diagram of standard package

Figure 2.4: TGP-751 thermo-generator package from Micropelt

resistance of TEGs tends to vary from a few ohms to a few hundred ohms, hence a MPPT system is required to extract the maximum amount of power from the TEG. While supporting multiple types of energy storage devices, it is desirable to have a battery charger on the same IC, to reduce the component count and complexity of the implementation. Furthermore, to prevent the power conditioner from draining the stored energy, when the thermal energy source is not available, it needs to have a very low quiescent current. Out of three power conditioners considered, the most appropriate device that fulfilled the requirements were selected.

2.2.2.1 S-8353/8354

The S-8353/8354 [56] is a step-up switching regulator from Seiko Instruments Inc. that is intended to be used in portable electronics. It has a relatively low startup voltage of around 0.9V and a high efficiency between 40% to 90%, even for light loads due to the presence of both a Pulse-Width Modulator (PWM) and a Pulse-Frequency Modulator (PFM) switching controller. The output voltage is selectable in 0.1V steps between 2V to 6.5V, and has a low leakage current of around 1μA. Figure 2.8 shows a typical application circuit and an efficiency graph, as depicted in the datasheet.

2.2.2.2 LTC3109

The LTC3109 [57] is an integrated step-up converter and power manager from Linear Technology, that is specifically made for TEGs with low electrical resistance, between 2Ω to 5Ω. It has a unique auto-polarity feature that allows it to operate on both a positive or negative voltage generated by the TEG, which, in this application, corresponds to the situation when the radiator is warmer than the room, and when the room is warmer than the radiator, respectively. The device is able to startup with a low input voltage between 40mV to 90mV,

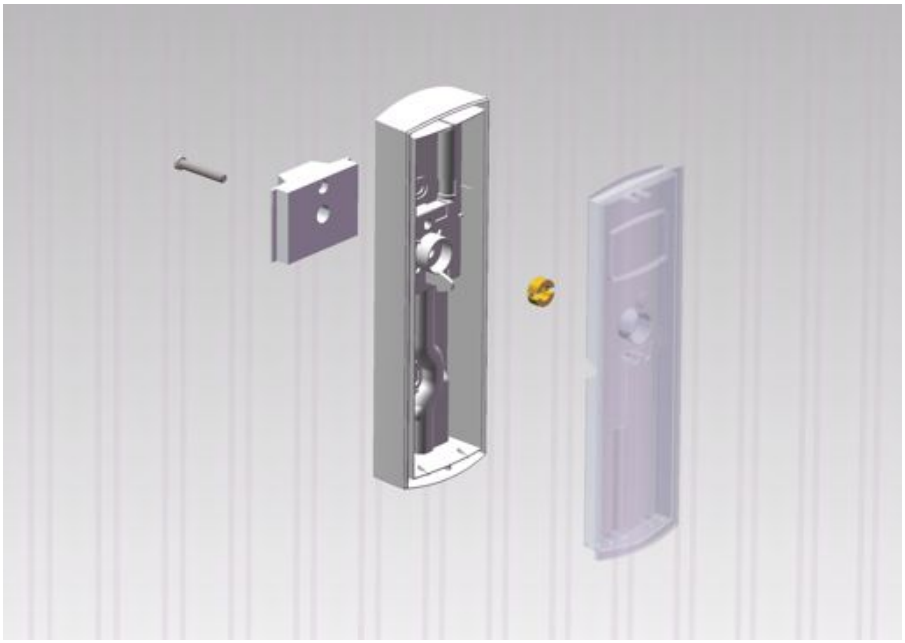

(a) Exploded diagram of the existing HCA

(b) Plastic housing

(c) Plastic lid

(d) Copper-plated steel bolt

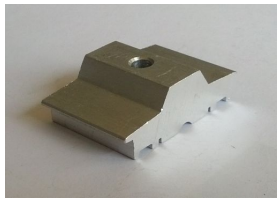

(e) Aluminium back part

(f) Brass nut

Figure 2.5: Components of the existing HCA

(a) Exploded diagram of the EH-HCA prototype

(b) New brass nut

(c) Thermo-plastic lid

(d) Tool for the new brass nut

Figure 2.6: New components for the EH-HCA prototype

(a) Mechanical construction of the general thermal energy harvester module

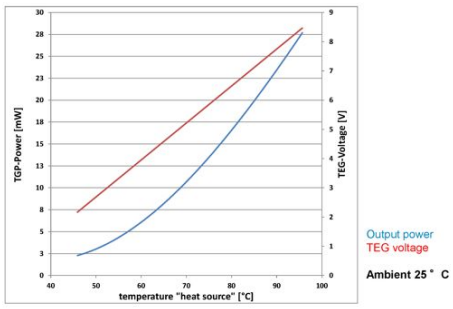

(b) Harvested thermal power

Figure 2.7: TE-gNODE module from Micropelt

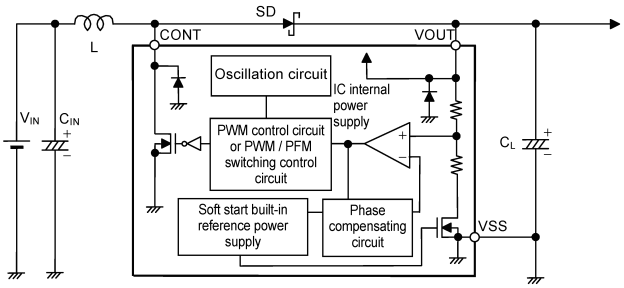

(a) Typical application circuit

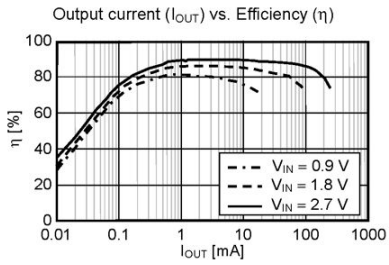

(b) Efficiency

Figure 2.8: S-8353/8354 from Seiko Instruments Inc.

and continue to operate up to 500mV. The output voltage is selectable among 2.3V, 3.3V, 4.1V, and 5.5V. The device also provides a power OK indicator to signal that the output voltage is within 7.5% of its selected value. However, the device has a low efficiency between 10% to 35% for low input voltages and a high quiescent current of around 10μA. The only energy storage device directly supported are capacitors, while an external charger IC can be used for batteries. A typical application circuit and an efficiency graph, as depicted in the datasheet is shown in figure 2.9.

The study presented in [58] uses the LTC3108, which is a single polarity version of the LTC3109, for harvesting thermal energy from the human body. A practical prototype is not constructed, instead opting for a breadboard setup. Nonetheless, the chosen power conditioner provides positive results, since the application does not require large energy storage and MPPT.

2.2.2.3 BQ25504

The BQ25504 is an ultra low-power boost converter with battery management from Texas Instruments, that is specially designed for energy harvesting applications. The startup voltage of the device is around 330mV, after which it supports very low input voltages between 80mV to 3V. It integrates a MPPT system than can be programmed to dynamically adjust the load resistance so that the optimal power is extracted from the TEG even at

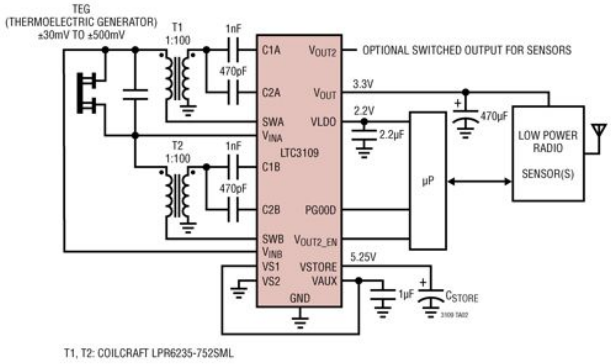

(a) Typical application circuit

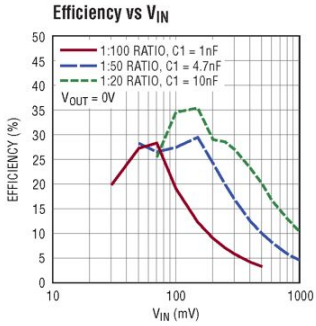

(b) Efficiency

Figure 2.9: LTC3109 from Linear Technology

very low temperature gradients. The dynamic MPPT system also supports input voltage regulation, where the maximum power is sacrificed by varying the load to ensure that the input voltage is higher than the minimum, to prevent the system from shutting down completely. A variety of energy harvesters can be used with the device due to this robust dynamic MPPT system. The output voltage can be programmed between 2V to 5.25V, and due to the battery management system, a variety of energy storage devices such as rechargeable Li batteries, thin-film batteries, super capacitors, or conventional capacitors, can be used. Furthermore, the device allows a programmable over-voltage level when charging and under-voltage level as protection when discharging the energy storage. A programmable threshold for a power OK indicator with hysteresis is provided to be used as a warning of pending loss of power. An efficiency between 20% to 70% can be obtained due to the PFM switching controller, and an extremely low quiescent current of 330nA. Figure 2.10 shows a typical application circuit and an efficiency graph, as depicted in the datasheet.

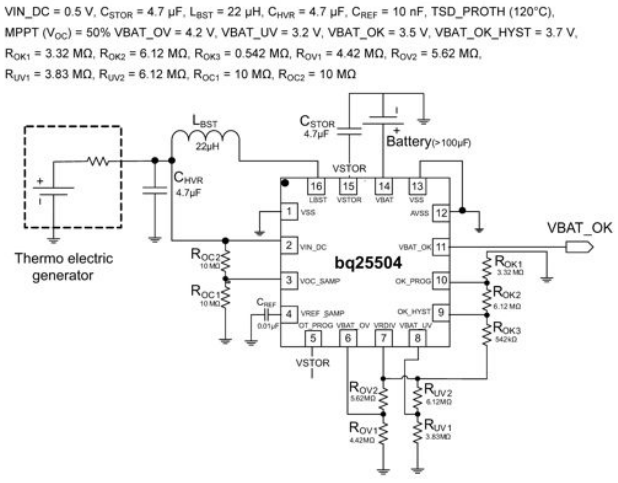

(a) Typical application circuit

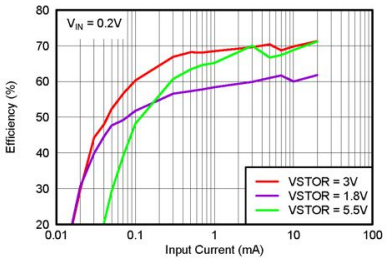

(b) Efficiency

Figure 2.10: BQ25504 from Texas Instruments

2.2.2.4 Summary

Table 2.1 presents a summary of the different power conditioners. Although the S-8353/8354 has a higher efficiency than the others, it is due to the higher startup voltage, which is not feasible to obtain from a TEG in a HCA. While the LTC3109's dual polarity is unique, the situation when the room is warmer than the radiator would not provide enough temperature gradient even during a hot summer. Furthermore, it has a very low efficiency and high leakage current making it unsuitable for this application. The BQ25504 is chosen for this study, because of its higher efficiency, low leakage current, presence of a dynamic MPPT system with a battery charger, and the flexibility of programming the required operating levels.

Table 2.1: Summary of DC-DC boost converters

Parameter	S-8353/8354	LTC3109	BQ25504
Startup voltage	0.9V	40mV to 90mV	330mV
Input voltage	0.9V to 10V	V_{startup} to 500mV	80mV to 3V
Output voltage	Programmable: 2V to 6.5V	Selectable: 2.3V, 3.3V, 4.1V, 5V	Programmable: 2.5V to 5.25V
Input resistance	Not defined	2Ω to 10Ω	Dynamic MPPT
Quiescent current	1μA	10μA	330nA
Efficiency, $V_{\text{in}} < 300$mV	40% to 90%	10% to 35%	20% to 70%
Power OK indicator	No	Yes	Programmable threshold
Battery charger	No	No	Programmable charging and protection
TEG polarity	Single	Dual	Single

2.2.3 Storage

The energy storage device is a crucial component in this application, especially since the power consumption rate of the system load is a non-zero amount. This is due to the mandatory measuring and displaying tasks of the HCA even during the non-heating seasons, e.g., the summer months. While there has been promising recent advancements in supercapacitors, the most practical component that can be used in this application still remain as rechargeable secondary batteries. It is worth noting that the BQ25504 power conditioner supports all types of storage devices.

2.2.3.1 Capacitor

The capacitor is a fundamental electronic component that stores energy in an electric field. While it exists in many variants in practice, fundamentally it is constructed with two parallel conductor plates separated with an insulating dielectric. Due to their large energy density, electrolytic capacitors, which are available in the range of a few hundred nanofarads to a few hundred millifarads, or supercapacitors, which are available in the range of a few tens of millifarads to a few tens of farads, are most suitable for EH applications.

The capacitance, C, of an ideal capacitor is defined as the ratio of the charge, Q, on each conducting plate and the voltage, V, between them. Therefore the charge stored in a capacitor can be described by equation (2.7).

$$C = \frac{\Delta Q}{\Delta V} \qquad \text{where} \begin{cases} C & \text{is in farad} \\ \Delta Q & \text{is in coulomb} \\ \Delta V & \text{is in volt} \end{cases}$$

$$\Delta Q = C \cdot \Delta V \tag{2.7}$$

The current, I, flowing through an electronic circuit can be defined as the rate of flow of charge over a period of time, Δt, given by equation (2.8).

$$I = \frac{\Delta Q}{\Delta t} \qquad \text{where} \begin{cases} I & \text{is in ampere} \\ \Delta t & \text{is in seconds} \end{cases} \tag{2.8}$$

Combining both equations (2.7) and (2.8), the capacitance required to sustain a stable voltage when the capacitor is discharged with a constant current for a period of time can be found using equation (2.9).

$$\begin{aligned} C \cdot \Delta V &= I \cdot \Delta t \\ C &= \frac{I \cdot \Delta t}{\Delta V} \end{aligned} \tag{2.9}$$

The energy, E, stored in the electric field of an ideal capacitor is related to the voltage between the conductor plates, and can be described by equation (2.10).

$$E = \frac{1}{2} \cdot C \cdot V^2 \qquad \text{where } E \text{ is in joule} \tag{2.10}$$

As shown in figure 2.11, the useful energy, ΔE, that is stored when a capacitor is charged is given by equation (2.11), while the average power, P_{avg}, is given by equation (2.12).

$$\Delta E = E_2 - E_1 = \frac{1}{2} \cdot C \cdot (V_2^2 - V_1^2) \tag{2.11}$$

$$P_{\text{avg}} = \frac{\Delta E}{\Delta t} \qquad \text{where } P_{\text{avg}} \text{ is in watt} \tag{2.12}$$

2.2.3.2 Battery

A battery is a device that converts chemical energy stored into electrical energy. Secondary batteries that can be recharged, due to the electrically reversible electrochemical reactions, are suitable for EH applications. Particularly, the need to sustain the HCA during the non-heating seasons, requires a large energy density which can only be satisfied by a battery with current technology. Various types of battery chemistries exist ranging from solid-state

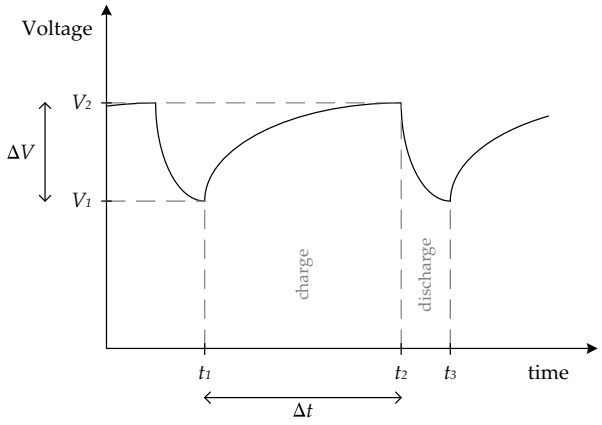

Figure 2.11: Energy stored in a capacitor when charging

thin-film batteries [59] with a capacity of tens of microampere hours to lithium-ion polymer batteries with a capacity of tens of ampere hours, in different constructions or packs.

A 100F supercapacitor that is discharged from 3V to 2.5V has a capacity of around 14mAh. In contrast, batteries provide a much larger energy density and a stable voltage for almost all of their operating lifetime. Capacitors can withstand significantly larger number of charge cycles compared to batteries. Nevertheless, its use is very application dependant, and is more attractive in applications that can afford the system load to be completely shut down when the energy source is depleted.

In this study the VL-3032 [60] Vanadium-Pentoxide (VL-type) rechargeable lithium coin cell from Panasonic Industrial Devices, shown in figure 2.12, is used. The specifications described in table 2.2 demonstrates the feasibility of the device for use in an EH-HCA. This battery has been successfully deployed in the automotive and metering industry because of its excellent reliability and robustness. Furthermore, the size of the battery is small enough to fit into the plastic housing of the HCA.

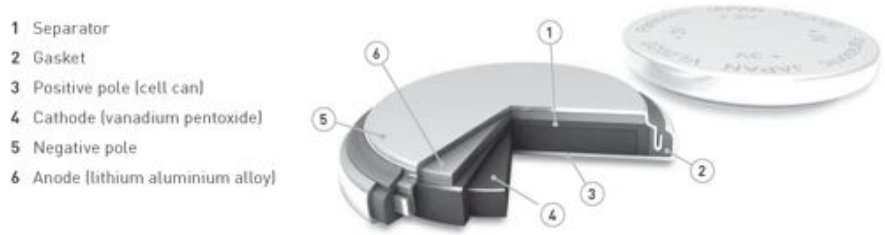

Figure 2.12: VL-3032 from Panasonic Industrial Devices

Since it is impractical to conduct a test over tens of years, the theoretical performance of the device was characterised by Panasonic, as shown in figure 2.13, by using accelerated tests. The results of such tests can be used as a good indication to evaluate the long term

Table 2.2: Specifications of VL-3032

Nominal voltage	3V
Nominal capacity	100mAh
Self-discharge	$\leq$ 2% per year
Continuous drain	0.2mA
Charge voltage	3.4V$\pm$0.15V
Charge current	$\leq$ 4mA
Operating temperature	$-20°$C to $+60°$C
Weight	6.2g
Diameter	30mm
Thickness	3.2mm

performance of the device.

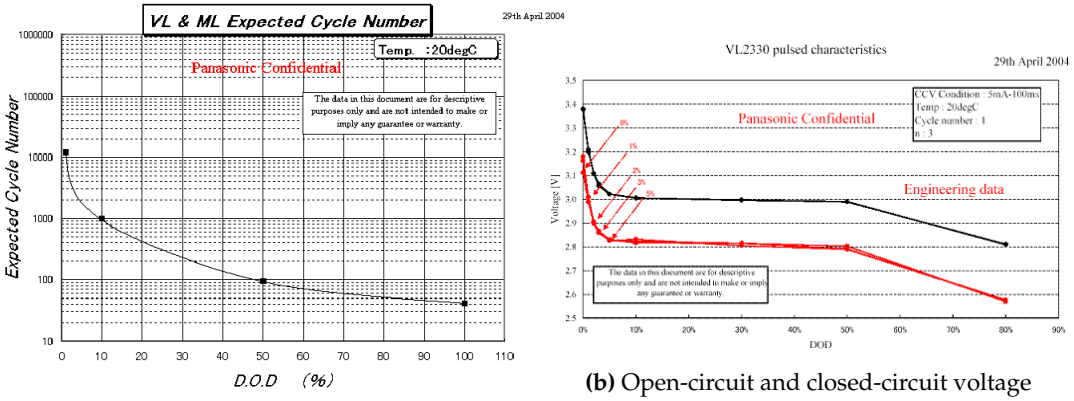

(a) Expected number of charge cycles

(b) Open-circuit and closed-circuit voltage

Figure 2.13: Impact of the depth of discharge on a VL-type rechargeable lithium battery

The maximum number of charge cycles, $N^{\text{max}}_{\text{cycles}}$, the battery can handle before it degrades is given by equation (2.13), where, D^{max}, represents the worst case Depth of Discharge (DOD) of the battery when used in an EH application.

$$N^{\text{max}}_{\text{cycles}} = \frac{30000}{(D^{\text{max}})^{1.474}} \qquad \text{where } D^{\text{max}} \text{ is in \%} \tag{2.13}$$

The number of years, N_{years}, that the battery can be operational depends on the number of charge cycles, $N^{\text{year}}_{\text{cycles}}$, it undergoes during an year as described by equation (2.14).

$$\begin{aligned} N^{\text{year}}_{\text{cycles}} * N_{\text{years}} &\leq N^{\text{max}}_{\text{cycles}} \qquad \text{where } N^{\text{year}}_{\text{cycles}} \text{ is in charge cycles per year} \\ N_{\text{years}} &\leq \frac{N^{\text{max}}_{\text{cycles}}}{N^{\text{year}}_{\text{cycles}}} \end{aligned} \tag{2.14}$$

Hence the total capacity of the battery, $C^{\text{total}}_{\text{battery}}$, depends on the capacity of the battery, C_{battery}, and the maximum charge cycles, as described by equation (2.15).

$$C_{\text{battery}}^{\text{total}} = C_{\text{battery}} * N_{\text{cycles}}^{\text{max}} \qquad \text{where } C_{\text{battery}} \text{ is in mAh} \tag{2.15}$$

Furthermore, each charge cycle results in a permanent loss of capacity, C_{loss}, in the battery. This is given by equation (2.16).

$$C_{\text{loss}} = \frac{C_{\text{battery}}}{N_{\text{cycles}}^{\text{max}}} \qquad \text{where } C_{\text{loss}} \text{ is in mAh per charge cycle} \tag{2.16}$$

2.3 Analysis

The thermal path of the mechanical construction is mathematically analysed to verify whether it is feasible to obtain a sufficient temperature gradient across the TGP. The heat energy is transferred from the radiator surface to the hot side of the TGP predominantly due to thermal conduction, while the heat energy is dissipated via thermal convection and radiation from the thermo-plastic lid, which is attached to the cold side of the TGP. These phenomena are included in the basic model.

As shown by figure 2.14, for a given room temperature and radiator surface temperature, the model can be used to obtain the actual temperature gradient across the thermal energy harvester, which can then help determine the feasibility of the EH-HCA.

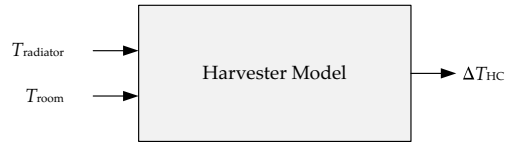

Figure 2.14: Block diagram of the thermal model

One-dimensional heat conduction is analogous to electrical conduction [61], since heat is transferred by vibrations between adjacent atoms, and electricity is conducted by free valence electrons of atoms. Table 2.3 shows the relationship between the different properties. The mechanical construction for thermal energy harvesting is modelled by exploiting this analogy.

Table 2.3: Analogy between thermal and electrical conduction

Thermal		$\Longleftrightarrow$	**Electrical**	
Heat flow	Q (W)	$\Longleftrightarrow$	Current flow	I (A)
Temperature difference	ΔT (K)	$\Longleftrightarrow$	Voltage difference	ΔV (V)
Thermal resistance	R_T ($\frac{K}{W}$)	$\Longleftrightarrow$	Electrical resistance	R (Ω)

Conduction
Thermal conduction occurs over a temperature gradient between a hot side temperature,

T_A, and a cold side temperature, T_B, through a cross-sectional area, A, due to the exchange of kinetic energy between atoms along the thermal path, l. The power, Q_{cond}, due to the heat flow can be described by equation (2.17), where, λ, is the thermal conductivity of the material. The thermal resistance, $R_{T\text{-}cond}$, is given by equation (2.18).

$$Q_{cond} = \lambda \cdot \frac{A}{l} \cdot (T_A - T_B) \qquad \text{where} \begin{cases} Q_{cond} & \text{is in watt} \\ \lambda & \text{is in watt per meter kelvin} \\ A & \text{is in square meter} \\ l & \text{is in meter} \\ T_A & \text{is in kelvin} \\ T_B & \text{is in kelvin} \end{cases} \tag{2.17}$$

$$R_{T\text{-}cond} = \frac{l}{\lambda \cdot A} \qquad \text{where } R_{T\text{-}cond} \text{ is in kelvin per watt} \tag{2.18}$$

Convection
Thermal convection occurs when a flow of fluid transports heat along with its matter. The EH-HCA is surrounded by air, which absorbs the heat from the thermo-plastic lid, becomes less dense and then rises. As this happens, cooler air moves into replace it, creating fluid motion in a process known as natural convection. The basic model presented in this study, assumes that the EH-HCA is not covered and that natural convection occurs. The convection coefficient, $h \approx 2.5 \frac{W}{mK}$, when natural convection exists. For a rectangular plate that is placed vertically, such as the thermo-plastic lid, the geometric constant, $G \approx 0.55$, while the length, l, represents the vertical dimension of the plate, and, A, represents the rectangular surface area of the exposed side of the plate. The power, Q_{conv}, due to the heat flow can be described by equation (2.19), while a thermal resistance, $R_{T\text{-}conv}$, can be modelled as given by 2.20.

$$Q_{conv} = h \cdot \frac{G \cdot A}{l^{0.25}} \cdot (T_A - T_B)^{1.25} \qquad \text{where } h \text{ is in watt per meter kelvin} \tag{2.19}$$

$$R_{T\text{-}conv} = \frac{l^{0.25}}{h \cdot G \cdot A} \cdot \frac{1}{(T_A - T_B)^{0.25}} \tag{2.20}$$

Radiation
Thermal radiation occurs when a sufficiently large temperature gradient exists, where heat energy is transferred as electromagnetic waves, even in the absence of a transfer medium. The power, Q_{rad}, due to the heat flow can be described by equation (2.21), where, A, is the surface area of the exposed hot side, while, σ, and, ϵ, represents the Stefan–Boltzmann constant and the emissivity of the material respectively. A thermal resistance, $R_{T\text{-}rad}$, can be modelled as described by equation (2.22).

$$Q_{rad} = \sigma \cdot \epsilon \cdot A \cdot (T_A^4 - T_B^4) \qquad \text{where } \sigma \text{ is in } \frac{W}{m^2 K^4} \tag{2.21}$$

$$R_{T\text{-}rad} = \frac{(T_A - T_B)}{\sigma \cdot \epsilon \cdot A \cdot (T_A^4 - T_B^4)} \tag{2.22}$$

2.3.1 Modelling of Harvester

To analyse the feasibility of obtaining a sufficient temperature gradient across the TGP, the model presented in figure 2.15 is used.

The temperature gradient between the hot surface of the radiator, T_{radiator}, and the cold ambient air of the room, T_{room}, is given by equation (2.23).

$$\Delta T = T_{\text{radiator}} - T_{\text{room}} \tag{2.23}$$

Assuming an ideal thermal conduction path with no losses, the thermal resistances of the components, due to conduction, can be described using equation (2.18). The thermal resistance of the bolt, $R^{\text{bolt}}_{\text{T-cond}}$, welded onto the surface of the radiator, is given by 2.24. It has a diameter, D^{bolt}, and a length, l^{bolt}, where the material steel has a thermal conductivity, λ^{steel}.

$$R^{\text{bolt}}_{\text{T-cond}} = \frac{l^{\text{bolt}}}{\lambda^{\text{bolt}} \cdot A^{\text{bolt}}} = \frac{l^{\text{bolt}}}{\lambda^{\text{steel}} \cdot \pi \cdot \frac{(D^{\text{bolt}})^2}{4}} \tag{2.24}$$

The thermal resistance of the nut, $R^{\text{nut}}_{\text{T-cond}}$, that is screwed onto the bolt to fasten the plastic housing to the radiator and support the TGP, is given by equation (2.25). It has a diameter, D^{nut}, and a length, l^{nut}, where the material brass has a thermal conductivity, λ^{brass}.

$$R^{\text{nut}}_{\text{T-cond}} = \frac{l^{\text{nut}}}{\lambda^{\text{nut}} \cdot A^{\text{nut}}} = \frac{l^{\text{nut}}}{\lambda^{\text{brass}} \cdot \pi \cdot \frac{(D^{\text{nut}})^2}{4}} \tag{2.25}$$

While the thermal resistance of the TGP, $R^{\text{TGP}}_{\text{T-cond}}$, is given in the datasheet of the device, the thermal resistance of the rectangular lid, $R^{\text{lid}}_{\text{T-cond}}$, that is used both as a cover and heat sink, is described by equation (2.26). The TGP, with a diameter, D^{TGP}, comes into contact with the lid, which has a thickness, H^{lid}, while the thermo-plastic material has a thermal conductivity, $\lambda^{\text{thermo-plastic}}$.

$$R^{\text{lid}}_{\text{T-cond}} = \frac{l^{\text{lid}}}{\lambda^{\text{lid}} \cdot A^{\text{lid}}} = \frac{H^{\text{lid}}}{\lambda^{\text{thermo-plastic}} \cdot \pi \cdot \frac{(D^{\text{TGP}})^2}{4}} \tag{2.26}$$

The total thermal resistance, $R^{\text{total}}_{\text{T-cond}}$, due to conduction is found by summing the individual series thermal resistances, as given by equation (2.27).

$$R^{\text{total}}_{\text{T-cond}} = R^{\text{bolt}}_{\text{T-cond}} + R^{\text{nut}}_{\text{T-cond}} + R^{\text{TGP}}_{\text{T-cond}} + R^{\text{lid}}_{\text{T-cond}} \tag{2.27}$$

The temperature, T_{H}, on the hot side of the TGP, is given by equation (2.28), where, T_{S}, is the surface temperature of the thermo-plastic lid.

$$T_{\text{H}} = \frac{(R^{\text{TGP}}_{\text{T-cond}} + R^{\text{lid}}_{\text{T-cond}}) \cdot T_{\text{radiator}} + (R^{\text{bolt}}_{\text{T-cond}} + R^{\text{nut}}_{\text{T-cond}}) \cdot T_{\text{S}}}{R^{\text{total}}_{\text{T-cond}}} \tag{2.28}$$

The temperature, T_{C}, on the cold side of the TGP, is given by equation (2.29).

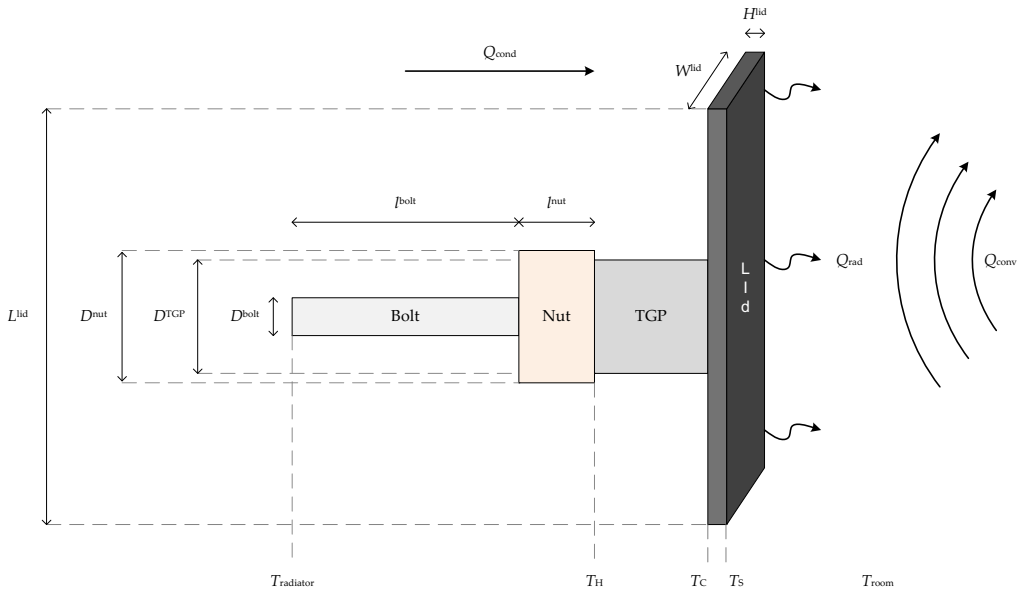

(a) Basic model

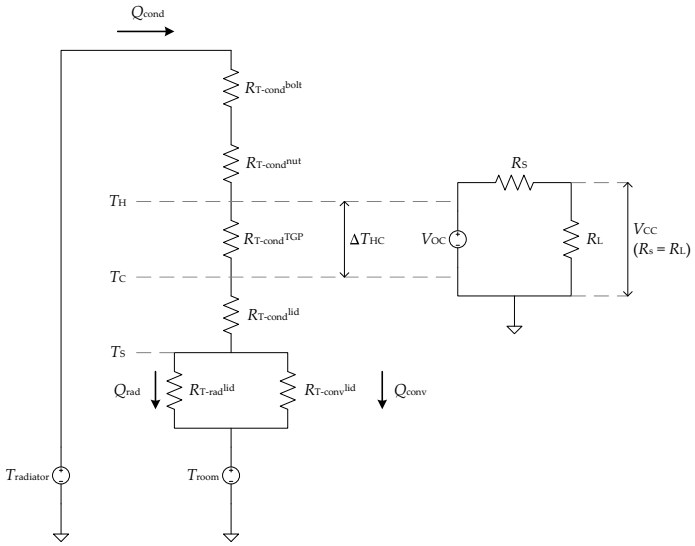

(b) Equivalent circuit

Figure 2.15: Thermal model of harvester

$$T_{\mathrm{C}} = \frac{R^{\mathrm{lid}}_{\text{T-cond}} \cdot T_{\text{radiator}} + (R^{\mathrm{bolt}}_{\text{T-cond}} + R^{\mathrm{nut}}_{\text{T-cond}} + R^{\mathrm{TGP}}_{\text{T-cond}}) \cdot T_{\mathrm{S}}}{R^{\mathrm{total}}_{\text{T-cond}}} \tag{2.29}$$

Finally, the temperature gradient, ΔT_{HC}, across the TGP, is given by equation (2.30).

$$\Delta T_{\mathrm{HC}} = T_{\mathrm{H}} - T_{\mathrm{C}} = \frac{R^{\mathrm{TGP}}_{\text{T-cond}}}{R^{\mathrm{total}}_{\text{T-cond}}} \cdot (T_{\text{radiator}} - T_{\mathrm{S}}) \tag{2.30}$$

The open-circuit voltage, V_{OC}, generated by the TGP can be found from equation (2.5), and described as equation (2.31).

$$V_{\mathrm{OC}} = \alpha_{\mathrm{TGP}} \cdot \Delta T_{\mathrm{HC}} \tag{2.31}$$

According to the maximum power transfer theorem, which MPPT [62] is based on, the optimum power transfer occurs when the load electrical resistance, R_{l}, is equal to the electrical resistance, R_{s}, of the TGP. In other words, the maximum power transfer occurs when the closed-circuit voltage, V_{CC}, generated by the TGP is half of the open-circuit voltage, as a result of a simple voltage division, shown by equation (2.32).

$$V_{\mathrm{CC}} = \frac{1}{2} \cdot V_{\mathrm{OC}} \qquad \text{when} \quad R_{\mathrm{l}} = R_{\mathrm{s}} \tag{2.32}$$

Therefore the optimum power, P_{in}, available for the power conditioner is given by equation (2.33).

$$\begin{aligned} P_{\mathrm{in}} &= \frac{(V_{\mathrm{OC}})^2}{4 \cdot R_{\mathrm{s}}} \\ &= \frac{(V_{\mathrm{CC}})^2}{R_{\mathrm{s}}} \\ &= \frac{(\alpha_{\mathrm{TGP}} \cdot \Delta T_{\mathrm{HC}})^2}{4 \cdot R_{\mathrm{s}}} \end{aligned} \tag{2.33}$$

Finding the surface temperature of the thermo-plastic lid

The power, Q_{cond}, due to thermal conduction is proportional to the temperature gradient between the hot surface of the radiator and the cold surface of the thermo-plastic lid and can be described by equation (2.34).

$$Q_{\mathrm{cond}} = \frac{(T_{\text{radiator}} - T_{\mathrm{S}})}{R^{\mathrm{total}}_{\text{T-cond}}} \tag{2.34}$$

The heat dissipated from the thermo-plastic lid due to convection between the hot surface of the thermo-plastic lid and the cold ambient air in the room is given by equation (2.19). The power, $Q^{\mathrm{lid}}_{\mathrm{conv}}$, from the heat flow caused by natural convection is shown by equation (2.35), where, L^{lid}, is the vertical length parallel to the direction of the air flow, and, W^{lid}, is the horizontal width, of the thermo-plastic lid.

$$
\begin{aligned}
Q_{\text{conv}}^{\text{lid}} &= h \cdot \frac{G \cdot A^{\text{lid}}}{(l^{\text{lid}})^{0.25}} \cdot (T_{\text{S}} - T_{\text{room}})^{1.25} \\
&= \frac{2.5 \frac{\text{W}}{\text{mK}} \cdot 0.55 \cdot L^{\text{lid}} \cdot W^{\text{lid}}}{(L^{\text{lid}})^{0.25}} \cdot (T_{\text{S}} - T_{\text{room}})^{1.25}
\end{aligned} \tag{2.35}
$$

Furthermore, the heat radiated from the hot thermo-plastic lid to the cold room is described by equation (2.21). The power, $Q_{\text{rad}}^{\text{lid}}$, from the heat flow caused by radiation is given by equation (2.36), where, ϵ^{lid}, is the emissivity of the thermo-plastic material.

$$
\begin{aligned}
Q_{\text{rad}}^{\text{lid}} &= \sigma \cdot \epsilon^{\text{lid}} \cdot A^{\text{lid}} \cdot (T_{\text{S}}^4 - T_{\text{room}}^4) \\
&= \sigma \cdot \epsilon^{\text{thermo-plastic}} \cdot L^{\text{lid}} \cdot W^{\text{lid}} \cdot (T_{\text{S}}^4 - T_{\text{room}}^4)
\end{aligned} \tag{2.36}
$$

The thermo-plastic lid reaches thermal equilibrium when the net heat flow, Q^{total}, given by equation (2.37), is zero.

$$
Q^{\text{total}} = Q_{\text{cond}} - Q_{\text{conv}}^{\text{lid}} - Q_{\text{rad}}^{\text{lid}} \tag{2.37}
$$

The energy, $Q^{\text{total}} \cdot \Delta t$, required to change the surface temperature, ΔT_{lid}, of the thermo-plastic lid in a given time, Δt, depends on its mass, m^{lid}, and the specific heat capacity, $C^{\text{thermo-plastic}}$, of the material, as described by equation (2.38).

$$
\Delta T_{\text{lid}} = \frac{Q^{\text{total}} \cdot \Delta t}{m^{\text{lid}} \cdot C^{\text{thermo-plastic}}} \tag{2.38}
$$

The steady-state surface temperature of the thermo-plastic lid can be found by employing numerical methods. Iterating over n for the net heat flow of the thermo-plastic lid from equation (2.37). Updating the changing surface temperature of the thermo-plastic lid from equation (2.39) using the specific heat equation (2.38), which describes the energy required to produce the change in temperature, until, $Q^{\text{total}} \rightarrow 0$. The initial surface temperature, T_{S}, is assumed to be the average of the temperature gradient between the surface of the radiator and the room.

$$
T_{\text{S}}^{n+1} = T_{\text{S}}^{n} + \Delta T_{\text{lid}} \tag{2.39}
$$

Preliminary results

A preliminary feasibility study can be performed using the thermal harvester model. The values from the datasheets and drawings used in the analysis are shown in table 2.4. The results from the analysis, shown in figure 2.16, demonstrate that the temperature gradient, ΔT, between the surface of the radiator and the room, provides a temperature gradient, ΔT_{HC}, across the TGP, which is reduced by approximately an order of magnitude. The power conditioner, BQ25504, should still be able to harvest energy down to around a 10K temperature gradient between the radiator surface and the room since the open-circuit voltage is sufficiently high. It is interesting to note that due to the low Carnot efficiency, out of the milliwatts of power, only microwatt amounts would be harvested.

Table 2.4: Values used from the datasheets and drawings

l^{bolt}	$=$	15 mm
λ^{steel}	$=$	$15\ \frac{\text{W}}{\text{mK}}$
D^{bolt}	$=$	3 mm
l^{nut}	$=$	4.2 mm
λ^{brass}	$=$	$115\ \frac{\text{W}}{\text{mK}}$
D^{nut}	$=$	10.7 mm
$R^{\text{TGP}}_{\text{T-cond}}$	$=$	$18\ \frac{\text{K}}{\text{W}}$
D^{TGP}	$=$	9.5 mm
α_{TGP}	$=$	$110\ \frac{\text{mV}}{\text{K}}$
R_{s}	$=$	300 Ω
V^{lid}	$=$	Volume = 9145 mm^3
H^{lid}	$=$	$\frac{\text{Volume}}{\text{Area}} = 1.8$ mm
$\lambda^{\text{thermo-plastic}}$	$=$	$10\ \frac{\text{W}}{\text{mK}}$
L^{lid}	$=$	127.9 mm
W^{lid}	$=$	38.9 mm
σ	$=$	$5.670373 \cdot 10^{-8}\ \frac{\text{W}}{\text{m}^2\text{K}^4}$
$\epsilon^{\text{thermo-plastic}}$	$=$	0.9
Δt	$=$	1 ms
ρ^{lid}	$=$	Density $= 1.8\ \frac{\text{g}}{\text{cm}^3}$
m^{lid}	$=$	Density $\cdot$ Volume $= 16.461$ g
$C^{\text{thermo-plastic}}$	$=$	$1\ \frac{\text{J}}{\text{gK}}$
T_{radiator}	$=$	$[20\ ^\circ\text{C}, 50\ ^\circ\text{C}] = [293\ \text{K}, 323\ \text{K}]$
T_{room}	$=$	$20^\circ\text{C} = 293$ K

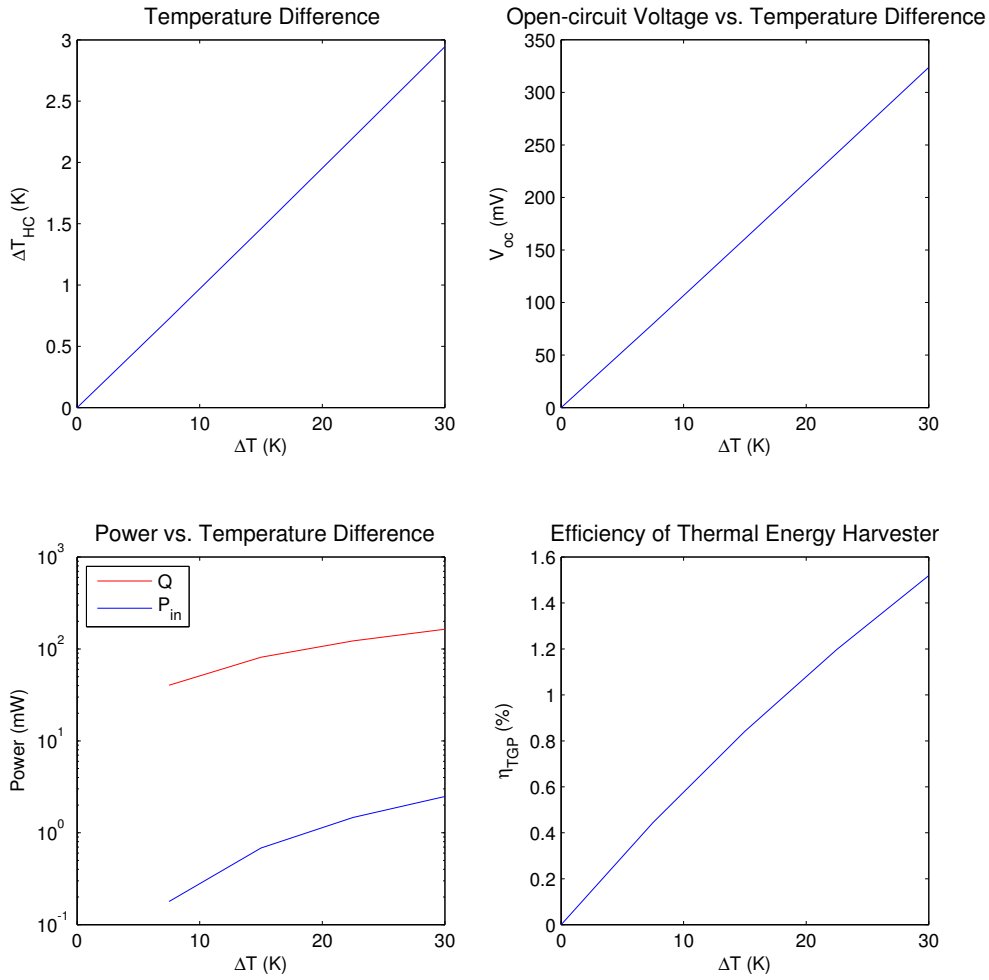

Figure 2.16: Preliminary results from the model

2.4 Experiment Setup

The experiments to measure the amount of power that can be harvested from the heat of the radiator, was carried out in a temperature-controlled room at Brunata, with an area of approximately 12m^2. This room was used in the design of the Futura+ HCA, and provided a good test environment. The layout of the test facility is shown in figure 2.17, where the surface temperature of the radiator is regulated by a Proportional-Integral-Derivative (PID) controller that adjusts the inlet and outlet water temperature to maintain a certain surface temperature of the radiator. A ventilator installed in the room ensures that a certain room temperature is maintained by circulation of the air.

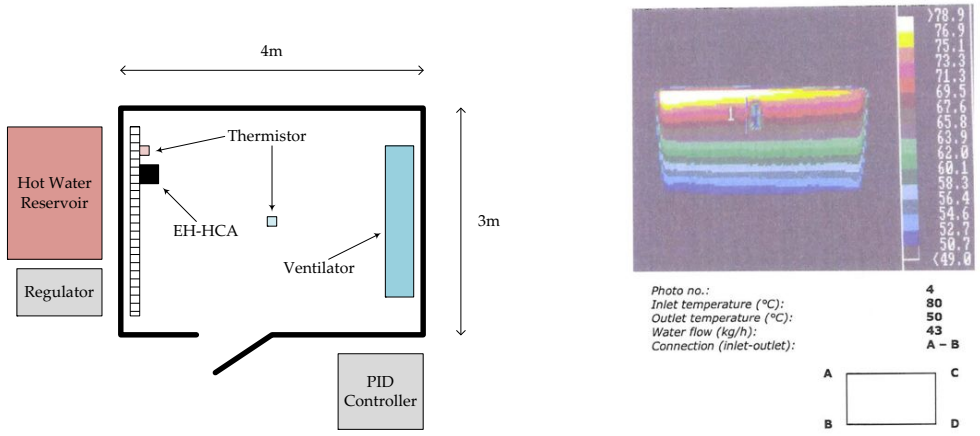

(a) Temperature-controlled room **(b)** Thermographic view of a radiator

Figure 2.17: Layout of the experiment setup

In apartments, the HCA is installed at a vertical distance of $\frac{2}{3}$ of the height from the bottom, and horizontally at the center of a radiator. Brunata has empirically verified that the measured surface temperature at this point provides the most accurate value of the average surface temperature of the radiator.

Since there were other HCAs already installed on the radiator for tests, the EH-HCA prototype was installed with a horizontal offset. The thermographic picture shown in figure 2.17b demonstrates that, while the surface temperature of the radiator varies vertically, it remains constant in horizontal regions, and would not significantly affect the outcome of the experiment.

A Low Surface Temperature (LST) radiator[1] is considered in this study, which has a maximum allowed surface temperature of 43°C [63]. LST radiators are used wherever high efficiency is required, yet where safety demands a low surface temperature, i.e., where people may injure themselves if left in contact with a standard radiator. They are typically used in hospitals, nurseries and residential homes, as well as children's bedrooms.

[1] conforms to BS EN 442: *Specification for radiators and convectors. Evaluation of conformity*

2.4.1 Measurement Equipment

The experiment to measure the power harvested by the EH-HCA prototype used several pieces of equipment as shown in figure 2.18. To speed up the setup of the experiment, a ready made Evaluation Module (EVM) of the BQ25504 power conditioner [64] was used, while a 820μF electrolytic capacitor was chosen as the energy storage device due to its simple mathematical model, and because it is the same capacitor currently used in the Futura+ HCA as an energy buffer for current spikes. The energy harvested from the heat of the radiator was discharged over a fixed resistance using the power OK indicator as a trigger. The temperature on the surface of the radiator and the temperature of the room was measured using 303ET Negative Temperature Coefficient (NTC) thermistors [65] from ATC Semitec. Finally, the data was measured using the ADC-16 high-resolution logger [66] from Pico Technology and was gathered on a computer for analysis using the PicoLog data acquisition software [67] from Pico Technology. The measurement equipment used in the experiment are shown in figure 2.19.

Figure 2.18: Overview of experiment setup

Power Conditioner
The BQ25504 EVM was modified to program the MPPT system to dynamically track 50% of the open-circuit voltage, instead of the default 78% intended for photo-voltaic cells. A summary of the performance specification is shown in table 2.5.

(a) EH-HCA and thermistor on the radiator

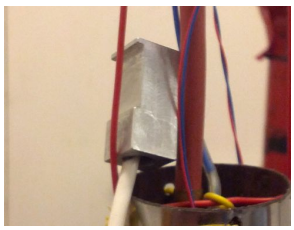

(b) Room thermistor

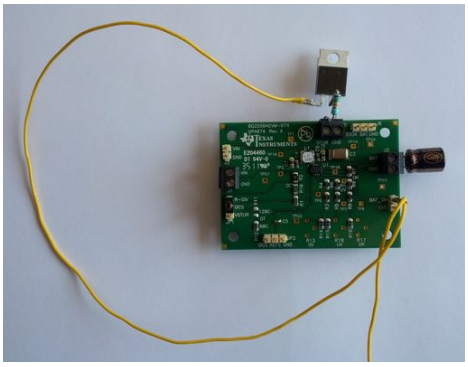

(c) Power conditioner, energy storage, and load

(d) High-resolution data logger

Figure 2.19: Equipment used in the experiment

Table 2.5: Performance specification of BQ25504 EVM

Parameter	Description	Value
V_{in}	DC input voltage	0.13V to 3V
$V_{\text{in}}^{\text{startup}}$	DC minimum startup voltage	330mV
V_{OV}	Over voltage level - Sets maximum output voltage	3.1V
V_{UV}	Under voltage setting to disconnect V_{BAT} from V_{SYS} system voltage	2.2V
$V_{\text{BAT\_OK}}^{\text{rising}}$	$V_{\text{BAT\_OK}}$ indication toggles high when V_{SYS} ramps up to this level	2.8V
$V_{\text{BAT\_OK}}^{\text{falling}}$	$V_{\text{BAT\_OK}}$ indication toggles low when V_{SYS} ramps down to this level	2.4V
MPPT	Maximum Power Point Tracking - Programmed % of open-circuit voltage for TEGs	50%

System Load

From equation (2.9), the system load was emulated by discharging over a resistor, $R_{\text{load}} = 18\text{k}\Omega$, to give a discharge time that is greater than 2s so that it is greater than the sampling time of the ADC16, as described by equation (2.40).

$$\begin{aligned} t &= \frac{C \cdot \Delta V}{I_{\text{avg}}} \\ &= \frac{C \cdot \Delta V \cdot R_{\text{load}}}{V_{\text{avg}}} \\ &= \frac{C \cdot (V_{\text{BAT\_OK}}^{\text{rising}} - V_{\text{BAT\_OK}}^{\text{falling}}) \cdot R_{\text{load}}}{0.5 \cdot (V_{\text{BAT\_OK}}^{\text{rising}} + V_{\text{BAT\_OK}}^{\text{falling}})} \\ &= \frac{820\mu\text{F} \cdot (2.8\text{V} - 2.4\text{V}) \cdot 18\text{k}\Omega}{\frac{2.8\text{V}+2.4\text{V}}{2}} = 2.3\text{s} \end{aligned} \tag{2.40}$$

The $V_{\text{BAT\_OK}}$ signal is used to switch an n-channel metal-oxide-semiconductor field-effect transistor (MOSFET) , which pulls the resistor to ground, as shown in figure 2.20.

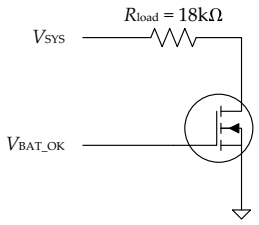

Figure 2.20: Schematic diagram of the emulated system load

Temperature Sensors
The 303ET NTC thermistors were used to measure the surface temperature of the radiator and the room. A thermistor is a resistor whose resistance varies significantly with the temperature of the environment, and the relationship between temperature, T, and resistance, R, can be modelled by using the Steinhart-Hart thermistor model give by equation (2.41).

$$T(R) = \frac{1}{A + B \cdot \ln(R) + C \cdot \ln(R)^2 + D \cdot \ln(R)^3} \quad \text{where} \begin{cases} T & \text{is in degree Celsius} \\ R & \text{is in ohm} \end{cases} \tag{2.41}$$

Equation (2.41) needs to rewritten for resistance as a function of temperature. Using the raw data points described in the datasheet of the thermistor, a curve fit can be found. By transforming R using a natural logarithm, a third-degree polynomial curve fit can be obtained as described by equation (2.42), where $A, B, C,$ and D are the coefficients[2].

$$R(T) = \exp\left(\frac{1}{A \cdot T^3 + B \cdot T^2 + C \cdot T + D}\right) \quad \text{where} \begin{cases} A & = 481.298455 \cdot 10^{-12} \\ B & = 409.194239 \cdot 10^{-9} \\ C & = \frac{15}{40847} \\ D & = \frac{491}{5608} \end{cases} \tag{2.42}$$

Current flowing through a thermistor dissipates heat, and raises its temperature above that of its environment, $T_{\text{environment}}$. This phenomena is known as the self-heating effect of a thermistor. The actual environment temperature can be described with equation (2.43), where the dissipation factor, $\delta = 0.7$, of the thermistor can be obtained from its datasheet, and, ΔV_{R}, is the voltage across the thermistor.

$$T_{\text{environment}} = T - \frac{\Delta V_R^2}{\delta \cdot R(T)} \quad \text{where} \begin{cases} T_{\text{environment}} & \text{is degree Celsius} \\ \Delta V_R & \text{is in volt} \\ \delta & \text{is in } \frac{\text{mW}}{^\circ\text{C}} \end{cases} \tag{2.43}$$

The simple voltage division circuit shown in figure 2.21 with an input voltage, $V_{\text{in}} = 3\text{V}$, is used to convert the temperature of the environment to a voltage, V_{out}. The equation (2.44) for V_{out}, also takes into account an input impedance, $R_{\text{in}} = 1\text{M}\Omega$, of the ADC-16 data logger.

$$V_{\text{out}} = V_{\text{in}} \cdot \frac{R_{\text{fixed}} \cdot R_{\text{in}}}{R_{\text{fixed}} \cdot R_{\text{in}} + R(T) \cdot (R_{\text{fixed}} + R_{\text{in}})} \quad \text{where} \begin{cases} V_{\text{out}} & \text{is in volt} \\ V_{\text{in}} & \text{is in volt} \\ R_{\text{fixed}} & \text{is in ohm} \end{cases} \tag{2.44}$$

A fixed resistance, $R_{\text{fixed}} = 19.1\text{k}\Omega$, was found to give the lowest voltage error and a large dynamic range. The temperature of the environment can then be given as described by equation (2.45) for the 303ET NTC thermistor.

$$\Delta V_{\text{R}} = V_{\text{in}} - V_{\text{out}}$$

[2]not related to the coefficients of the Steinhart-Hart equation

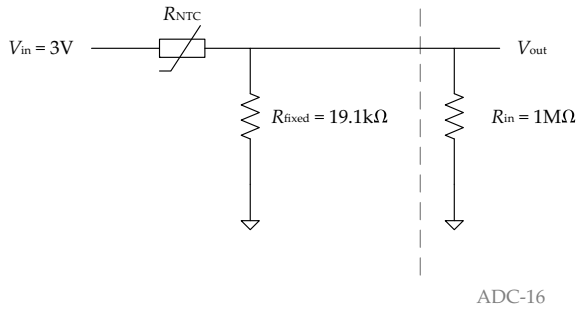

Figure 2.21: Schematic diagram of the 303ET NTC thermistor

$$T_{\text{environment}} = T - \frac{(V_{\text{in}} - V_{\text{out}})^2}{0.7 * R(T)} \tag{2.45}$$

Figure 2.22 shows the polynomial curve fit obtained from the data set given in the datasheet of the 303ET NTC thermistor. It also shows a plot of the output voltage calculated using the polynomial curve fit.

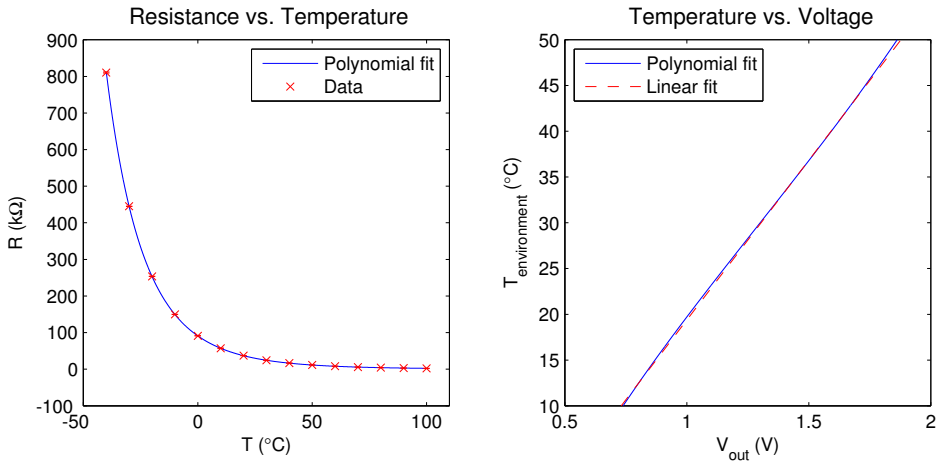

Figure 2.22: Curve fits for the 303ET NTC thermistor

Within the region of interest for the temperature of the environment, a linear approximation can be obtain as described by equation (2.46), which is better suited for the PicoLog data acquisition software.

$$V_{\text{out}} = \frac{539}{18805} \cdot T_{\text{environment}} + \frac{302}{679} \qquad \text{where } T_{\text{environment}} \in [10, 50]$$

$$T_{\text{environment}} = \frac{18805}{539} \cdot V_{\text{out}} - \frac{5679110}{365981} \tag{2.46}$$

Data Logger
The performance specification of the ADC-16 high-resolution logger is shown in table 2.6, where the input signals can be in the range $\pm$2.5V, and is sampled in millivolts.

Table 2.6: Performance specification of ADC-16

Description	Value
Sample resolution	13 bits to 16 bits
Accuracy	$\pm$0.2%
Number of inputs	8 single-ended and 4 differential
Output voltage references	$\pm$5V and 2.5V
Linearity	0.003% (max.)
Input voltage range	$\pm$2.5V
Input impedance	1MΩ
Input connector	D25 female
Output connector	D9 male to PC serial port

The ICL7611 [68], low-power operational amplifier (opamp) from Maxim Integrated Products is configured as a voltage follower to provide a low impedance input to the ADC-16. Since the maximum voltage of the BQ25504 EVM is set to around 3V, a scale factor of $\frac{5}{6}$ is used to scale the input signal. Figure 2.23 shows the schematic and circuit diagram of the voltage follower and the voltage divider. The ADC-16 connects to a computer over the serial port, and the PicoLog data acquisition software installed, is then used to store the sampled data.

The output voltage, V_{out}, is given by equation (2.47), where R_1 and R_2 form the voltage divider.

$$\begin{aligned} V_{\text{out}} &= V_{\text{in}} \cdot \frac{R_2 \cdot R_{\text{in}}}{R_2 \cdot R_{\text{in}} + R_1 \cdot (R_2 + R_{\text{in}})} \qquad \text{where} \begin{cases} R_1 & \text{is in ohm} \\ R_2 & \text{is in ohm} \end{cases} \\ &= V_{\text{in}} \cdot \frac{1\text{M}\Omega \cdot 1\text{M}\Omega}{1\text{M}\Omega \cdot 1\text{M}\Omega + 100\text{k}\Omega \cdot (1\text{M}\Omega + 1\text{M}\Omega)} \end{aligned}$$

$$V_{\text{out}} = \frac{5}{6} \cdot V_{\text{in}} \tag{2.47}$$

2.4.2 Measurement Metrics and Rationale

The signals measured in the experiment are shown in figure 2.24. The compiled data was gathered using the PicoLog data acquisition software, and saved in a plain text file for analysis.

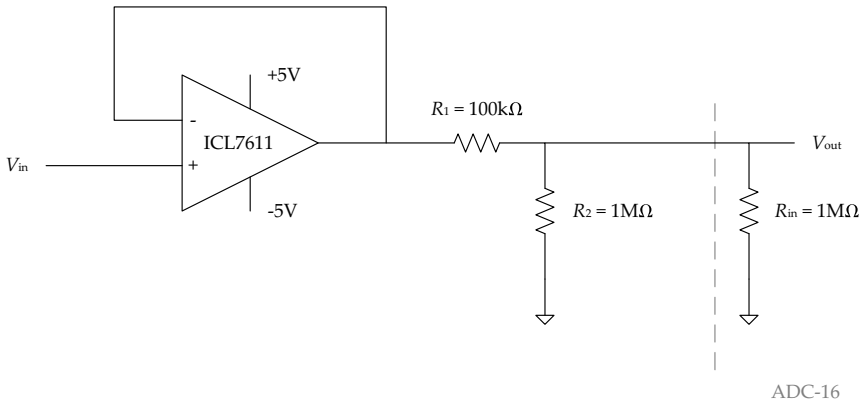

(a) Schematic diagram

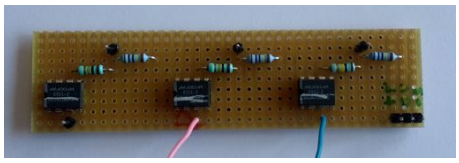

(b) Circuit

Figure 2.23: ICL7611 voltage follower and divider

TGP voltage
The closed-circuit voltage across the TGP, V_{TGP}, was measured with the parameters described in table 2.7, where the sample measured, S, is in millivolt. Since the voltage across the TGP is relatively small compared to the other measurements, it was scaled by a factor of 10.

Table 2.7: Parameters for the TGP voltage

Name	$10 \cdot V_{\text{TGP}}$
Resolution	13 bits
Conversion time	78ms
Scaling	$10 \cdot \frac{S}{1000}$

This measurement can be used to verify the validity of the harvester model. It can also be used to verify whether the TGP performs as described in the datasheet. Furthermore, the voltage generated by the TGP can be used to calculate the amount of power, P_{in}, delivered to the BQ25504 EVM using equation (2.33).

System and battery voltage
The output voltage of the BQ25504 EVM available to the system, V_{SYS}, was measured, along

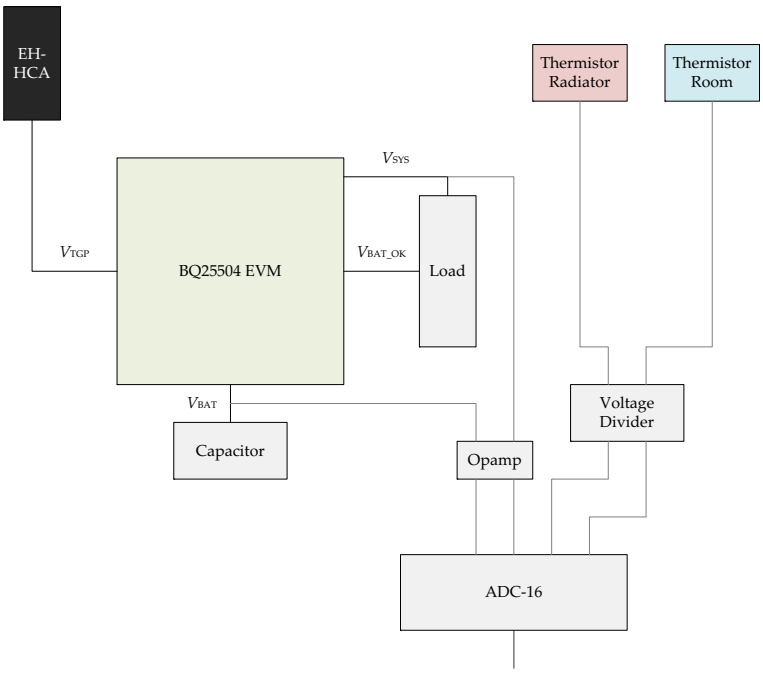
EH-
HCA
Thermistor
Radiator
Thermistor
Room
V_{SYS}
V_{TGP}
BQ25504 EVM
V_{BAT_OK}
Load
V_{BAT}
Capacitor
Opamp
Voltage
Divider
ADC-16

used to convert the voltage measured into temperature.

Table 2.9: Parameters for the radiator and room temperature

Name	T_{radiator}, T_{room}
Resolution	14 bits
Conversion time	151ms
Scaling	$\frac{18805}{539} \cdot \frac{S}{1000} - \frac{5679110}{365981}$

The temperature difference between the temperature on the surface of the radiator and the room, ΔT, was found using equation (2.23). The measured temperatures were also used to calculate the temperature gradient across the TGP using equation (2.30), and validate the model.

2.4.3 Methodology

The experiment was conducted in the temperature-controlled room over a time period of 22 hours. To represent a LST radiator, the temperature on the surface of the radiator was varied approximately between 30°C to 40°C, while the room temperature was maintained at around 20°C, giving a temperature difference approximately ranging between 10K to 20K. The experiment is also conducted in three phases, initially with a low temperature difference, then the temperature difference is allowed to further decrease to a unsustainable level, finally the temperature difference is increased significantly. The second phase is used to observe the impact of insufficient heat on the radiator, where the surface temperature drops below the level at which the BQ25504 EVM is able to operate. Furthermore, the experiment was carried out several times, to ensure that the results did not vary significantly. To reach the conclusions, a final data set was selected and analysed using MATLAB.

2.5 Results

A plot of all the measurement data gathered is shown in figure 2.25, where the closed-circuit voltage across the TGP is scaled by a factor of 10.

As the harvester converts heat energy into electrical energy, the BQ25504 EVM converts this power into a stable system voltage, charging the capacitor. As the rising system and battery voltage crosses the $V_{\text{BAT\_OK}}^{\text{rising}}$ level, the power OK indicator, $V_{\text{BAT\_OK}}$, toggles high activating the n-channel MOSFET, which then grounds the load resistor, discharging the capacitor. When the capacitor is discharging, the system and battery voltage decreases, and as it crosses the $V_{\text{BAT\_OK}}^{\text{falling}}$ level, the power OK indicator toggles lows disconnecting the load. If there is power available for harvesting, the system and battery voltage rises once again. This process continues until the temperature gradient across the harvester drops below a level where not enough power is available to the BQ25504 EVM to operate. If the amount of harvested power is insufficient for the EH system, the system voltage gradually drops. The battery voltage is disconnected from the system voltage when it crosses the V_{UV} level, preventing a deep discharge of the energy storage device. At this stage, the system is completely shut down, and no power is delivered to the load. If the temperature gradient increases once again, the BQ25504 EVM undergoes a cold-start. This startup level is higher than the minimum input voltage supported when the device is operational.

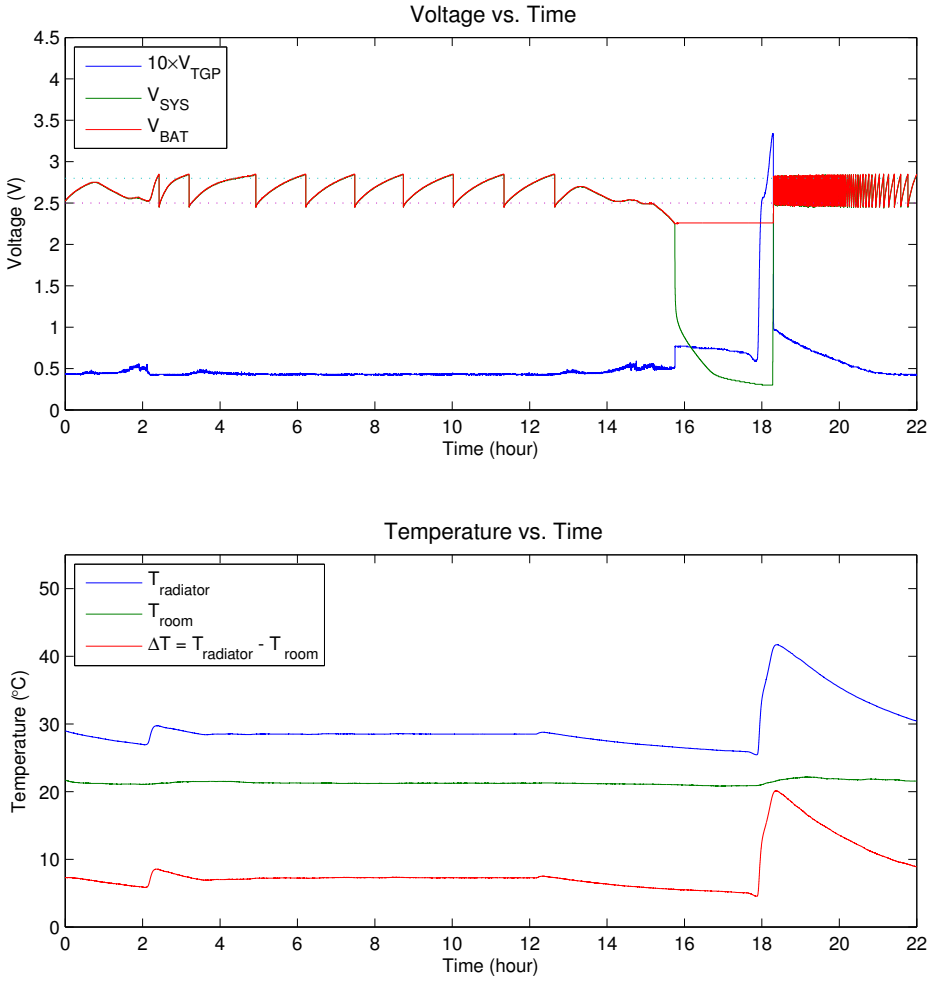

Figure 2.25: Measured values

Figure 2.26 and 2.27 shows a closeup of the period when the temperature gradient across the harvester is low and high respectively. It can be seen that a large temperature difference provides much more energy for the power conditioner, in contrast to the low energy available when the temperature difference is small.

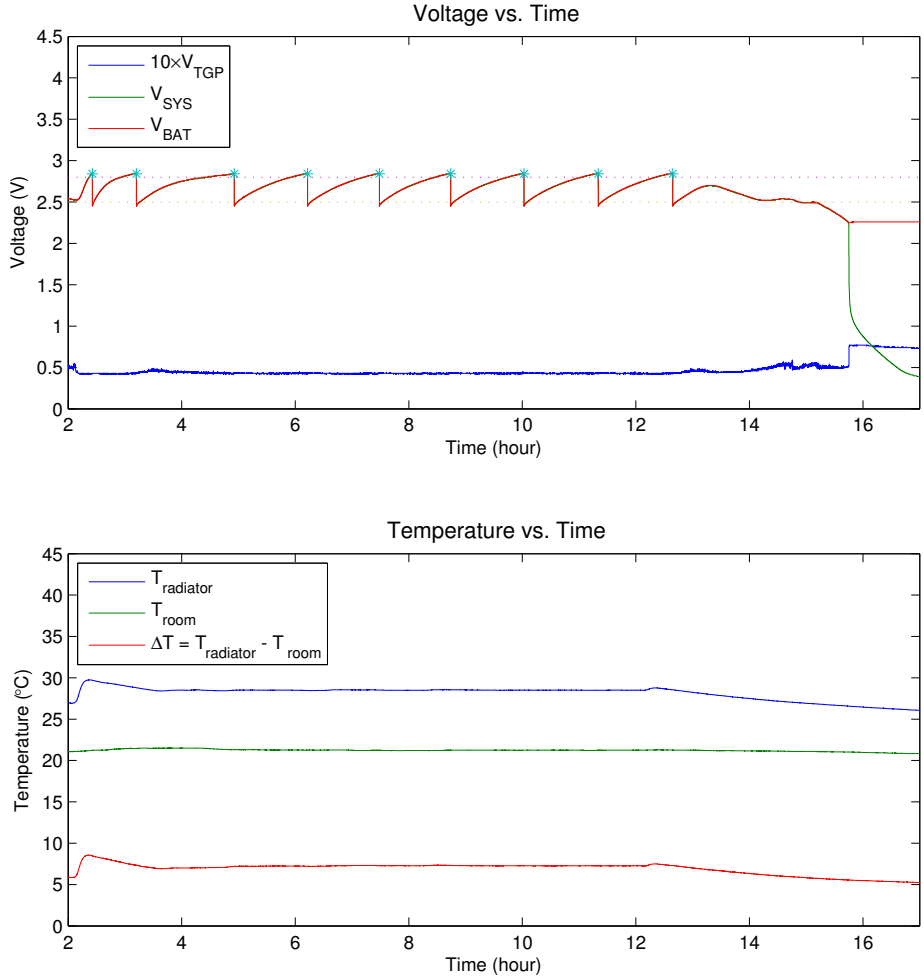

Figure 2.26: Period when a low amount of energy is harvested

2.5.1 Comparison

The measurements can be used to validate the results obtained from the model of the harvester. Figure 2.28 shows a plot of the results from the model and data from the measurements.

The data shown in figure 2.28a can be separated into a period when the BQ25504 EVM

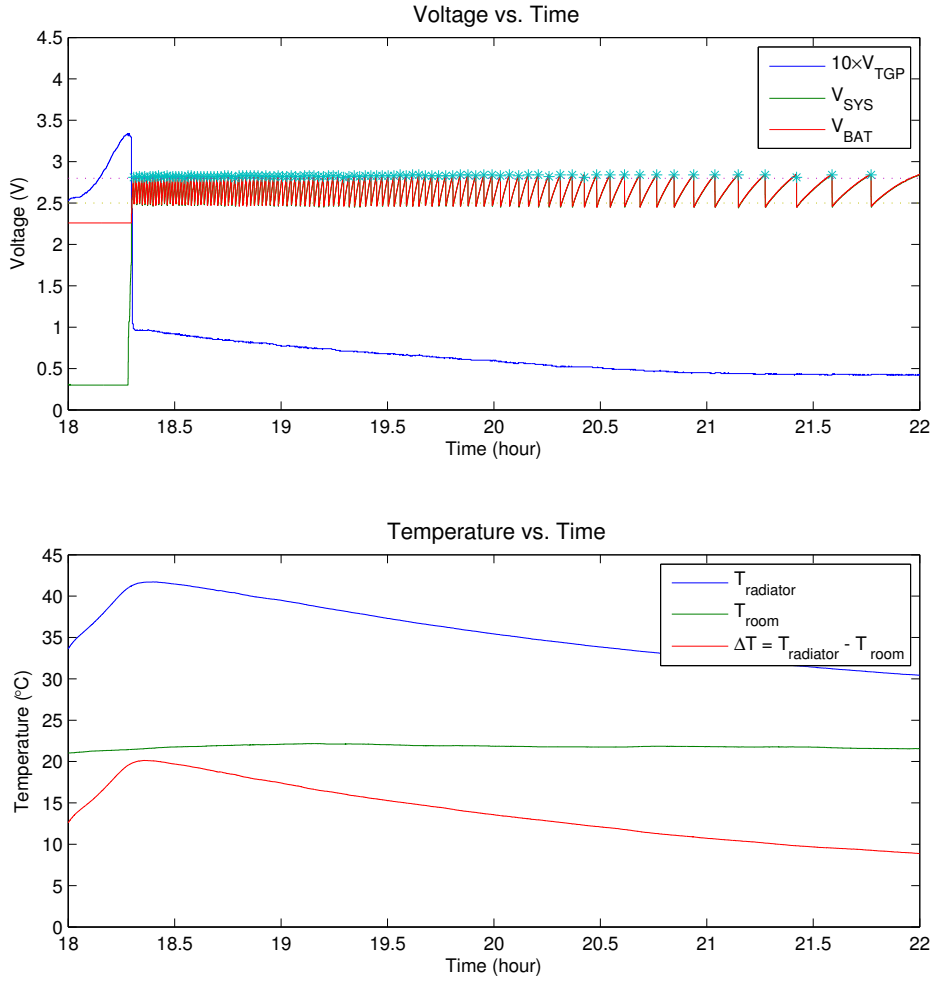

Figure 2.27: Period when a high amount of energy is harvested

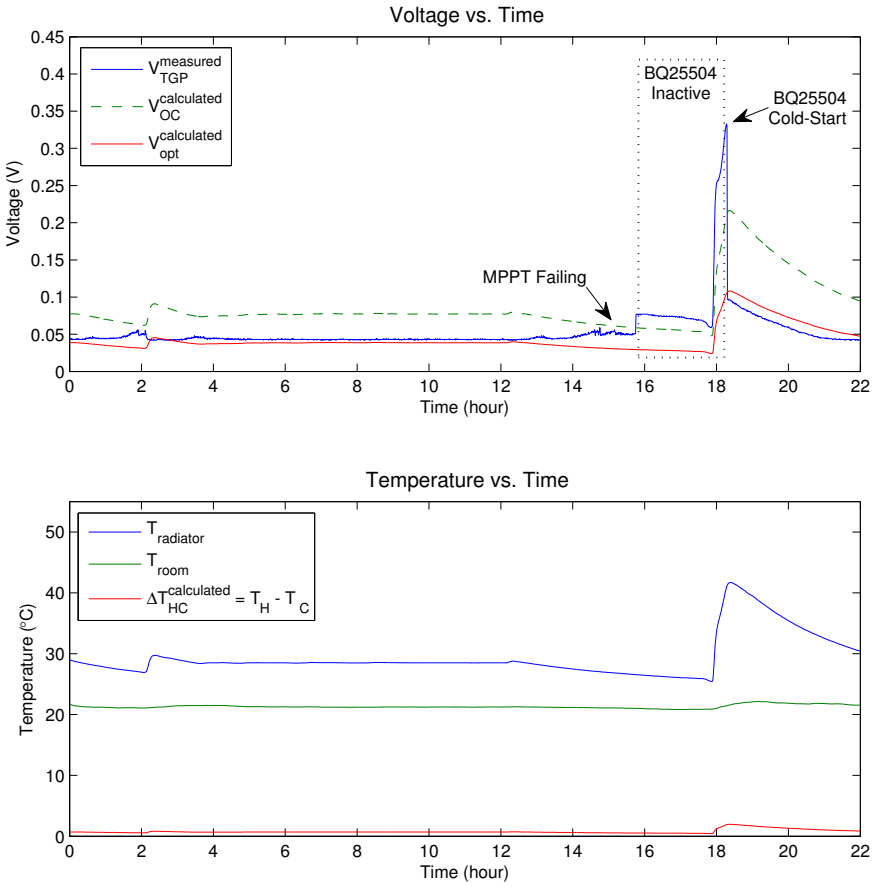

(a) Output voltage of the TGP-751 over time

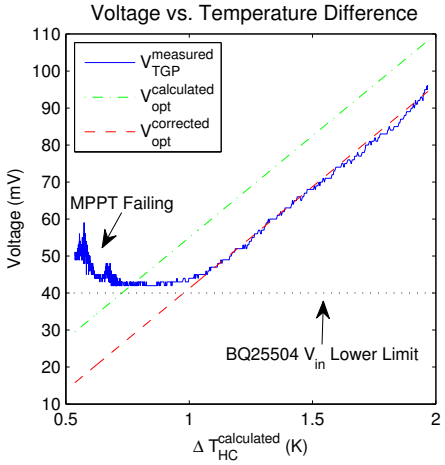

(b) Output voltage over a temperature range across the TGP-751 in the active period

Figure 2.28: Measured voltage (V_{TGP}) compared to the calculated voltage (V_{opt}) of the TGP-751 with MPPT

is active and when it is inactive. In the active period, the power conditioner has undergone a cold-start and is converting the harvested power. During this period, while the calculated closed-circuit voltage, $V_{\text{opt}}^{\text{calculated}}$, closely follows the measured voltage, $V_{\text{TGP}}^{\text{measured}}$, there seems to be a small error. In the inactive period, the power conditioner is not operational, and this error seems to increase when a rapid change in the temperature gradient occurs. This could be explained as a result of the steady-state calculation considered in the model. The function of the MPPT system can be seen by comparing the measured voltage between the active and inactive periods of the BQ25504 EVM power conditioner. It is also interesting to notice that the MPPT fails as the temperature gradient across the harvester decreases. This is a result of the BQ25504 EVM sacrificing the state of converting the maximum power to maintain the TGP voltage above the minimum operational level. Furthermore, the measurements reassure the validity of the information described in the datasheet of the BQ25504, such as the input voltage range and the startup voltage.

Figure 2.28b shows the measured closed-circuit voltage of the TGP and the calculated result from the model. It clearly shows a constant absolute error in the calculated closed-circuit voltage. While the relative error would not be significant at higher temperature gradients, the low temperature focus of this study requires the temperature gradient across the TGP, calculated using equation (2.30) of the model, to be modified with an offset of 0.25K, as given by equation (2.48). Furthermore, the MPPT system compensating to maintain the voltage above the lower limit can be clearly seen.

$$\Delta T_{\text{HC}}^{\text{corrected}} = \Delta T_{\text{HC}} - 0.25 \tag{2.48}$$

2.5.2 Empirical Modelling

The power input to the power conditioner, along with its output, which is the average power available, $P_{\text{out}}^{\text{avg}}$, from the EH system is shown in figure 2.29. The input power curve is incorrect below a temperature gradient of 11K between the surface of the radiator and the room, due to the MPPT compensation. Although this affects the efficiency plot, the trend and order of the results above a temperature gradient of 11K are the same as described in the datasheet of the power conditioner.

The power output obtained from the model with the correction applied, is a good fit to the measured data. This also shows the error region below a temperature gradient of 11K. Since the efficiency is not constant over the range of temperature difference, the average power output from the EH system can be obtained with a curve fit as described by equation (2.49), which can be used in emulating EH in nodes as part of an experiment, when deploying tens or hundreds of EH-HCAs are impractical.

$$\boxed{P_{\text{out}}^{\text{fit}} = \frac{0.15}{\Delta T^{-1.45} - 0.006} - 3} \qquad \text{where } \Delta T \in [8, 20] \tag{2.49}$$

It should be noted that this empirically obtained model is only a valid representation for the construction of the harvester presented in this study, within the specified temperature gradient.

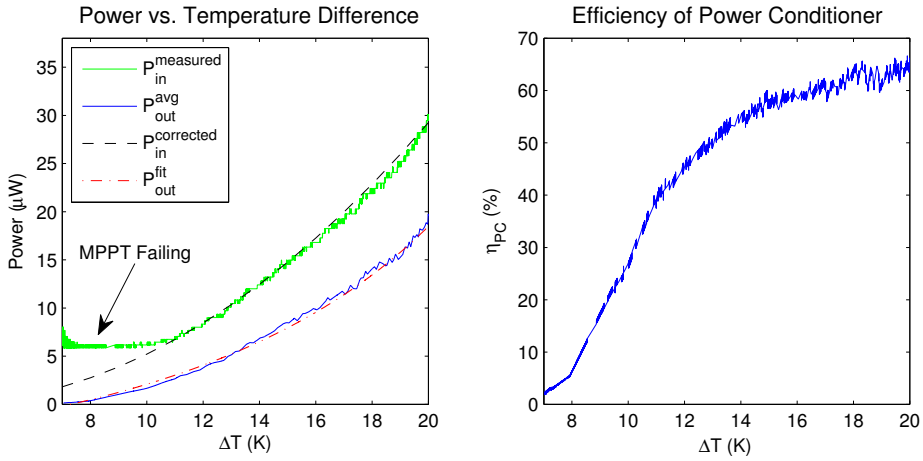

Figure 2.29: Power converted by the BQ25504

2.6 Summary

A prototype of an EH-HCA was designed with a complete thermal EH system using new manufacturable materials and state-of-the-art electronic components. An ideal thermal model of the mechanical construction was used to determine the feasibility of the prototype before implementation, while an experiment was designed to determine the feasibility of practically harvesting thermal energy. In cooperation with an industrial partner, a suitable battery was identified for field deployment, although an electrolytic capacitor was used for its simplicity in the experiment.

The experiment was conducted over a time period of 22 hours in a temperature-controlled room. The results obtained from experiment was used to refine the thermal model, which was needed for preliminary feasibility testing. The refined analytical model presented, accurately describes the behaviour of the thermal energy harvester for an EH-HCA, within a temperature gradient of 11K to 20K between the surface of the radiator and the ambient air of room. Furthermore, an empirical model was presented to estimate the amount of power harvested by the EH system. The empirical model shows that approximately 1μW to 20μW can be harvested from the heat of the radiator when the temperature difference between the surface of the radiator and the room is within 8K to 20K respectively. It is further noted that the transient period that occur when the temperature on the surface of the radiator changes, provide the best opportunity to harvest heat energy. This is due to the rapid increase in the temperature difference during the transient period, before settling into a low steady state temperature difference between the surface of the radiator and the room.

A conservative conclusion can be drawn, which states that an EH-HCA can harvest between 1μW to 10μW of power during the heating season for radio communication. Furthermore, the general thermal energy harvesting module used by collectors, can extract between 100μW to 1mW of power from hot water pipes in buildings.

2.7 Further Improvements

The one-dimensional analytical model presented, while being specific to this particular mechanical construction, does not consider any losses. Hence, it can be considered as a best case scenario, and any further theoretical improvement requires modifying the construction of the thermal path.

Since the main means of heat flow is through conduction, it is interesting to note that while the cross sectional area of a component is proportional to the heat flow, it is inversely proportional to the temperature difference. This means that decreasing the cross sectional area would increase the temperature gradient, which in turn would increase the Carnot efficiency and the overall efficiency of the energy conversion, but it also decreases the heat flow, which reduces the amount of actual energy present for the conversion. This indicates that an optimum cross sectional area exists, which should be considered in any future modifications of the mechanical construction, as it is beyond the scope of this study.

The validity of the model should be verified beyond the range of the temperature gradient used in this study. Furthermore, it can be extended to two-dimensions to account for temperature gradients across the thermo-plastic lid, which would allow a better calculation of the optimum area. Also the assumption that no temperature drop occurs between the components in the thermal path, due to losses, should be removed. Furthermore, the impact of solar insolation, which could heat up the surface of the lid, should be examined.

This study is based on the hypothesis that during the winter season, the system load would be able to operate continuously with the energy harvested. However, the thermal energy source present is discontinuous during the other three seasons of a year. Therefore, a study should be conducted at least over a period of one year, to determine the average amount of power harvested from the thermal energy source, and the power consumed by the system, such that this hypothesis can be verified.

Chapter 3

Wireless Sensor Node

This chapter presents an overview of common platforms of sensor nodes used by academia in a testbed. It also describes requirements that are typically found in industrial applications, such as AMI. An explanation of the design for ıota, which is a wireless sensor node platform that supports energy harvesting and emulation, is provided. Finally, ıota is manufactured to be used in a testbed for experiments related to protocol design in EH-WSNs.

3.1 Background

Sensor nodes are resource constrained devices, that process data collected from onboard sensors. Wireless sensor nodes, also known as motes , are sensor nodes that are connected in a network over a wireless medium. Distributed sensing nodes collaborate together to achieve a common objective, such as environment monitoring, by exchanging measurement data with each other.

Since motes are typically deployed in much larger numbers than nodes in a conventional ad-hoc network, they are composed of low-cost components. Most of the applications where motes are deployed, require them to operate autonomously, for a long period of time ranging from months to years. However, motes typically use a battery driven power source, making the energy efficiency of the device a main design challenge. Recent advancements in EH technologies have enabled motes to be designed to also be energy autonomous by scavenging ambient energy from its environment, significantly increasing its operating life-time, which is only limited by the service life of the electronic hardware.

Traditional low-power design techniques are focused on single devices. In contrast, energy-centric design in motes of a WSN is much more complex, since it requires optimising not only a single device, but the energy efficiency of the entire network. To achieve this, energy-awareness needs to be included in all the operations within a WSN, so that a trade-off between power consumption and performance can be found dynamically. This extreme focus on energy efficiency poses several system and network design challenges that needs to be overcome, in order to deploy a sustainable WSN.

Figure 3.1 shows the main components of a typical wireless sensor node. It is composed of four main subsystems, the computing subsystem, the communication subsystem, the sensing subsystem, and the power supply subsystem.

The computing subsystem consists of a microcontroller unit (MCU) with internal or external memory. Typically a microcontroller is used in embedded systems because of its low-cost, low-power consumption, and the ease of programming, where as a general purpose

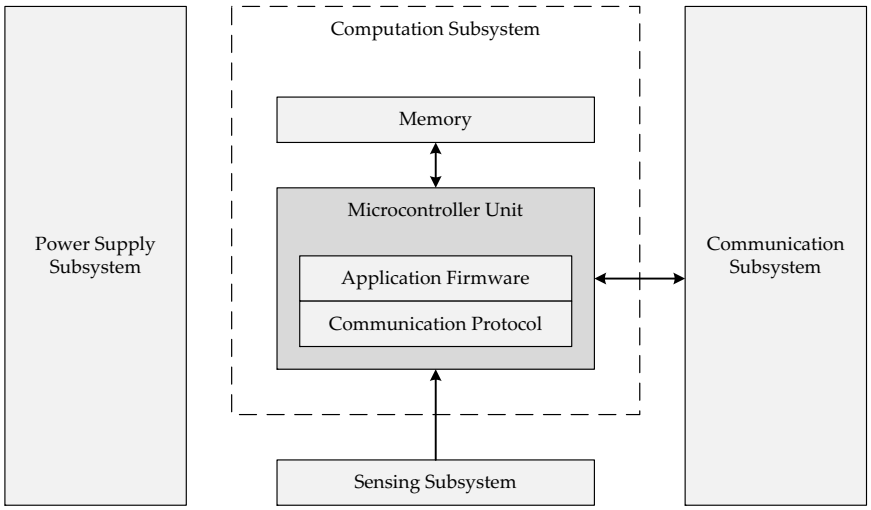

Figure 3.1: System architecture of a canonical wireless sensor node

microprocessor has significantly higher power consumption and programming overhead. The microcontroller performs all tasks required by the mote, such as controlling the sensors, executing the communication protocols, and processing the data gathered from the sensors. The choice of the MCU in a mote is primarily dictated by its power dissipation characteristics, while required performance levels are a secondary criterion. The optimal trade-off between the two parameters heavily depends on the application scenario. Modern MCUs provide various operating modes, such as active, idle, and sleep modes, for power management. Furthermore, Dynamic Voltage Scaling (DVS) and Dynamic Frequency Scaling (DFS) , which allows the core voltage and frequency to be adjusted, respectively, can be used to manage the power consumption of the MCU.

The memory requirements are very much application dependant. Memory use can be categorised into two types: program memory, is the memory space used by the firmware of the mote; user application memory, is used to store application related data. For applications with low memory requirements, internal volatile Random Access Memory (RAM) or non-volatile FLASH memory is used, where as, for high memory requirements, external non-volatile Electrically Erasable Programmable Read-Only Memory (EEPROM) is used. In FLASH memory, fairly large blocks of data must be erased before they can be rewritten with new data, where each block has a write endurance of about 10 thousand cycles. In contrast, EEPROM memory supports byte access, where each byte has a write endurance of about 1 million cycles. Therefore, the memory access controller should ideally support wear levelling to prolong the service life of the device, by ensuring that access to all blocks or bytes is uniform.

The communication subsystem consists of a radio transceiver and other expansion ports, such as Universal Serial Bus (USB) or Universal Asynchronous Receiver / Transmitter (UART) . Typically, the radio transceiver is based on the free ISM frequency band, where the functionality of both the transmitter and the receiver are combined into a single device.

There are several factors affecting the power consumption characteristics of a radio, such as the modulation scheme, data rate, carrier frequency, transmission power, and the operational duty cycle. Transceivers often define several operating modes, such as transmit, receiver, idle, and sleep modes, where the use of these modes are dictated by the communication protocol. Few transceivers define an extra low-power listening mode, but the power consumption during this state is almost equal to the power consumed in the receive mode [69]. Thus it is desirable to completely shutdown the transceiver instead of entering into a low-power listening mode, when not transmitting or receiving data. Expansion ports are optionally introduced to add new functionality in the future, or to be used during debugging of the design. Furthermore, ports such as USB can even be used to provide power to the mote.

The sensing subsystem is dependant on the application scenario. Typically, it consists of several hardware devices that translate physical phenomena, such as temperature or light intensity, into electrical signals. Sensors could either contain an internal Analog-to-Digital Convertor (ADC) , which provides a digital interface to the MCU, or provide an analog signal directly to the MCU. There are several sources of power consumption in a sensor, such as signal sampling and conversion to electrical signals, signal conditioning, and optionally an ADC. Generally, sensors consume much less power relative to the rest of the components in a mote.

The power supply subsystem can consist of multiple power sources, such as primary or secondary batteries, capacitors, or an EH system. It is responsible for dynamically regulating the power consumption of the system, by shutting down parts of the mote after they have completed their task. The Dynamic Power Manager (DPM) also varies the operating modes of the MCU depending on the non-deterministic workload, while using DVS and DFS to obtain a near optimum power consumption characteristic of the mote.

A summary of the technical specification of most common mote platforms that are used in a WSN testbed for experimental research by academia is shown in table 3.1, while a more comprehensive survey can be found in [70,71]. Since existing mote platforms do not fulfill the requirements of the application scenario at Brunata, a new mote platform is designed and manufactured in this study.

3.2 IOTA

The Information Over The Air (*ıota*) mote is a complete wireless sensor node designed to support the evaluation of various EH systems, while providing the use of a primary battery. *ıota* is designed with standard components that is used at Brunata, so that the cost is kept at a reasonable level and it can be easily industrialised when the need arises. The basic design of *ıota* reflects both a sensor node (meter/sender) and gateway node (receiver/collector). Although the GPRS connection used by a gateway node is not included in the basic design, expansion slots are provided to quickly integrate such extra devices. Since Brunata uses FSK modulation in the free 433.92MHz ISM band, *ıota* is also required to operate with this modulation and frequency. Furthermore, the antenna connector used in *ıota* is required to easily support both a cable and an antenna, so that different experiments can be performed where the effects of the channel are both ignored and considered.

Table 3.1: Summary of popular mote platforms [72,73]

	BTnode3	**MICA2**	**TelosB**
Research institution	ETH Zurich	Crossbow	UC Berkeley
Active mode current (Maximum)	91mA	55mA	24.8mA
Sleep mode current (Maximum)	9mA	18μA	6.1μA
Microcontroller	8-bit Atmel ATmega128L AVR	8-bit Atmel ATmega128L AVR	16-bit Texas Instruments MSP430
Clock	32 kHz, 7.3728MHz	7.37MHz	8MHz
RAM (kB)	64+180	4	10+16
ROM (kB)	128	128	48
Storage (kB)	4	512	1024
Radio transceiver	Chipcon CC1000 ISM	Chipcon CC1000 ISM	Chipcon CC2420 IEEE 802.15.4
Frequency band	300MHz to 1000MHz	300MHz to 1000MHz	2.4GHz
Bit rate	38.4kbps	38.4kbps	250kbps
Power	Dual AA batteries	Dual AA batteries	Dual AA batteries
PC connector	External programming board	External programming board	USB
Sensors	External	External	Hamamatsu S1087 light intensity, Sensirion SHT11 humidity and temperature
Expansion connector	40 pin + 15 pin	51 pin	None
Extras	Zeevo ZV4002 Bluetooth 2.4GHz	None	None

3.2.1 System Design

The system architecture of ɪota is composed of several components as shown in figure 3.2. It consists of a power supply subsystem, communication subsystem, computing subsystem, sensing subsystem, and an optional display subsystem.

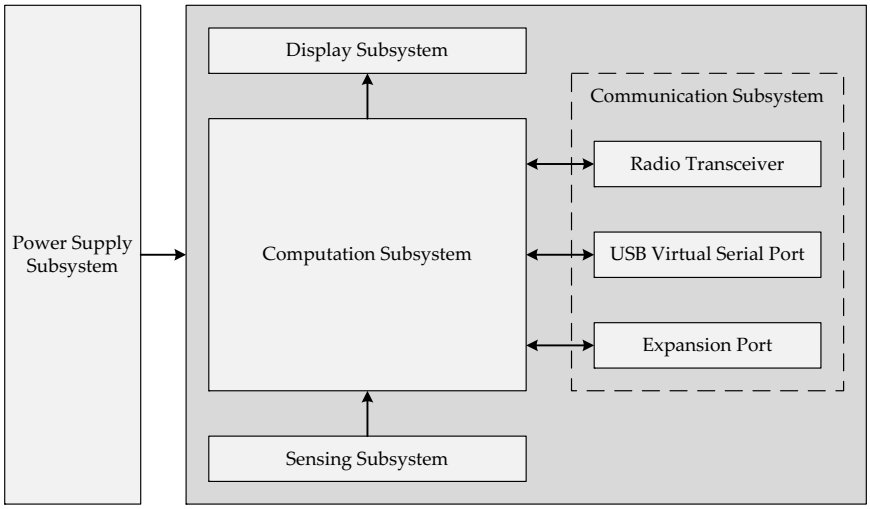

Figure 3.2: System architecture model

3.2.1.1 Power Supply Subsystem

The power supply subsystem of ɪota does not use a DC-DC convertor due to losses, instead supports three protected direct power sources. Since Brunata presently uses primary Li batteries as the main power source, a size AA battery holder is provided to maintain support for such applications. A connector for external power input is provided to support different EH systems. Finally, power via a USB connector is provided as a stable power source. These three power sources can be used to emulate scenarios such as battery powered sensor nodes with a limited energy source, mains powered sensor nodes with an unlimited energy source, EH sensor nodes with an unpredictable energy source, or a combination of them. Although wireless sensor nodes that are deployed, typically do not contain a main on/off power switch, it is included in ɪota to be able to safely store the device without draining the power source, when not in use. Furthermore, the power supply is stabilised with a large electrolytic capacitor to act as an energy buffer for the peak currents drawn by the radio transceiver during operation.

3.2.1.2 Communication Subsystem

The communication subsystem consists of the mandatory radio transceiver, and an optional USB virtual serial port and expansion ports. The radio chosen in this study is the SX1212 ultra low-power integrated 300-510MHz transceiver from Semtech [74], which is

the only radio transceiver with a receive power consumption of 3mA and a single-ended RF output available in the industry. Table 3.2 provides a summary of the technical specifications, while figure 3.3 shows a simplified block diagram of the SX1212.

Table 3.2: Technical specification of SX1212

Supply voltage	2.1V to 3.6V
Supply current in sleep mode	100nA to 2μA
Supply current when frequency synthesiser is running	1.3mA to 1.7mA
Supply current in receive mode	3mA to 3.5mA
Supply current in transmit mode	25mA to 30mA @ 10dBm
Frequency band	300MHz to 510MHz
Modulation	FSK and OOK
Bit rate (FSK)	$0.78\frac{\text{kb}}{\text{s}}$ to $150\frac{\text{kb}}{\text{s}}$
Frequency deviation (FSK)	33kHz to 200kHz
Crystal oscillator frequency	9MHz to 15MHz
Frequency synthesiser step size	2kHz
Wake up time from sleep mode	1.5ms to 5ms
Wake up time from standby mode	500μs to 800μs
Transmit power	-8.5dBm to +12.5dBm
Transmit power step size	3dBm
Transmitter wake up time when frequency synthesiser is running	120μs to 500μs
Transmitter wake up time from standby	600μs to 900μs
Receiver sensitivity (FSK)	-104dBm @ 434MHz, $25\frac{\text{kb}}{\text{s}}$
Receiver bandwidth	50kHz to 250kHz
Receiver wake up time when frequency synthesiser is running	280μs to 500μs
Receiver wake up time from standby	600μs to 900μs
Maximum RSSI sampling time	$\frac{1}{\text{frequency deviation}}$
RSSI dynamic range from sensitivity level	70dB

The SX1212 is a low-cost single-chip integrated radio transceiver that is optimised for low-power operation. It includes data handling features such as a 64 byte FIFO for data buffering, a packet handler to automatically generate packet headers, a 16 bit Cyclic Redundancy Check (CRC) generator to maintain data integrity, and a Linear Feedback Shift Register (LFSR) to randomise the transmission data similar to DSSS for robustness. All of the RF communication parameters are programmable, maintaining flexibility and allowing dynamic frequency hopping for FHSS implementations.

Since the supply voltage range is large enough, Li based primary batteries can be used to directly power the radio transceiver. The very low current consumption of the SX1212 during all the operational modes are vital to a wireless sensor node. In particular, a typical sleep current of 100nA is essential because motes spend most of the time in this mode. FSK modulation with a high bit rate is also supported. The SX1212 has built-in load capacitors for the crystal oscillator to ease implementation. The communication protocol implemented on *ιota* should take into account the current consumption and time duration of switching operating modes, which could be significant for small transmission data packets. To obtain a reasonable wireless communication range, it is important for the radio

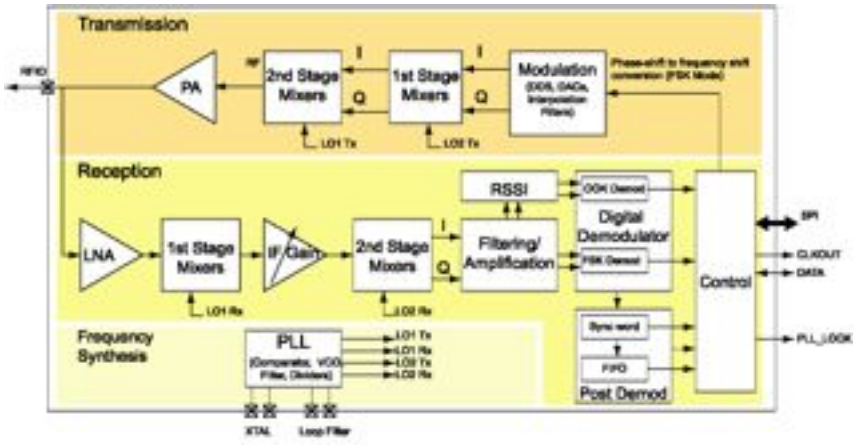

Figure 3.3: Simplified block diagram of SX1212 [74]

transceiver to support a large transmit power output, due to losses in the RF path from the chip to the antenna on the PCB . The Received Signal Strength Indicator (RSSI) on the SX1212 can be used to listen for signals before a transmission is performed. The RSSI can be also used to estimate the transmission range of the sender, although it is not an accurate representation of the physical distance.

The supply voltage of the SX1212 is filtered using an LC pi low-pass filter, to prevent both noise from the rest of the system reaching the electronics of the radio, and noise from the radio from reaching the rest of the system. The RF path is matched to 50Ω and a MEMS based single-ended bandpass Surface Acoustic Wave (SAW) filter is used to prevent unwanted harmonic frequencies from being transmitted, as required by legal regulations. A single SAW filter has two main advantages: it is a cost-effective solution considering the cost involved in mounting several discrete components, and it incurs less losses of the RF signal compared to discrete components.

The FT230X USB to basic UART IC from Future Technology Devices International Ltd. [75], with a micro-AB USB connector is used as the USB virtual serial port. The USB virtual serial port can be used as support for debugging, or provide connectivity for an application software on a computer. The FT230X is chosen for its simple standard UART interface and royalty free driver support for all the major operating systems. The entire USB protocol is handled on-chip with no extra programming required. An internal non-volatile programmable memory is provided to store the USB device descriptors, and configuration settings. Clock generation and power supply filtering is fully integrated within the single chip, thus an external crystal and filter is not required. The FT230X is configured to operate as a USB bus-powered device, and hence does not require power from the power supply subsystem. On the contrary, it includes a 3.3V Low-Dropout (LDO) voltage regulator, which is used to power the rest of the system when the USB is connected. Figure 3.4 shows a block diagram of the FT230X.

The expansion ports provided are the General Purpose Input/Output (GPIO) pins of the MCU, where they can be also configured as a UART port or an Inter-Integrated Circuit (I2C) port.

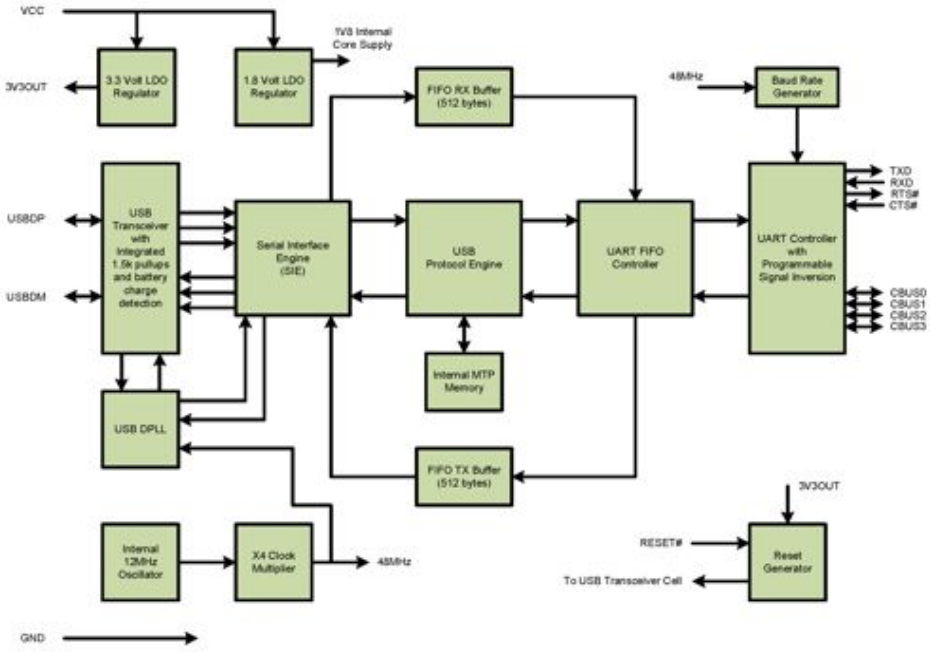

Figure 3.4: Block diagram of FT230X [75]

3.2.1.3 Computing Subsystem

The computing subsystem of *ıota* uses the STM32L162RD ultra low-power 32-bit ARM Cortex-M3 MCU from STMicroelectronics [76]. It is part of the STM32 L1 ultra low-power family of microcontrollers. This MCU uses the 7^{th} generation 32-bit Reduced Instruction Set Computing (RISC) Central Processing Unit (CPU) from ARM Holdings, while adding an extra array of peripherals and features. The STM32L162RD is chosen because of the high performance low-power core that is able to support tasks of both a node and a gateway node. The Cortex Microcontroller Software Interface Standard (CMSIS) defined by ARM provides a vendor independent hardware abstraction layer to speed up application development. Furthermore, the ARM Cortex family of microcontrollers have a rich set of open source tools for application development, that support all the major PC operating systems. Table 3.3 provides a summary of the technical specifications, while figure 3.5 shows the low-power operating modes and an overview of the peripherals on the STM32 L1.

Table 3.3: Technical specification of STM32L162RD

Supply voltage	1.8V to 3.6V
Dynamic core voltage scaling	1.2V, 1.5V, 1.8V
Maximum leakage current per pin	50nA
Maximum core frequency	32MHz
Performance benchmark [77]	$2\frac{\text{CoreMark}}{\text{Mhz}}$
Internal reference voltage	1.2V

The STM32L162RD does not require any external memory, since it has an on-chip EEPROM. If extra memory is required, the internal FLASH memory can be used for application

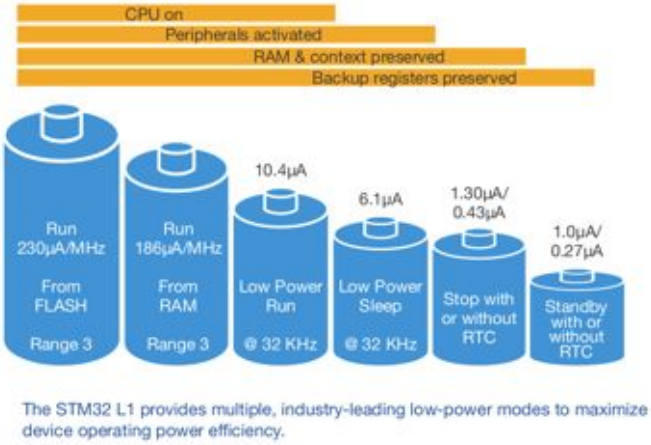

(a) Operating modes

(b) Peripheral overview

Figure 3.5: STM32 L1 family of microcontrollers [78]

data as well, or an external memory can be connected to the expansion port over I2C. The operating range of the supply voltage is large enough to be able run directly from a primary Li battery. An internal reference voltage can be used along with an ADC to measure the supply voltage if necessary. All meters produced at Brunata use a Real-Time Clock (RTC) with an external 32.768kHz crystal to maintain an event log, as well as a Liquid Crystal Display (LCD) to provide the user with measurement information as required by legal regulations. The STM32L162RD has an on-chip RTC and a LCD driver that can be used for this purpose. An on-chip Advanced Encryption Standard (AES) hardware accelerator can be used for experiments related to security in WSNs. An efficient power manager can be designed to utilise the various low-power operating modes, DVS of the core voltage, and DFS using the different internal clock sources. Furthermore, the MCU is factory programmed with a 96 bit unique Identifier (ID) , which can be used to generate a unique MAC address for the node.

3.2.1.4 Sensing Subsystem

The sensing subsystem of *ιota* consists of the SHT25 digital Relative Humidity (RH) and temperature sensor IC from Sensirion [79], which is a fully calibrated single chip device in a small package. The package contains a capacitive RH sensor, band gap temperature sensor, amplifier, ADC, One-Time Programmable (OTP) memory, and a digital processing unit. The SHT25 is a widely used low-power sensor that has good long term stability. It is currently used in the Futura Comfort meter produced by Brunata, and thus chosen as the on-board sensor of *ιota*. The temperature sensor can be used to measure the room temperature, when emulating a thermal EH application, while the RH sensor can be used to emulate a real application scenario, such as the Futura Comfort meter. Table 3.4 provides a summary of the technical specifications of the SHT25.

Table 3.4: Technical specification of SHT25

Supply voltage	2.1V to 3.6V
Supply current when measuring	200μA to 330μA
Supply current in sleep mode	150nA to 400nA
Resolution of the RH measurement	8 bit or 12 bit
Accuracy tolerance of the RH measurement	$\pm$2% to $\pm$4%
Operating range of the RH measurement	0 to 100%
Long term drift of the RH measurement	$< 0.5\frac{\%}{\text{year}}$
Resolution of the temperature measurement	12 bit or 14 bit
Accuracy tolerance of the temperature measurement	$\pm$0.4% to $\pm$1.4%
Operating range of the temperature measurement	-40°C to +125°C
Long term drift of the temperature measurement	$< 0.04\frac{^\circ\text{C}}{\text{year}}$
Communication interface	I2C

The supply voltage range of the sensor is large enough to be directly powered with a primary Li battery. The extremely low sleep mode current consumption of the SHT25 is vital for nodes that spend most of its time in this mode. The high resolution and accuracy of the sensor is beneficial when emulating real application scenarios dependant on these parameters, while the standard I2C interface provides easy access to the measurement data.

3.2.1.5 Display Subsystem

The Futura range of meters produced by Brunata has an LCD as required by legal regulations of the HCA. Hence, the same display is chosen to be optionally mounted on *ıota* to resemble a meter produced by Brunata. The LCD peripheral on the MCU can be used to generate the waveforms required to drive the display. Table 3.5 shows a summary of the technical specifications, while figure 3.6 shows a diagram of the LCD used by Brunata.

Table 3.5: Technical specification of LCD

Supply voltage	2.5V $\pm$1V
Duty	$\frac{1}{3}$
Bias	$\frac{1}{2}$
7 segments	5
Radix	2
Icons	8
Minimum lifetime	100,000 hours

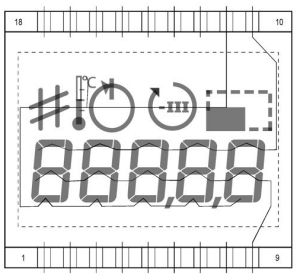

Figure 3.6: LCD used in meters produced by Brunata

3.2.2 Hardware Implementation

The hardware implementation of *ıota* was performed using Altium Designer. A right-angled Sub-Miniature version A (SMA) connector was used in the RF front-end to ensure that the mote can support both an antenna and a coaxial cable. This helps when emulating a scenario with or without channel effects. Test points for all the main communication tracks were included to ease the debugging process. Two jumper shunts are introduced, one to measure the power consumption of the SX1212 radio transceiver, and another to measure the power consumption of the entire system. This can be used to accurately measure the power consumption of a communication protocol, both on the radio and the entire system. Figure 3.7 shows a 3D view of the designed device and the actual manufactured device, where the optional LCD is not mounted on the manufactured device.

3.2.2.1 Schematic Design

A simplified top-level system schematic is shown in figure 3.8 with all the main components. The power supply provides power to the entire system. The LCD is connected to the

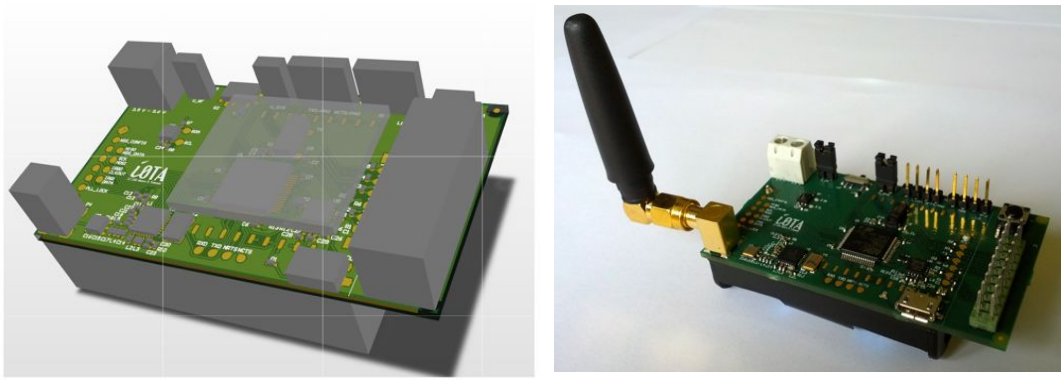

(a) 3D view

(b) Actual implementation

Figure 3.7: *ıota* wireless sensor node

driver in the STM32L162RD with 15 segment lines and 3 common lines. The SX1212 radio transceiver is connected over a Serial Peripheral Interface (SPI) bus, while the FT230X USB virtual serial port is connected over a UART interface, and the humidity and temperature sensor SHT25 connects over an I2C interface, to the STM32L162RD. The expansion port can be configured either as GPIOs, a UART interface, or an I2C interface.

3.2.2.2 Layout Design

A four layer PCB is chosen for *ıota* due to the compact size as shown in figure 3.9. Inspired by other mote designs, all the components are placed on the top, while the battery holders are placed on the bottom such that the two battery holders form stable feet for *ıota*. The electrolytic capacitor is placed within a AA battery holder, next to the AA Li battery holder. The RF trace was routed with impedance control to match the standard 50Ω. The standard ARM Joint Test Action Group (JTAG) connector, which is used for programming and debugging the STM32L162RD microcontroller is placed on right of the PCB. When a bootloader for the MCU is ready and tested, this connector can be removed, further reducing the size of the PCB. A bed-of-nails fixture can be used on the exposed test points of the JTAG connector in case more debugging of the firmware is required.

3.3 Summary

As existing motes does not provide the flexibility required by a mote for an EH-WSN, a new wireless sensor node, known as *ıota*, is designed and manufactured as a state-of-the-art testbed for research on EH-WSN. Table 3.6 summarises the specifications of the new mote. *ıota* can be used to perform experiments on EH-WSNs, battery powered WSNs, mains powered WSNs, or a combination of them. It also provides a high performance MCU along with an ultra low-power radio transceiver for implementing advanced communication protocols and sensing applications. The USB virtual serial port provides easy connectivity to a PC, for use by an application software such as a protocol sniffer. The jumper shunts on the PCB of *ıota* can be used to accurately measure the power consumption of both the radio and the entire system, while the mote can be either used in a wired or wireless network to consider or ignore channel effects.

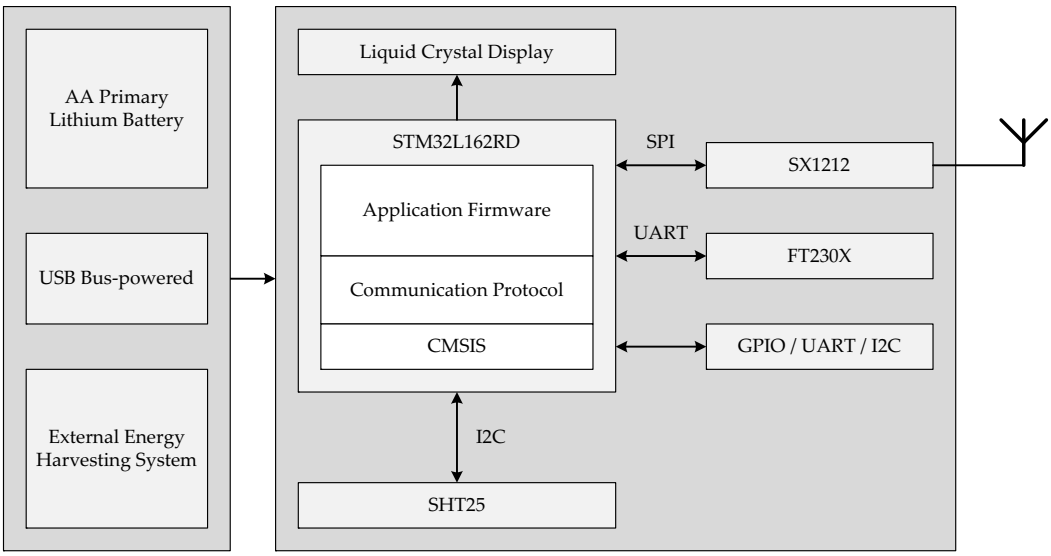

Figure 3.8: Top-level system schematic

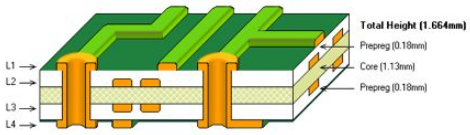

(a) PCB layer stackup

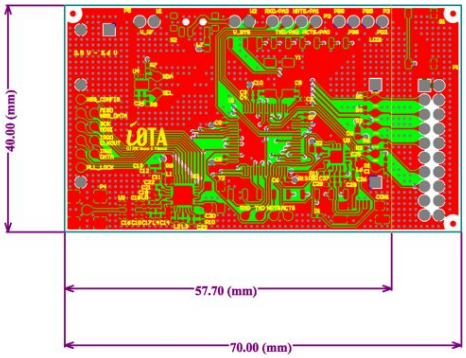

(b) Top view of the layout

Figure 3.9: Layout of *ιota*

Table 3.6: Summary of the *ιota* wireless sensor node

	ιota
Maximum active mode current	43mA @ +10 dBm
Maximum sleep mode current	10μA (with RTC + LCD)
Microcontroller	STMicroelectronics STM32L162RD
Clock	32.768kHz, 32MHz (Maximum)
RAM (kB)	48
ROM (kB)	384
Storage (kB)	12+384
Radio	Semtech SX1212 ISM
Frequency band	300MHz to 510MHz
Bit rate	$0.78\frac{\text{kb}}{\text{s}}$ to $150\frac{\text{kb}}{\text{s}}$
Power	Single 3.6V AA primary lithium battery, USB bus-powered, External power input
PC connector	USB
Sensors	Sensirion SHT25 humidity and temperature
Expansion connector	8 pin
Extras	LCD

3.4 Further Improvements

The BQ25504 power conditioner should be integrated into the PCB of *ιota*. The BQ25504 should be configurable with jumper shunts, so that it can support multiple energy harvesters. A secondary rechargeable battery should be included to complete the EH system, while allowing the use of an optional primary AA battery. All the through-hole components on the PCB should be replaced with surface-mounted components, that can be reflow soldered.

A free software toolchain should be established to speed up the development of application firmware. Furthermore, a compact bootloader should be designed to allow new application firmware to be uploaded via the USB virtual serial port.

Chapter 4

Media Access Control

This chapter describes the results of the literature survey of MAC schemes designed for WSNs, ending with a general overview of all the schemes examined. Then a qualitative analysis of receiver-initiated MAC schemes, along with a mathematical analysis of MAC schemes suitable for EH-WSNs is presented. A sketch of a novel collision avoidance scheme known as Collision Avoidance with Opportunistic Data Aggregation (CAODA) is proposed. The chapter concludes with a comparison to the MAC scheme used by Brunata, and a summary of the analysis.

4.1 Background

The medium access controller (MAC) of the data-link layer plays a key role in wireless sensor networks. It is primarily responsible for the establishment of communication links between nodes, vital to form the network infrastructure. Then the MAC scheme regulates access to the shared wireless channel. Certain additional features such as automatic re-transmissions and error correction may also be included in the MAC scheme.

In contrast to conventional networks where Quality of Service (QoS) and bandwidth efficiency are considered the main priority, energy efficiency remains the primary objective of a EH-WSN, rendering traditional MAC schemes inapplicable.

Since the radio communication of a sensor node consumes the highest amount of power, the main method of conserving power is to duty cycle the node. This is accomplished by alternating the node between active and sleep states, where the node is operational in the active state and shut down in the sleep state. In a contention-based MAC scheme this poses a particular problem of deciding the rendezvous point between a sender and receiver so that a communication link can be established. As shown in figure 4.1, contention-based MAC schemes take a synchronous or asynchronous approach to solve this problem.

4.1.1 Synchronous

In synchronous schemes, nodes organise the active and sleep states to overlap each other, as shown in figure 4.2. A portion of the active state is used to synchronise all the nodes to a global active/sleep schedule. When a source node has data to transmit, it waits until the active state to initiate the data transfer. Unlike contention-free schemes, synchronous schemes are more tolerant to schedule misalignment, however, it still requires a globally synchronised schedule.

A few schemes using this concept are:

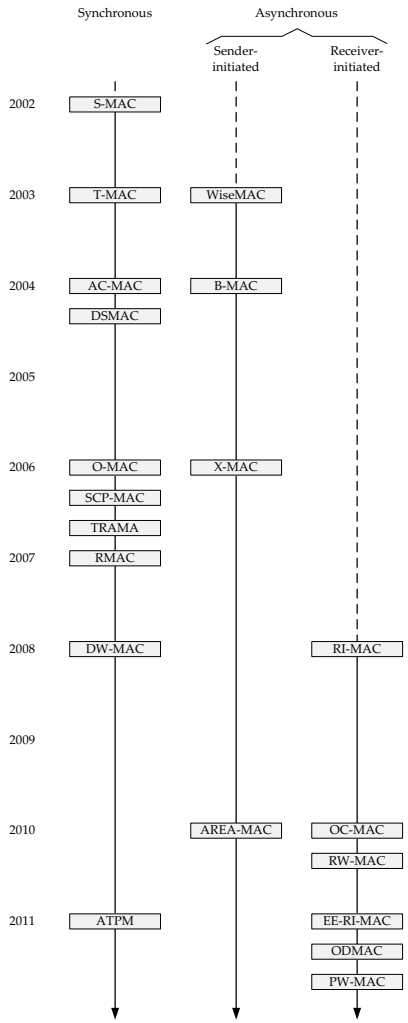

Figure 4.1: Chronology of contention-based media access schemes

- Sensor MAC (**S-MAC**) , was a major milestone in synchronous schemes, where neighbouring nodes align their active and sleep phases, forming virtual clusters with independent fixed schedules [80]. The active phase is divided into the *listen for synchronising* and *listen for handshaking* portions, where a source node coordinates the data transfer with a receiver and, if necessary, continues into the sleep phase for the transmission. Those nodes on the border of two clusters superimpose both the schedules of the two clusters.

- Timeout MAC (**T-MAC**) , introduces adaptive duty cycling into S-MAC, where a node in the active state prematurely goes to sleep if nothing is received, varying the active state, reducing power consumption [81].

- Adaptive Coordinated MAC (**AC-MAC**) , improves upon S-MAC using the adaptive duty cycling concept used by T-MAC [82]. However, unlike T-MAC, where a node

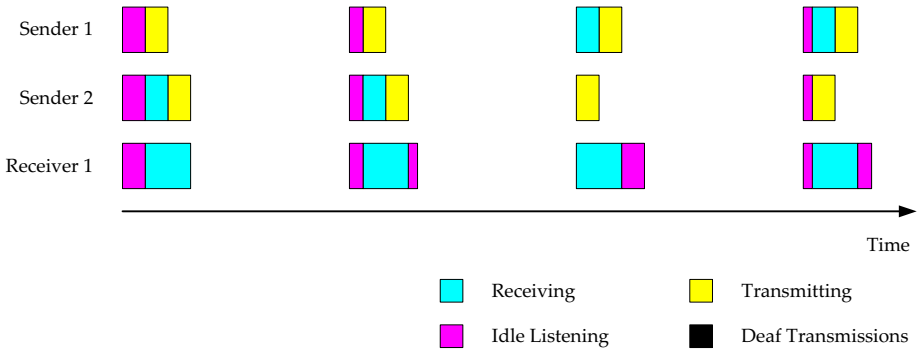

Figure 4.2: Timing diagram of the synchronous approach

suffers from the *early sleeping* problem when a neighbouring node has data to transfer after the node has gone to sleep, within the active period, AC-MAC divides the active state into two sub regions, where the node alternates between an active and sleep state. This provides two chances of communication within a single cycle.

- Dynamic Sensor MAC (**DSMAC**) , uses an adaptive duty cycle technique, where all nodes in a virtual cluster use a base duty cycle like in S-MAC, but can reduce its sleep period by half if a lower latency is required [83]. Synchronisation is maintained by sharing the schedule information, so that neighbouring nodes can choose to either adopt the new duty cycle, or communicate using the base duty cycle.
- Staggered On MAC (**O-MAC**) , takes a receiver centric approach on the assumption that the receiver would be the dominant user of energy in future transceiver architectures [84]. Hence, the concept of *staggered on* receivers is proposed, where the active state of receivers are temporally distributed, such that no two receivers can hear from a sender at the same time. After a classification of MAC schemes, O-MAC presents a careful analytical study, including analysing the efficiency of the relationship between the message generation rate and the receiver duty cycle, on which the new protocol is based. It attempts to predict the wake-up time of the receiver so as to synchronise the communication, and uses a pseudo-random staggered scheduler to define the wake-up slot of a receiver within a frame.
- Scheduled Channel Polling MAC (**SCP-MAC**) , is designed for ultra-low duty cycles ($< 0.1\%$) [85]. As in S-MAC, receivers have a very short synchronised active period, and the senders use a short preamble to indicate that it has data to transmit. Unlike S-MAC, once such communication is initiated, the receiver reduces the sleep period, and listens to the channel more frequently to reduce the latency of a bursty data stream, returning to the ultra-low duty cycle when the channel is idle.
- Traffic-Adaptive Medium Access protocol (**TRAMA**) , divides time into two slotted sections within a frame, the random access section and the scheduled section [86]. The duration of the sections depend on the traffic and network conditions. The random access slots are used for small control messages, so that nodes are able to learn the two-hop topology of their neighbours, while the scheduled slots with no contention are used for longer data messages. All nodes are synchronised so that they

are active during the control period, and during the final data slot of each neighbour.

- Routing Enhanced MAC (**RMAC**) , is based on S-MAC, with the exception that RMAC can deliver a data packet multiple hops within a single operational cycle [87]. This is accomplished by having a large enough synchronised active state where a control message travels across the full forwarding path and establishes a schedule, such that during the sleep state, all the nodes along the path can consecutively enter the active state to pass along the data.

- Demand Wake-up MAC (**DW-MAC**) , is optimised for bursty and high traffic loads [88]. It improves upon the weaknesses of RMAC, where collisions are likely to occur due to hidden sources, as a source node always starts transmitting a data packet at the beginning of the sleep period. DW-MAC includes the destination address in the control message and uses a simple proportional mapping scheme to schedule the wake-up of nodes during the sleep period.

- Adaptive Transmit Power MAC (**ATPM**) , is an improvement of the power consumption of S-MAC by reducing the transmission power for nodes that are closer to each other [89]. ATPM uses the control messages, which are transmitted at full power, to estimate the distance between two nodes. By sampling the received signal on one node, ATPM determines the minimum transmission power required for transferring data to the other node.

Advantages: The inherent synchronicity of these MAC schemes, allows the support of all of the types of communication patterns required by an EH-WSN. It also has the possibility of operating over a single channel and extending into a multi-hop topology.

Disadvantages: However, these MAC schemes fundamentally require a notion of a globally synchronous clock, which creates an additional overhead for EH-WSN. This coupling of nodes via a global clock also hinders a node's ability to have a fully independent duty cycle. Furthermore, from an energy perspective, the size of a virtual cluster and handling of border nodes are not trivial issues.

4.1.2 Asynchronous

Studies of asynchronous schemes have demonstrated its energy saving capabilities [90, 91], it is therefore desirable to explore these possibilities. Asynchronous schemes decouple the duty cycles of the nodes, allowing them to have individual duty cycles, which is essential for an EH-WSN. This leads to the need of techniques on deciding a rendezvous point for nodes to communicate. The Aloha System (**ALOHA**) [92, 93], was one of the earliest asynchronous schemes, where a node transmitted data as soon as it was ready, and if a collision occurred then the node retried at a later point in time. Brunata uses a simplified version of this approach, called the Inter-Meter Reading + (**IMR**+) protocol, using hardware consisting of only a transmitter, where a node transmits data periodically with randomised channel access to avoid collisions. The receiver does not duty cycle, remaining in a constant active state listening for incoming transmissions. This approach consumes an excessive amount of energy waiting for transmissions (idle listening) and is not optimal for use in an EH-WSN. As techniques using CSMA was introduced, asynchronous schemes evolved into two general approaches, the sender-initiated and receiver-initiated schemes.

4.1.2.1 Sender-Initiated

The basic technique used in a sender-initiated asynchronous MAC scheme is called preamble sampling, where the sender transmits a preamble to indicate that there is a pending need for communication. The receiver wakes up occasionally into the active state, to listen to such a preamble transmission. Once the preamble is detected, the receiver replies with a positive acknowledgement to the sender when the preamble transmission stops. As shown in figure 4.3, this establishes a communication link between the sender and receiver.

A thorough survey of sender-initiated schemes is performed in [94], concluding with a guideline to select MAC schemes for a given application. Some schemes applicable to the topology in this study are:

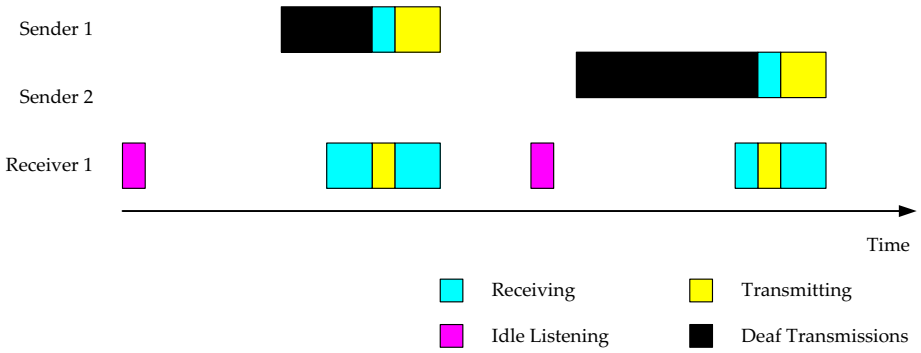

Figure 4.3: Timing diagram of the preamble sampling approach

- Wireless Sensor MAC (**WiseMAC**) , is based on the preamble sampling technique, where all the nodes follow a static duty cycle [95, 96]. The sender always initiates the communication, where the first communication between two nodes uses a long preamble lasting at least the period of the receiver. The receiver duty cycles between the active and sleep state, while listening to the channel to check if it is busy during the active state. If a preamble is detected, then the receiver listens until a data frame is received and replies with an acknowledgement, otherwise it goes back to the sleep. The acknowledgement contains information regarding the remaining time until the next active state, and is used by the sender to initiate a preamble transmission just before the receiver wakes up. WiseMAC introduces this novel concept of learning the duty cycle of the neighbours to minimize the preamble length by predicting the wake up time of a receiver.

- Berkley MAC (**B-MAC**) , uses the conventional preamble sampling approach with a long preamble lasting for at least the duty cycle period of a receiver [90]. In contrast to other schemes, B-MAC provides the core MAC functionality, such as carrier sensing, backoffs, and acknowledgements, with a set of interfaces allowing upper layer services to optimise the performance, rather than enforcing any particular policy.

- Short Preamble MAC (**X-MAC**) , uses a short strobed preamble to further improve upon the weaknesses of B-MAC [97]. In the conventional preamble sampling approach, a receiver has to remain active until the end of the long preamble, even if

it has woken up at the start of the preamble. Also, nodes that are unintentionally woken up, due to overhearing the preamble, waste energy until it realises that the communication was not intended for it. X-MAC embeds the address of the intended receiver in the short preamble so that any unintentionally woken up nodes can go back to sleep immediately, reducing energy waste and potential collisions. A series of short preambles are transmitted by the sender with pauses in between, so that a receiver can interrupt the series with an acknowledgement, decreasing the length of the preamble. It also introduces an adaptive algorithm to dynamically adjust the receiver duty cycles to optimize for varying traffic load in the network. A variant of X-MAC is implemented in the TinyOS embedded operating system [98], called X-MAC Unified Power Management Architecture (**X-MAC-UPMA**) , which transmits a series of data frames instead of short preambles [99]. The receiver simply transmits an acknowledgement as soon as valid data has been received. Presently, X-MAC is the most widely used sender-initiated scheme.

- Asynchronous Real-time Energy-efficient and Adaptive MAC (**AREA-MAC**) , share the same strobed preamble approach, however, in contrast to X-MAC, if a receiver has not replied with an acknowledgement after transmitting the preamble and listening for a reply, the sender in AREA-MAC introduces a short sleep period in between the series of short preambles [100, 101].

Advantages: A major strength of asynchronous schemes is the decoupling of nodes, removing the need for time synchronisation. This also makes the implementation of such schemes simpler. Another property resulting from this decoupling, which is an absolute requirement for EH-WSNs, is the ability for a single node to decide its own duty cycle to utilise the available energy efficiently. Sender-initiated schemes can also operate over a single channel, with support for routing in a multi-hop topology.

Disadvantages: Although broadcast communication can be supported by sender-initiated schemes, due to the presence of independent duty cycles in nodes, this approach performs worse than synchronised schemes. Furthermore, in low duty cycle networks, energy is wasted in the long preamble waiting for the receiver to wake up, and in dense networks, energy is wasted when multiple nodes contend for the same receiver.

4.1.2.2 Receiver-Initiated

In contrast to the preamble sampling technique in sender-initiated schemes, receiver-initiated schemes use a new novel approach to asynchronous communication. Here, instead of long preambles, the sender listens to the channel, waiting for small beacons transmitted by the receiver. The receiver transmits the beacons with an independent duty cycle, and is used by the sender to synchronise with the receiver. As shown in figure 4.4, these beacons essentially provide time slots for communication to take place.

Some receiver-initiated schemes are:

- Receiver-Initiated MAC (**RI-MAC**) , was a major milestone in MAC schemes, as S-MAC was to synchronous schemes and B-MAC was to sender-initiated schemes [23]. It introduced a novel concept of asynchronous communication for single channel multi-hop duty cycling MAC schemes. In RI-MAC, the sender enters the active state and silently listens to the medium until the receiver explicitly signals the start of data transmission with the use of short periodic beacon frames. The duty cycle of the

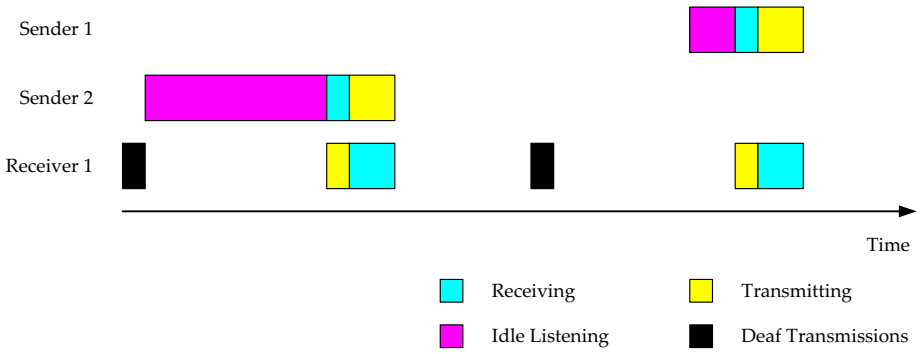

Figure 4.4: Timing diagram of the beaconing approach

receiver is dynamic, in the sense that the sleep period is randomised to prevent unintended synchronisation between nodes. The absence of preamble transmissions occupying the channel, allows for more nodes to exchange data, increasing the throughput. RI-MAC also performs well under a wide range of traffic loads, including light and heavy loads, and bursty traffic.

- Opportunistic Cooperation MAC (**OC-MAC**) , is an extension of RI-MAC, which exploits the opportunistic properties in a asynchronous network [102]. In OC-MAC, neighbouring active senders aggressively exchange data with each other, while waiting for the beacon from a receiver. Once the data is passed onto another waiting sender, a sender can prematurely enter the sleep state, instead of waiting for the receiver. Although this approach only works when multiple senders are active, in a dense network, opportunistic cooperation reduces energy wasted while listening and decreases the end-to-end latency.

- Receiver Wake-up MAC (**RW-MAC**) , is an improvement of RI-MAC [103]. Inspired by WiseMAC, it reduces the time a sender listens for a beacon, by predicting the wake up time of the receiver, piggy backing the remaining wake up interval in the beacon. To minimize collisions, RW-MAC, also staggers the active state of nodes, as in O-MAC.

- Energy-Efficient RI-MAC (**EE-RI-MAC**) , is another approach to improve the energy wasted by the sender while waiting for a beacon in RI-MAC [104]. The concept behind EE-RI-MAC is inspired by AC-MAC, where the sender alternates between the active and sleep state while listening for a beacon. The duration of this active and sleep period within the listening time is shown to be crucial for the performance of this scheme.

- On-Demand MAC (**ODMAC**) , is the first receiver-initiated MAC scheme which is specifically designed for EH applications [32]. It is based upon the concept introduced by RI-MAC and the ENO [25] concept. However, unlike RI-MAC, ODMAC employs dynamic duty cycling [25, 105, 106], specifically for the purpose of regulating the power consumption, where each node can be tuned to minimize the energy consumption and even assign the excess of energy for tasks unrelated to networking,

such as for security. Like O-MAC, ODMAC introduces an important concept of decoupling the sensing period of a sender and the beacon period of a receiver, providing the network administrator with a tool to choose whether energy saving should either favour receiving/relaying or sensing tasks, according to the application requirements [107]. Furthermore, ODMAC incorporates an Opportunistic Forwarding (OF) mechanism, that is beyond the MAC layer, to help decrease the energy wasted on idle listening.

- Predictive Wake-up MAC (**PW-MAC**) , is another scheme that reduces the energy consumption of senders, inspired by WiseMAC [108]. PW-MAC, introduces the use of an independently generated pseudo-random sequence to control the wake up times of each node, allowing senders to accurately predict the time when a receiver will wake up. Furthermore, an on-demand prediction error correction mechanism helps compensate for timing challenges caused by unpredictable hardware, operating system delays, and clock drift.

Advantages: With the receiver-initiated approach, in contrast to the sender-initiated approach, sender preambles are replaced by listening to receiver beacons. Since the beacon length is substantially shorter than a preamble, the channel usage and collisions are reduced. Furthermore, nodes are able to support independent dynamic duty cycles, crucial for EH-WSNs, operate over a single channel, and provide multihop functionality

Disadvantages: The performance of broadcast communication is less efficient than synchronous schemes.

4.2 Evaluation Criteria

The requirements of an EH-WSN is different from conventional wireless networks. For example, energy efficiency is of paramount importance in EH-WSN, where as, throughput and delay would be of high importance in a traditional wireless network. For this reason, it is important to find an optimal compromise between different performance metrics to suit the application.

4.2.1 Energy Efficiency

Collisions occur at the receiver when two or more nodes transmit data at the same time to a single receiver, wasting energy both at the senders and the receiver. In dense networks, collisions pose a significant problem and collision detection or avoidance techniques, such as Clear Channel Assessment (CCA) using carrier sensing, RTS/CTS Handshaking (RCH) , or Random Backoff (RB) mechanisms, should be incorporated into the MAC scheme.

Deaf Transmissions take place when a node is transmitting data and no other node is listening for the reception of the data. The transmitting node is wasting energy on the transmission.

Error Control is specially important for WSNs deployed in noisy environments. There are two general mechanisms employed by MAC schemes for error control, FEC and ARQ. ARQ based techniques use retransmissions to recover lost data, where as FEC

based techniques recode the data with information necessary to reconstruct the original message. While FEC can achieve significant improvements of the BER, it is not a trivial problem to decide whether the additional power consumed due to the overhead and processing are worth it.

Idle Listening happens when a node is in the active state, listening, but not receiving any data. Nodes waiting for incoming data wastes energy, and hence should be minimized.

Overhearing occurs during unicast communication, when a node is listening to the channel, and receives the transmitted data unintentionally. Avoiding overhearing can significantly reduce power consumption.

Protocol Overhead is a result of the control information in the MAC scheme. For example, ready-to-send (RTS) , clear-to-send (CTS) , ready-to-receive (RTR) , clear-to-receive (CTR) , and synchronisation (SYNC) frames use part of the available bandwidth. Furthermore, packet headers and trailers, also increase the overhead, resulting in a decrease in energy efficiency. Therefore, It is important for MAC schemes in WSN to be low in complexity.

4.2.2 Performance

Channel Utilisation reflects how well the full bandwidth of the channel is used by the communications in the network. In conventional wireless networks, such as mobile phone networks, the density of a cell can rapidly change, and bandwidth is a valuable resource. In contrast, the number of nodes in a WSN is dependant on the application, and hence, the channel utilisation is of less importance.

Fairness represents the ability of different nodes to share the channel equally. It is an important consideration in networks such as voice networks, where users desire an equal opportunity to communicate. However, in WSNs, nodes cooperate to fulfill a common objective. For example, in a multi-hop network, nodes acting as relays will have much more data to forward than nodes in the boundary. Therefore, it is desirable to measure the performance of the entire application, instead of a per-node basis.

Latency is the delay from the moment a sender transmits a packet of data, until it successfully arrives at the receiver. It can be specified either as, node-to-node latency, which is the delay of data successfully reaching a neighbouring node from a node, or as, end-to-end latency, which is the delay of data successfully reaching the sink from the source over several hops. The importance of latency varies depending on the application of the WSN.

Reliability in a WSN is the guarantees that the MAC scheme provides with respect to the delivery of data to the intended receiver. For example, it can be specified as the packet delivery ratio of the network, which is the ratio of the sum of the number of data packets received to the sum of the number of data packets sent.

Scalability and robustness refers to the ability of the network to maintain its integrity and functionality upon changes in network size, node density, and topology. For example, a substantial increase in the number of nodes, making the network denser, or a decrease in the number of nodes, making a sparse network, could reduce the network

performance and eventually result in the disintegration of the network. Therefore, a scale-free network is very robust and desirable, since it is able to gracefully accommodate such random additions or failures of nodes.

Throughput is the total amount of data successfully transferred from a sender to a receiver without errors in a given amount of time, typically measured in bits per second. Factors such as collisions, protocol overhead, and channel utilization affect the throughput. Another related measure is *goodput*, the amount of application data, excluding overhead, successfully received without errors over a period of time.

4.3 Assessment

The radio of a wireless sensor is the major component of power consumption. The power consumed can be divided into the Radio Frequency (RF) power that is transmitted and the one required to power the electronics involved in frequency synthesis, frequency converting, mixing, etc. Traditional approaches of Dynamic Voltage Scaling (DVS) or Dynamic Frequency Scaling (DFS) is not a feasible approach for power management in radios, since slowing down the analog electronics could end up consuming more power. Therefore, the primary approach to manage the power consumption is by duty cycling. This means, that the radio alternates between an active state, for communication, and enters a sleep state, where the radio is completely shut down. A major requirement for MAC schemes in EH-WSNs is then the ability to fully independently adjust the duty cycle of an individual node.

The duty cycles of nodes in a synchronous network are tightly or loosely coupled to each other. This limitation excludes synchronous MAC schemes that was previously examined, leaving the possibility of using asynchronous MAC schemes. Within the asynchronous approach, the receiver-initiated scheme is shown to be more energy efficient than the sender-initiated scheme [23, 107] . For this reason, only receiver-initiated schemes will be considered.

Out of the receiver-initiated MAC schemes explored, RI-MAC is the scheme that describes this approach fundamentally. OC-MAC defines an opportunistic policy exploiting certain features of RI-MAC. It acts as a collision avoidance mechanism, increasing the throughput in dense networks. However, although OC-MAC out performs the collision avoidance mechanism defined in RI-MAC, it is not trivial to determine that it is better than other mechanisms proposed in academia. RW-MAC and PW-MAC use prediction algorithms to determine the wake up time of receivers, reducing energy wasted during idle listening. Despite this benefit, both MAC schemes assume a static duty cycle, making it infeasible to use in an EH-WSN. Additionally, due to assumptions [A2] and [A3], it is not feasible to predict the power harvested from the energy source, which is the main parameter determining the duty cycle of a single node. EE-RI-MAC is an interesting solution to the idle listening problem. Nonetheless, the duration of intermediate sleep states is heavily dependent of the specific application, and requires a detailed analytical examination. ODMAC remains the only MAC scheme that has extended the receiver-initiated approach specifically towards EH-WSNs.

Therefore, this study considers ODMAC as the state-of-the-art MAC scheme for EH-WSNs, and will be further analysed. The current MAC scheme used at Brunata, IMR+ , is analysed to explore the benefits of ODMAC. RI-MAC is also analysed to identify the changes introduced by ODMAC. Furthermore, OC-MAC and EE-RI-MAC is assessed to verify its benefits.

An overview of the energy efficient properties of the discussed MAC schemes are shown in table 4.1.

4.3.1 Inter-Meter Reading +

Brunata uses a simplified adaptation of the ALOHA protocol, called IMR+. This scheme only supports a single-hop, single channel network. The sender nodes only contain a radio transmitter, while the receiving gateway node only contains a radio receiver. Both the senders and receiver use a static duty cycle, although, the simplicity of the scheme allows to dynamically adjust the duty cycle of the nodes according to the energy available. Figure 4.5 shows an overview of this approach.

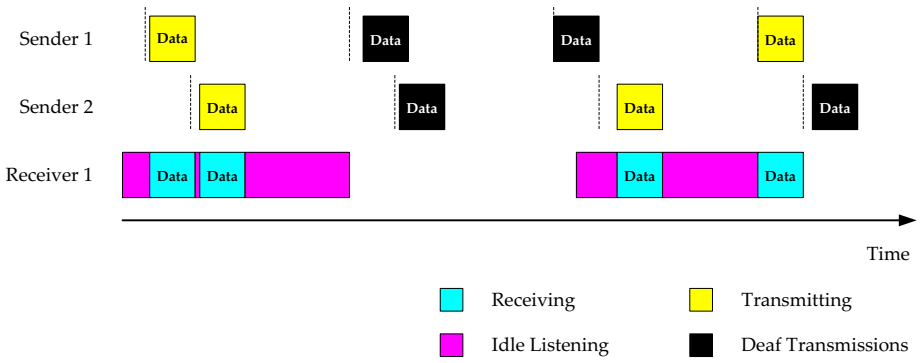

Figure 4.5: Mechanics of inter-meter reading + communication

In IMR+, collisions occur continuously if the duty cycle period of senders happens to be synchronised. To avoid this problem, the transmission is delayed a random amount of time at the beginning of each period. Due to this simple collision avoidance technique, small payload sizes used by Brunata, and ultra-low duty cycling of the senders, the probability that a collision will happen is quite low. Nevertheless, several significant sources of energy waste exist in this simple approach:

- Senders continuously transmit data even though the receiver might be in the sleep state.
- In a sparse network, the receiver might spend most of the active period listening for data, but not receiving any.
- Senders that are within range of more than one gateway node will transmit data to all the receivers.

4.3.2 Receiver-Initiated MAC

In RI-MAC, a node periodically wakes up to check for incoming data. Immediately after waking up, a CCA is performed and a beacon is broadcasted if the channel is idle. If the channel is busy, the node does a backoff and transmits the beacon later. This beacon announces to the neighbours that it is ready to accept incoming data. After the beacon has been transmitted, the receiver continues to listen to the channel for a short period of

Table 4.1: Overview of the energy efficiency attributes of MAC schemes for WSNs

MAC	Collision Avoidance	Deaf Transmissions	Duty Cycling	Error Control	Idle Listening	Overhearing	Protocol Overhead
S-MAC	CCA/RCH/RB	Very low	Static	Not defined	Medium	Medium	Synchronisation
T-MAC	CCA/RCH/RB	Very low	Dynamic	Not defined	Low	Low	Synchronisation
AC-MAC	CCA/RCH/RB	Very low	Static	Not defined	Low	Low	Synchronisation
DSMAC	CCA/RCH/RB	Very low	Dynamic	Not defined	Medium	Medium	Synchronisation
O-MAC	CCA/Staggered on receivers	Very Low	Dynamic	ARQ	Low	Very low	Synchronisation
SCP-MAC	CCA/RCH/RB/ Two-phase contention	Low	Static	ARQ	Low	Low	Synchronisation
TRAMA	CCA/RCH/ Transmission schedule	Very low	Dynamic	ARQ	Low	Low	Synchronisation
RMAC	CCA/RCH/RB	Very low	Static	None	Medium	Low	Synchronisation
DW-MAC	CCA/ Proportional mapping/ RB	Very low	Static	ARQ	Low	Low	Synchronisation
ATPM	CCA/RCH/RB	Very low	Static	Not defined	Medium	Low	Synchronisation
ALOHA	CCA/RB	High	Static	ARQ	High	High	ACK
IMR+	None	High	Static	None	High	High	None
WiseMAC	CCA/ Wake up schedule	Low	Static	Not defined	Low	Low	Preambling
B-MAC	CCA/RB	High	Static	ARQ	Low	High	Preambling
X-MAC	CCA/RB	Medium	Dynamic	Not defined	Low	Low	Preambling
AREA-MAC	CCA	Medium	Dynamic	Not defined	Low	Low	Preambling
RI-MAC	CCA/RB	Low	Static	ARQ	High	Very Low	Beaconing
OC-MAC	CCA/RB/ Opportunistic senders	Low	Static	ARQ	Medium	Very Low	Beaconing
RW-MAC	CCA/RB/ Staggered wake up	Low	Static	ARQ	Low	Very Low	Beaconing
EE-RI-MAC	CCA/RB	Low	Static	ARQ	Medium	Very Low	Beaconing
ODMAC	CCA/RB	Low	Dynamic	Not defined	Medium	Very Low	Beaconing
PW-MAC	CCA/RB/ Prediction-based	Low	Static	ARQ	Low	Very Low	Beaconing

time. A node with data ready to be sent, enters the active state and listens silently to a beacon from the intended receiver. Once the beacon is received, the sender immediately starts transmitting the data, and waits for a time period to receive another beacon which acknowledges (ACK) the reception of the data. If the sender has more data packets to send, it uses this acknowledgement beacon as a RTR indicator, to start transmitting the next data packet. If there is no incoming data from the sender after transmitting the beacon, the receiver enters the sleep state. Then both the sender and receiver, resume the cycle of beacon transmissions. An overview of the communication in RI-MAC is shown in figure 4.6.

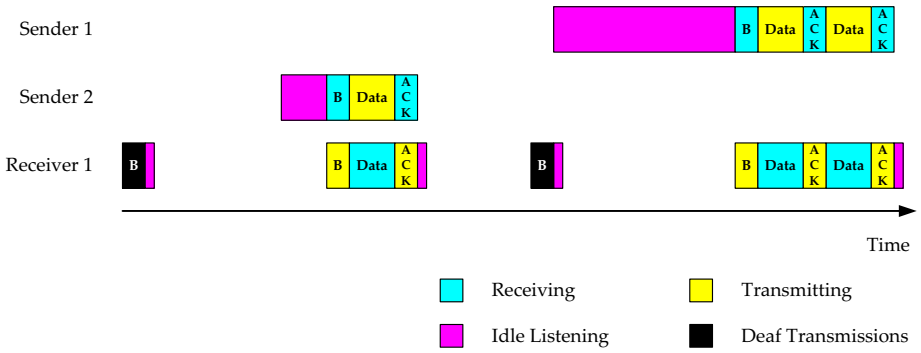

Figure 4.6: Mechanics of RI-MAC communication

The communication mechanism defined by RI-MAC significantly reduces the amount of time a pair of nodes occupy the channel, allowing more contending nodes to communicate with each other, thus increasing the capacity and throughput of the network. RI-MAC is more efficient in detecting collisions and recovering lost data, because access to the channel is mainly controlled by the receiver. Since receivers only wait a short period of time for incoming data, after beacon transmission, overhearing is greatly reduced. All these benefits culminate in a very energy efficient MAC scheme.

4.3.2.1 Beacon Frames

The structure of a beacon frame, is shown in figure 4.7. The base beacon contains mandatory fields that are required for the protocol, while it can be expanded with optional fields. The mandatory fields contain: the hardware preamble, to indicate the start of a transmission and synchronise the radio receiver; the frame length, used to filter and process the frame in the radio receiver; the source address, as an identification of the node that is transmitting the beacon. The optional fields contain: the backoff window size, used as a collision avoidance mechanism; the destination address, used in unicast communication to identify the intended receiver. Apart for these fields, RI-MAC beacons also has the overhead from the IEEE 802.15.4 standard [109] frame format, which it uses as a container in its experiments.

The beacon frame in RI-MAC plays a dual role. It is used both as a RTR, broadcasting the request to initiate data transmission, in essence, creating a time slot for rendezvous, and as an ACK, which informs the sender that the data has been received successfully. The base beacon, with only the mandatory fields, are used in the RTR broadcast, while the optional

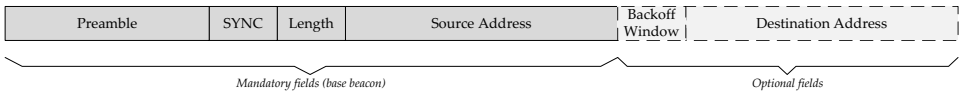

Figure 4.7: Beacon frame structure

destination address field is used in the ACK reply to signify a unicast transmission, so that other nodes waiting for a beacon can ignore it. The frame length field is used by the receiver to differentiate between the types of beacons.

The duty cycle of the beacon transmissions are controlled by varying the sleep state, L, of the node. To prevent coincidental synchronization, a node sets the sleep period randomly between $0.5L$ and $1.5L$, before entering the sleep state. This essentially makes the average duty cycle of RI-MAC static.

4.3.2.2 Collision Detection and Retransmissions

If two or more senders contend for the same base beacon, the data packets will be transmitted simultaneously. The experiments conducted in RI-MAC, has shown that due to the presence of the capture effect in FM radios, also called co-channel interference tolerance, such a contending scenario does not necessarily lead to collisions [110]. This property demonstrates that the traditional assumption that a packet collision always results in data corruption is false.

For this reason, senders in RI-MAC immediately transmits the data upon receiving a base beacon, without any backoff. The receiver listens for a short period of time after transmitting the beacon, known as the dwell time, which is determined by the current backoff window size. Concurrently, it measures the channel power level and processes the bit pattern received. If a valid data frame header is not detected in time, and the measured power level indicates that a transmission is in progress, then, this condition is classified as a collision. Figure 4.8 shows the collision avoidance technique used by RI-MAC.

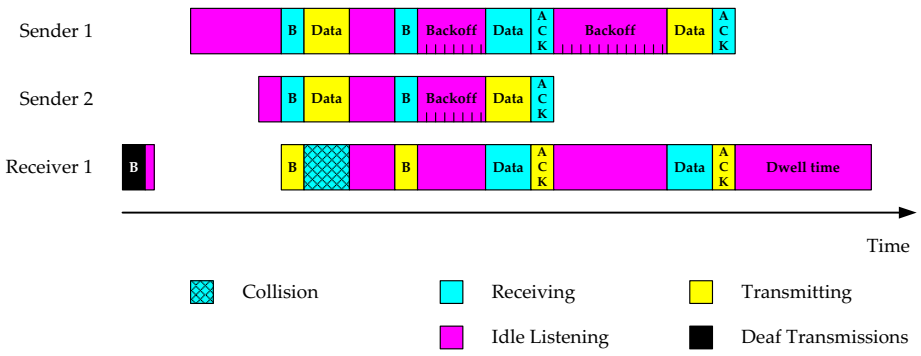

Figure 4.8: Collision avoidance mechanism

If a collision occurs, the receiver performs a CCA, waiting for the channel to be free.

Once a clear channel is determined, the receiver transmits a beacon with a backoff window specified, informing the senders of the failed transmission. The senders, waiting for an ACK use the backoff window specified in the beacon to perform a random backoff. The senders listen to the channel, while waiting for the random period to expire, before retransmitting the data. If a transmission from another sender is detected, the sender withholds the transmission, and waits for an ACK beacon, before resuming with a new random backoff. If a collision happens again, the receiver increments the backoff window using a Binary Exponential Backoff (BEB) strategy [14], until the maximum window size is reached, after which, both the senders and receivers accept a failed transmission and goes back to sleep, retrying at a later point in time.

4.3.2.3 Beacon-on-Request

An optimization to utilize an instance when the intended receiver is already active is defined in RI-MAC, as shown in figure 4.9. After a CCA, a sender that has data to transmit, immediately broadcasts a beacon with a backoff window size specified and the destination address set to the intended receiver. The beacon acts as a RTS indicator, and if the receiver happens to be awake, it replies with a base beacon after a random backoff period. Then data exchange proceeds using the normal RI-MAC communication mechanism.

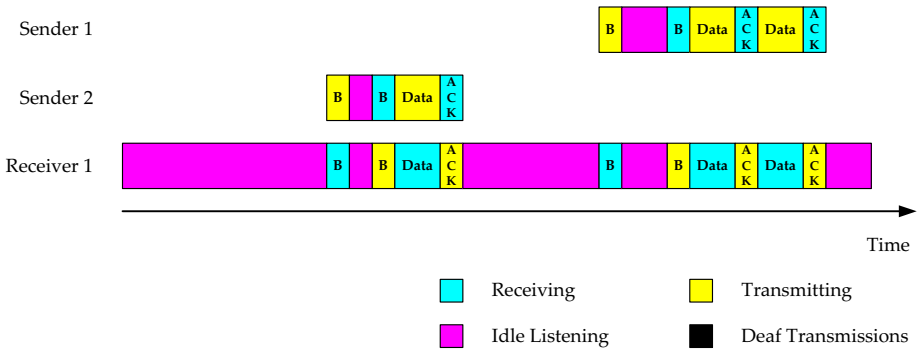

Figure 4.9: Beacon-on-request mechanism

4.3.2.4 Broadcast support

RI-MAC does not describe a mechanism for broadcast communication. After its publication, the authors of RI-MAC described the Asynchronous Duty cycle Broadcasting (**ADB**) protocol for RI-MAC [111], adding this functionality. Since broadcast communication is not used in the topology discussed in this study, ADB will not be further analysed.

4.3.3 Opportunistic Cooperation MAC

In a low duty cycling network, a sender in RI-MAC usually waits for a long period of time before a receiver wakes up and transmits a beacon. This idle listening time is the main cause of energy waste in RI-MAC. OC-MAC extends the beacon-on-request feature defined

in RI-MAC and defines two communication policies for contending and cascading scenarios, which reduce this waiting time. Neighbouring senders in OC-MAC are allowed to exchange data aggressively while waiting for the receiver to wake up. Figure 4.10 provides an overview of the mechanism used in OC-MAC.

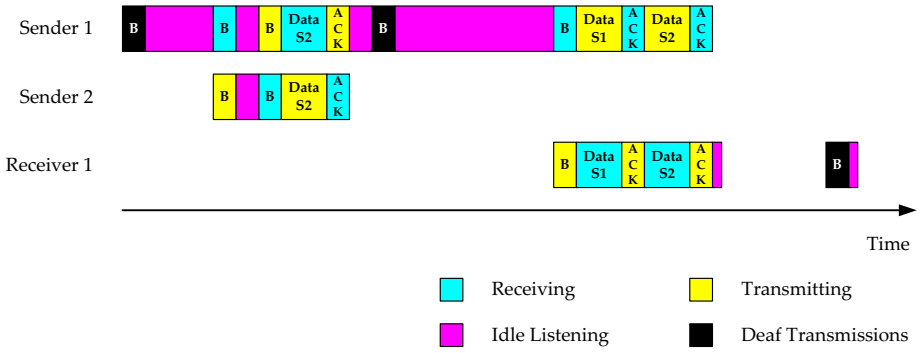

Figure 4.10: Mechanics of OC-MAC communication

Similar to the beacon-on-request feature, when a node has data ready, it transmits a RTS beacon, if the channel is idle. The beacon contains its residual energy, the destination address, and a request for other senders to relay the data. Notice that, in contrast to the beacon-on-request feature of RI-MAC, which is directed towards receivers, the beacon-on-request in OC-MAC is directed only towards senders. By not loading the receivers, this ensures that the channel is not deprived of beacons, which will reduce the throughput of the network. After the beacon is transmitted, the sender listens to the channel for a period of time. If it does not receive a response within this duration, the sender looses its right to cooperative communication and continues to wait silently for a beacon from the receiver or another contending sender.

When an RTS beacon is received by a sender that coincidentally happens to be awake, it compares its residual energy to the contender. The sender ignores the request if the contending sender has more residual energy than itself. If the contender has less residual energy than the sender, it transmits a CTS beacon, similar to the base beacon in RI-MAC, after a random backoff. The backoff prevents collisions, in case multiple senders are active. The rest of the mechanism is similar to the beacon-on-request feature in RI-MAC.

Once the exchange of data is completed, the contending sender enters the sleep state, while the sender which received the data, transmits another RTS beacon to check if any opportunity exists to relay both its own data, and the data from the contending sender. Hence, a sender is only permitted to broadcast a RTS beacon immediately after waking up, or after completing a cooperative communication with a contender.

4.3.3.1 Contending Scenario

Collisions can happen when two or more nodes contend for the same base beacon, increasing the latency and energy usage of the network. OC-MAC defines a policy for this scenario, that helps increase the efficiency of the network.

In OC-MAC, a sender aggressively delegates its data to a contending sender, and goes

to sleep before the receiver wakes ups, reducing the idle listening time. The selected delegator will then be responsible for delivering the data, including its own, to the receiver via another sender or by itself. An overview of this policy is shown in figure 4.11.

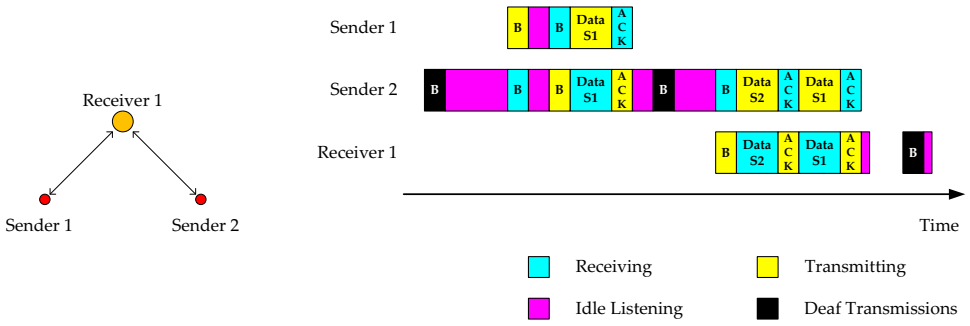

Figure 4.11: Contending nodes

4.3.3.2 Cascading Scenario

Although the topology studied in this thesis does not consider a multi-hop network, the cascading scenario is described for completeness sake.

Nodes in a multi-hop network have dual roles of being a sender and a receiver. Figure 4.12, shows a typical cascading flow in such a network. Here, node 1 is waiting silently for the node 0 to transmit a beacon before exchanging data. After a little while, node 2 wakes up to send data to node 1. In RI-MAC, node 2, has to wait until node 1 completes its communication with node 0 and transmit a beacon in its next cycle. However, OC-MAC allows node 2 to use the beacon-on-request mechanism to transmit its data to node 1 immediately.

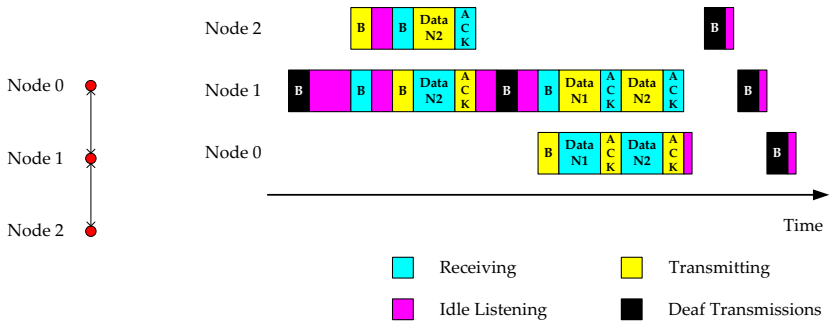

Figure 4.12: Cascaded nodes

4.3.4 Energy Efficient RI-MAC

EE-RI-MAC is an enhancement for RI-MAC, defining another approach to increase the energy efficiency of the senders. In particular, EE-RI-MAC uses a technique inspired by AC-MAC and X-MAC, where, instead of listening for a beacon, a sender alternates between the active state and sleep state within this duration. Figure 4.13 shows an overview of this approach.

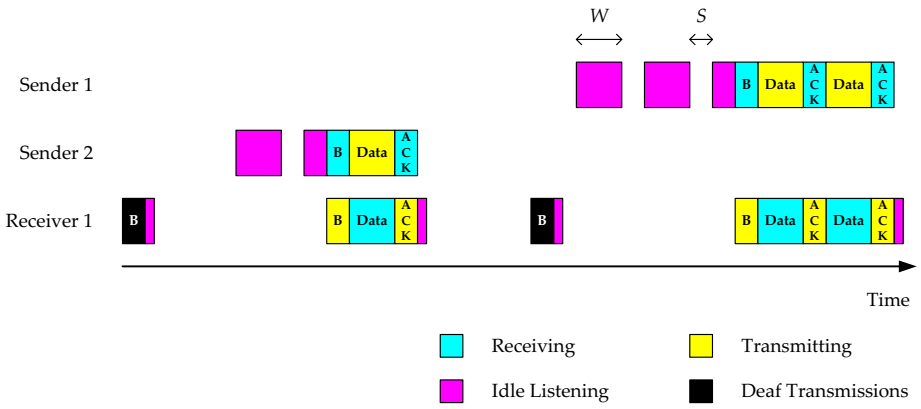

Figure 4.13: Mechanics of EE-RI-MAC communication

In order to further reduce the idle listening period of a sender, it enters the sleep state after listening for a period W, and wakes up after a duration S. The authors of EE-RI-MAC opt to use simulations to determine the optimal duty cycle for alternating between the active and sleep state during the idle listening period. It is found that a duty cycle of 37.5%, resulted in the optimum case, outperforming RI-MAC in terms of energy usage.

However, the simulations are performed on a specific network topology and application, and lack a general analytical solution, therefore EE-RI-MAC remains skeptical. The choice of the value used for the two important parameters, W and S, determines the performance of the scheme. Additionally, even though EE-RI-MAC achieves the same throughput as RI-MAC with higher energy efficiency, the latency of the network suffers.

4.3.5 On-Demand MAC

As the first MAC scheme specifically optimised for an EH-WSN, ODMAC builds upon the foundation of RI-MAC. It exploits the independent duty cycles of nodes to define a policy for dynamically adjusting the duty cycle of each node. Furthermore, for a scenario when more than a single receiver is present, it defines a forwarding policy to determine which receiver to pick.

4.3.5.1 Dynamic Duty Cycling

Since nodes in the network have a dual role of being a receiver for forwarding tasks and sender for measuring tasks, ODMAC decouples the duty cycles of these two roles in a single node. Hence, a node has a beacon duty cycle and a sensing duty cycle. The beacon duty

cycle controls the trade-off between energy consumption and end-to-end delay, while the sensing duty cycle controls the trade-off between energy consumption and measurement rate. An important feature of ODMAC is the ability for a network administrator to decide the trade-offs depending on the application.

ODMAC uses an adaptive duty cycle mechanism based on the ENO principle, where the energy consumed by a node is less than or equal to the amount of energy harvested. All nodes in the network dynamically adjust the beacon and sensing duty cycle, in order to achieve and maintain an ENO-Max state, which is defined as an ENO state with maximum performance. This means that when the node is consuming more energy that is harvested, the duty cycles are decreased to reduce the energy consumption. In the same manner, when the energy consumed is lower than the energy harvested, the duty cycles are increased so that the node is more active.

4.3.5.2 Opportunistic Forwarding

In a scenario with two or more receivers, where one receiver is on a high beacon duty cycle due to the high amount of energy it harvests, a sender has to wait a long time listening to the channel if it wants to exchange data with another receiver. To prevent such a situation from arising, ODMAC defines a forwarding policy based on opportunity.

This mechanism is a network layer policy, that assigns each sender a nontrivial task of maintaining an approved list of receivers. Nonetheless, a simplified OF policy where such an approved list is not used, can be applied in a multi-cluster single-hop network. Instead of waiting for the intended receiver to wake up, a sender opportunistically forwards data after the first beacon it receives. Since the probability of receiving beacons from a receiver with surplus energy is high, this policy creates a more robust network, that is adaptive to changes in energy, by maintaining a balanced load in the network. Furthermore, the idle listening time of senders is reduced in the region where the clusters overlap. Figure 4.14 shows an example of such an opportunistic policy in a multi-cluster network, where as the state of energy of the receivers change, the nodes that are in range of both the receivers adapt to the receiver with more energy.

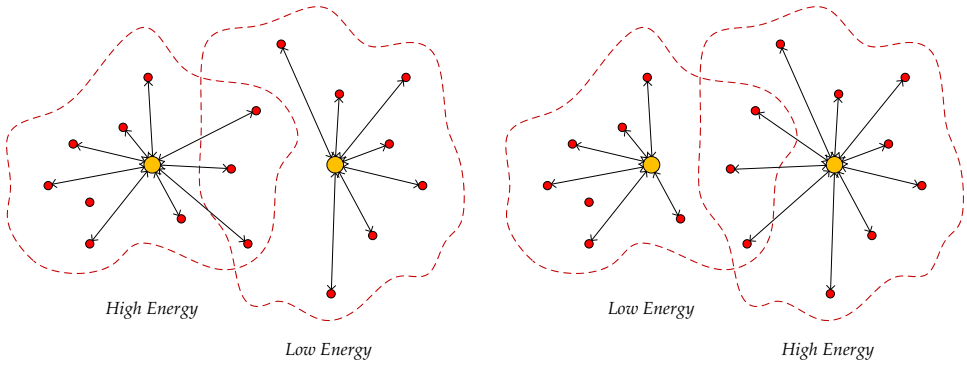

Figure 4.14: Opportunistic forwarding in a multi-cluster network

4.3.6 Summary

The asynchronous MAC schemes based on the receiver-initiated approach was qualitatively analysed. An overview of the analysis is shown in figure 4.15.

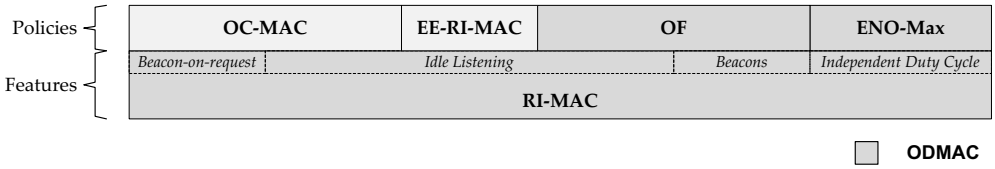

Figure 4.15: Receiver-initiated MAC for EH-WSNs

RI-MAC forms the foundation of the receiver-initiated paradigm, providing features that has been exploited by the other MAC schemes described. OC-MAC defines a policy based on the beacon-on-request feature, promoting aggressive cooperation among senders, which acts both as a collision avoidance mechanism and reduces idle listening. These properties help increase the throughput of the network while saving energy. EE-RI-MAC attempts to reduce idle listening of a sender by introducing an alternating duty cycle when waiting for a receiver. Although this policy has a benefit, it requires further analysis before validation. ODMAC is designed specifically for EH-WSNs and specifies a dynamic duty cycling policy based on the ENO principle. It also decouples the beaconing period from the sensing period, providing a network administrator a mechanism to tune the network to suit a particular application. Furthermore, ODMAC defines an opportunistic policy to forward data when multiple receivers are present.

ODMAC is chosen as the fundamental, and only MAC scheme available for EH-WSNs since it provides all the policies required in an EH-WSN. OC-MAC and EE-RI-MAC provide some interesting benefits for this topology, but this is considered to be beyond the scope of identifying a MAC scheme for EH-WSNs, since it can be quickly adapted into ODMAC.

The metering industry typically uses MAC schemes that are similar to ALOHA, due to the perceived belief that its simplistic nature out performs any other MAC scheme. Hence, a mathematical analysis of IMR+ will also be performed to compare with ODMAC, so that the benefits from ODMAC can be precisely identified.

4.4 Analysis

A mathematical analysis of both IMR+ and ODMAC is presented. Since the models are used to compare IMR+ and ODMAC, the properties of the channel are considered to be the same for both MAC schemes. Therefore, the models do not consider active collision avoidance mechanisms, such as BEB, and retransmissions due to channel errors. Furthermore, nodes are considered to transmit only a single packet within a duty cycle period, and the packet size is considered to be constant for all transmissions over all nodes.

In a single-hop topology, nodes do not relay data to each other. As a result, the model of a MAC scheme can be separated into the sender and receiver in a single cluster. The analysis is based on the available power for senders and receiver from the energy harvesting

system. This means, that the main parameters to the model are the power harvested by a single sender, and the power harvested by the receiver.

As shown in figure 4.16, for a given power budget of the senders and the receiver, the models can be used to determine the feasible measurement period of the senders.

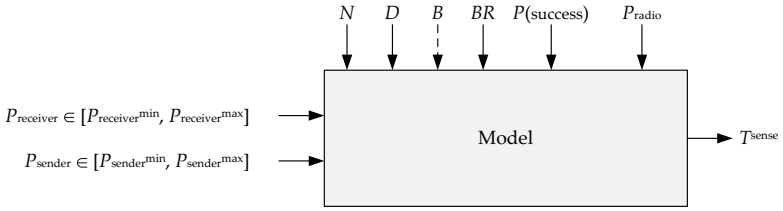

Figure 4.16: Block diagram of the model

4.4.1 Modelling of Inter-Meter Reading +

To analyse the one-way communication of IMR+ scheme, a model is presented, in figure 4.17, followed by a list of notations used in the analysis.

Sender
The duration of a single transmission is the time the channel will be used by a single node and can be expressed by equation (4.1).

$$\tau_{tx} = \frac{D \cdot 8}{BR} \tag{4.1}$$

The duty cycle period of a single packet transmission is inversely proportional to the available power of a sender. Equation (4.2) describes the duty cycle period for a given amount of power available.

$$P_{sender} = \frac{P^{startup} \cdot T^{startup} + P_{tx} \cdot (T_{tx}^{startup} + \tau_{tx})}{T_{tx}} \quad \text{where } P_{sender} \in \left[P_{sender}^{min}, P_{sender}^{max}\right]$$

$$T_{tx} = \frac{P^{startup} \cdot T^{startup} + P_{tx} \cdot (T_{tx}^{startup} + \tau_{tx})}{P_{sender}} \quad \text{where } T_{tx} \in \left[T_{tx}^{min}, T_{tx}^{max}\right] \tag{4.2}$$

$$T_{tx} \propto \frac{1}{P_{sender}}$$

Collisions can occur when two or more nodes transmit at the same point in time. The probability of a collision is dependent on the number of nodes in the cluster, and can be stated by equation (4.3).

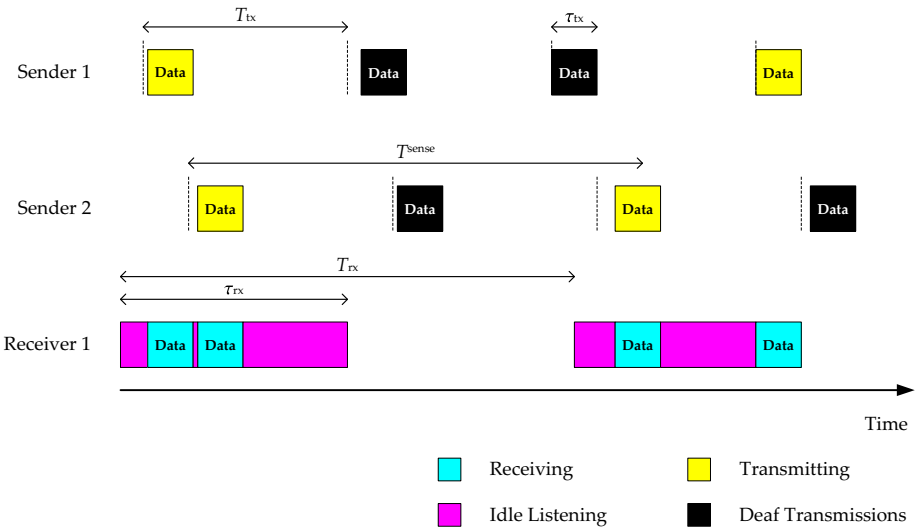

Figure 4.17: Inter-meter reading + model

D	is the packet size, in bytes
BR	is the transmission bit rate, in bits per second
N	is the number of nodes in a single cluster
P^{startup}	is the power consumed by the radio to enter the active state from the sleep state, in watts
T^{startup}	is the time it takes for the radio to enter the active state from the sleep state, in seconds
P_{tx}	is the power consumed by the radio during transmission, in watts
$T_{\text{tx}}^{\text{startup}}$	is the time it takes for the radio to begin transmission, in seconds
P_{sender}	is the power available from the harvesting system of the sender, in watts
τ_{tx}	is the transmission time of a single packet, in seconds
T_{tx}	is the duty cycle period of a single packet transmission, in seconds, which should be always less than the corresponding maximum legal duty cycle limit of the chosen frequency band
$P(\text{collision})$	is the probability that a collision will occur
$P(\text{success})$	is the probability that at least one out of n packets will be successfully delivered, collision-free, to the receiver
n	is the number of transmissions required to achieve the probability, $P(\text{success})$
P_{rx}	is the power consumed by the radio during reception, in watts
$T_{\text{rx}}^{\text{startup}}$	is the time it takes for the radio to enter the receive mode, in seconds
P_{receiver}	is the power available from the harvesting system of the receiver, in watts
τ_{rx}	is the worst case time for which the receiver should be in the active state, listening for incoming packets, to receive at least one valid packet from all the nodes in the cluster, in seconds
T_{rx}	is the duty cycle period of the receiver, in seconds
T^{sense}	is the measurement period of a sender, in seconds
g	*goodput*, is the amount of data successfully received without errors, in bits per second

$$P(\text{collision}) = (N-1) \cdot \frac{\tau_{tx}}{T_{tx}} \tag{4.3}$$

The probability of successfully delivering at least one out of n transmissions can be used to specify a guarantee, or reliability, of the network. The number of transmissions required to guarantee that at least one out of n transmissions is successfully delivered, collision-free, is described by equation (4.4).

$$P(\text{success}) = 1 - P(\text{collision})^n$$

$$n = \left\lceil \frac{\log(1 - P(\text{success}))}{\log(P(\text{collision}))} \right\rceil \tag{4.4}$$

Receiver
Since the receiver cannot communicate information back to the senders, it has to be prepared for the worst case active time. In order to ensure that at least one valid packet is received from all the nodes in the cluster, the receiver should listen to the channel for at least the time specified by equation (4.5), where the worst case duty cycle period of the sender, when is it running on the lowest power level, given by equation (4.2), is considered along with the corresponding number of transmissions required, given by equations (4.3) and (4.4).

$$\tau_{rx} = T_{tx}^{max} \cdot n \tag{4.5}$$

To ensure that the receiver can operate with the available power, the receiver has to duty cycle. The duty cycle period can be calculated using equation (4.6).

$$P_{\text{receiver}} = \frac{P^{\text{startup}} \cdot T^{\text{startup}} + P_{rx} \cdot (T_{rx}^{\text{startup}} + \tau_{rx})}{T_{rx}} \quad \text{where } P_{\text{receiver}} \in \left[P_{\text{receiver}}^{\text{min}}, P_{\text{receiver}}^{\text{max}} \right]$$

$$T_{rx} = \frac{P^{\text{startup}} \cdot T^{\text{startup}} + P_{rx} \cdot (T_{rx}^{\text{startup}} + \tau_{rx})}{P_{\text{receiver}}} \quad \text{where } T_{rx} \in \left[T_{rx}^{\text{min}}, T_{rx}^{\text{max}} \right] \tag{4.6}$$

$$T_{rx} \propto \frac{1}{P_{\text{receiver}}}$$

The sensing period represents how often a new measurement can be made by a node. Since within a single duty cycle period, the receiver has at least one valid packet from all the nodes in the cluster, the sensing period is the same as the duty cycle period of the receiver, expressed by equation (4.7).

$$T^{\text{sense}} = T_{\text{rx}} \tag{4.7}$$

The goodput of the receiver, defined as the amount of new measurements received from all the senders, in the worst case, within a given amount of time, can be calculated from equation (4.8).

$$g = \frac{N \cdot D \cdot 8}{T^{\text{sense}}} \tag{4.8}$$

4.4.2 Modelling of On-Demand MAC

The two-way communication of ODMAC is modelled as shown in figure 4.18. While the same notations from figure 4.17 are used, a list of new notations used in this analysis are also described.

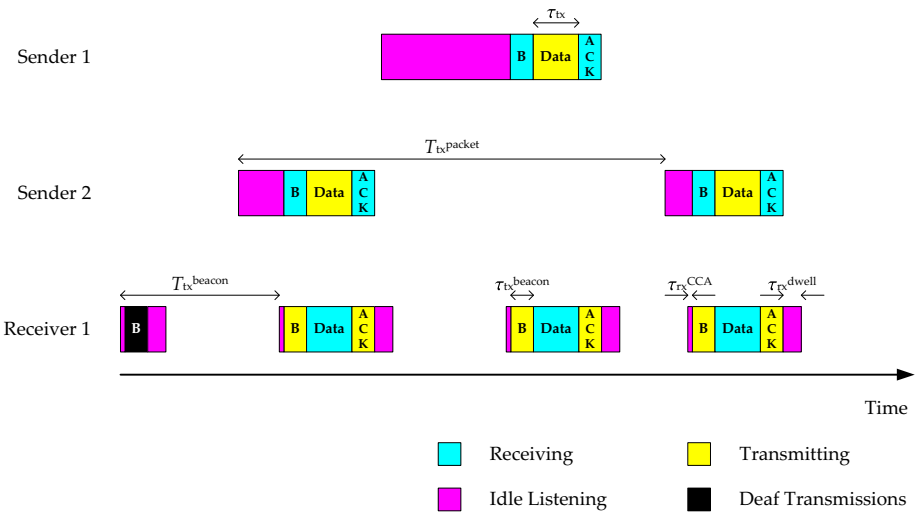

Figure 4.18: On-Demand MAC model

B	is the beacon size, in bytes
$T_{\text{tx}}^{\text{packet}}$	is the duty cycle period of the sender, in seconds
$\tau_{\text{rx}}^{\text{CCA}}$	is the time taken by the radio to perform a CCA using carrier sensing, in seconds
$\tau_{\text{rx}}^{\text{dwell}}$	is the time duration the receiver waits for a response from the sender, in seconds
$\tau_{\text{tx}}^{\text{beacon}}$	is the transmission time of a single beacon frame, in seconds
$T_{\text{tx}}^{\text{beacon}}$	is the duty cycle period of a beacon transmission, in seconds, which should be always less than the corresponding maximum legal duty cycle limit of the chosen frequency band

Receiver
The receiver performs a CCA to ensure that the channel is idle before transmitting a beacon. The time taken to perform a CCA, is specified for the radio that is used. Once the channel is free, the receiver transmits a single beacon frame. The duration of the beacon is described by equation (4.9). After broadcasting a beacon, the receiver continues to listen for a short period of time to receive a response from a sender.

$$\tau_{\text{tx}}^{\text{beacon}} = \frac{B \cdot 8}{BR} \tag{4.9}$$

The duty cycle of the beaconing depends on the amount of power the receiver is harvesting, where the period of the duty cycle is given by equation (4.10). After the sender receives the beacon, it transmits the data immediately, which is then acknowledged by the receiver with another beacon.

$$P_{\text{receiver}} = \frac{P^{\text{startup}} \cdot T^{\text{startup}} + P_{\text{rx}} \cdot (2T_{\text{rx}}^{\text{startup}} + \tau_{\text{rx}}^{\text{CCA}} + \tau_{\text{tx}}) + 2P_{\text{tx}} \cdot (T_{\text{tx}}^{\text{startup}} + \tau_{\text{tx}}^{\text{beacon}})}{T_{\text{tx}}^{\text{beacon}}}$$

$$\text{where } P_{\text{receiver}} \in \left[P_{\text{receiver}}^{\text{min}}, P_{\text{receiver}}^{\text{max}}\right]$$

$$T_{\text{tx}}^{\text{beacon}} = \frac{P^{\text{startup}} \cdot T^{\text{startup}} + P_{\text{rx}} \cdot (2T_{\text{rx}}^{\text{startup}} + \tau_{\text{rx}}^{\text{CCA}} + \tau_{\text{tx}}) + 2P_{\text{tx}} \cdot (T_{\text{tx}}^{\text{startup}} + \tau_{\text{tx}}^{\text{beacon}})}{P_{\text{receiver}}}$$

$$\text{where } T_{\text{tx}}^{\text{beacon}} \in \left[T_{\text{beacon}}^{\text{min}}, T_{\text{beacon}}^{\text{max}}\right] \tag{4.10}$$

$$T_{\text{tx}}^{\text{beacon}} \propto \frac{1}{P_{\text{receiver}}}$$

Sender
The transmission duration of a single packet is given by equation (4.1). When the sender has data to exchange, in the worst case, it has to wait for a full beacon period before receiving a beacon from the receiver. It then immediately transmits the data, and receives an acknowledgement from the receiver. The duty cycle period of the sender is given by equation (4.11).

$$P_{\text{sender}} = \frac{P^{\text{startup}} \cdot T^{\text{startup}} + P_{\text{rx}} \cdot (2T_{\text{rx}}^{\text{startup}} + T_{\text{tx}}^{\text{beacon}} + \tau_{\text{tx}}^{\text{beacon}}) + P_{\text{tx}} \cdot (T_{\text{tx}}^{\text{startup}} + \tau_{\text{tx}})}{T_{\text{tx}}^{\text{packet}}}$$

$$\text{where } P_{\text{sender}} \in \left[P_{\text{sender}}^{\text{min}}, P_{\text{sender}}^{\text{max}}\right]$$

$$T_{\text{tx}}^{\text{packet}} = \frac{P^{\text{startup}} \cdot T^{\text{startup}} + P_{\text{rx}} \cdot (2T_{\text{rx}}^{\text{startup}} + T_{\text{tx}}^{\text{beacon}} + \tau_{\text{tx}}^{\text{beacon}}) + P_{\text{tx}} \cdot (T_{\text{tx}}^{\text{startup}} + \tau_{\text{tx}})}{P_{\text{sender}}}$$

$$\text{where } T_{\text{tx}}^{\text{packet}} \in \left[T_{\text{packet}}^{\text{min}}, T_{\text{packet}}^{\text{max}}\right] \tag{4.11}$$

$$T_{\text{tx}}^{\text{packet}} \propto \frac{1}{P_{\text{sender}}}$$

A collision occurs in ODMAC, when two or more nodes that has data to transmit, wakes up and waits for the same beacon. Since beacons essentially form time slots for communication, these senders collide when transmitting data after receiving the same beacon. The probability of such an event happening can be expressed by equation (4.12).

$$P(\text{collision}) = (N-1) \cdot \frac{T_{\text{tx}}^{\text{beacon}}}{T_{\text{tx}}^{\text{packet}}} \tag{4.12}$$

As described by equation (4.4), in the worst case, a sender has to transmit data for n times to ensure that with a probability $P(\text{success})$, at least one transmission is successful.

The sensing period of a sender, which is the shortest time duration a sender has to wait before performing a new measurement, is represented by equation (4.13).

$$T^{\text{sense}} = T_{\text{tx}}^{\text{packet}} \cdot n \tag{4.13}$$

The goodput of the receiver can be calculated using equation (4.8).

4.4.3 Comparison

The models for IMR+ and ODMAC can be used to compare the performance to determine the benefits of ODMAC. Only a relative comparison can be made, since channel errors are not included in the model. However, the models are sufficient to determine the advantages and disadvantages of the two MAC schemes.

The harvested and consumed power levels used in this analysis are described in table 4.2. The range of measured power levels harvested from the heat of the radiator by the senders, and the power levels harvested from the heat of hot water pipes in buildings by the receiver, is explained in chapter 2. Furthermore, the power levels consumed by the SX1212 radio transceiver from Semtech is described in chapter 3.

The analysis of the impact of harvested power on how often a new measurement can be performed by the senders are shown in figure 4.19. Since the receiver cannot communicate any information back to the sender in IMR+, the receiver has to be designed for the worst case. This means that the active period of the receiver listening for incoming data should be long enough to ensure that at least one valid packet will arrive successfully from all the senders, even if they are harvesting the lowest amount of power. For this reason,

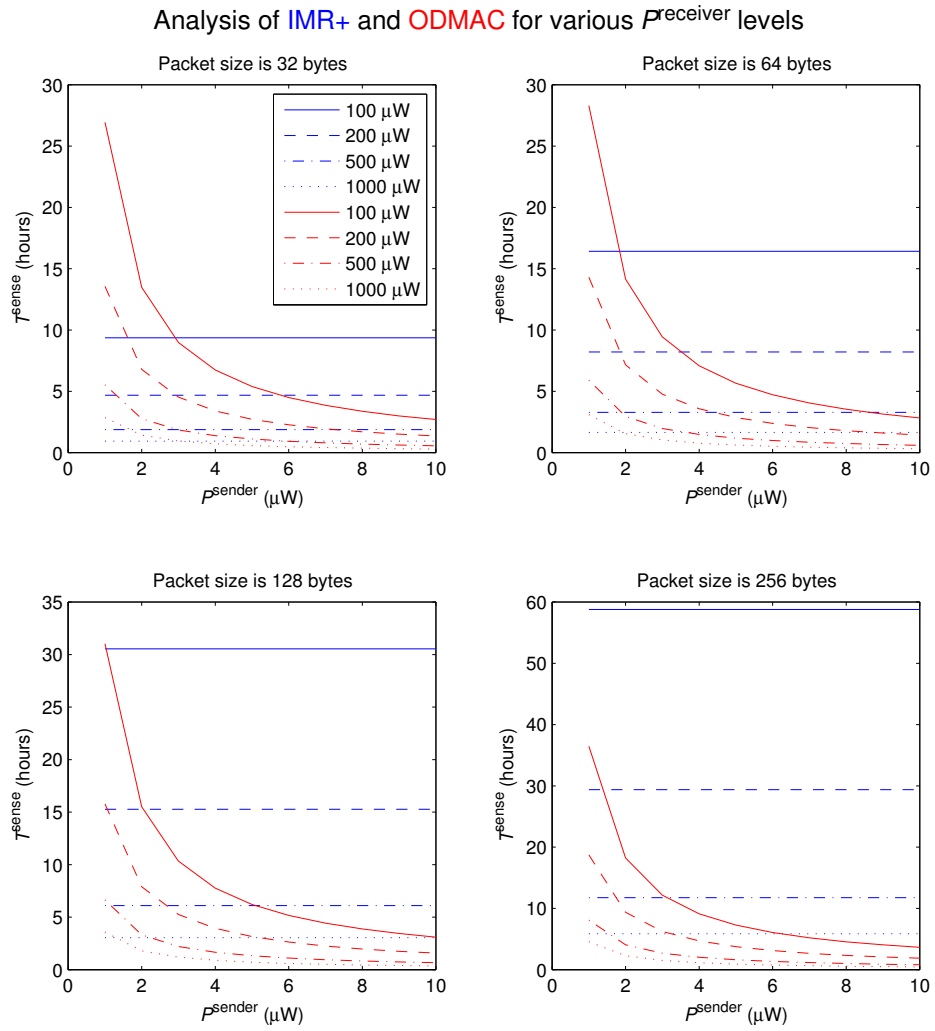

Figure 4.19: Impact of harvested power on the measurement period

Table 4.2: Values used for the analysis

B	=	18 bytes
BR	=	153600 $\frac{\text{bits}}{\text{second}}$
P^{startup}	=	1.02 mW
T^{startup}	=	5.8 ms
P_{tx}	=	132 mW
$T^{\text{startup}}_{\text{tx}}$	=	0.5 ms
$P^{\text{min}}_{\text{sender}}$	=	1 μW
$P^{\text{max}}_{\text{sender}}$	=	10 μW
$P(\text{success})$	=	99.99 %
P_{rx}	=	11.55 mW
$T^{\text{startup}}_{\text{rx}}$	=	0.5 ms
$P^{\text{min}}_{\text{receiver}}$	=	100 μW
$P^{\text{max}}_{\text{receiver}}$	=	1000 μW
$\tau^{\text{CCA}}_{\text{rx}}$	=	100 μs

IMR+ cannot efficiently use the power available to increase its performance. In an EH-WSN application, where the senders can afford to completely shut down when there is no energy to harvest, IMR+ cannot be used, because the receiver would have to remain constantly active. In contrast, ODMAC demonstrates its ability to dynamically adjust to the energy harvested from its environment. For very low harvested power, ODMAC sacrifices the frequency of measurements to keep the network stable. As soon as the harvested power increases, the sensing period reduces exponentially, far out performing IMR+.

Another observation of the analysis is the impact of the packet size. In IMR+, the sensing period is severely affected by the increase in the packet size, where as ODMAC is more resilient to the increase in packet size while still maintaining the same adaptivity.

The optimal network performance is achieved, when both the senders and receivers are able to harvest the maximum amount of power from the energy source. This scenario is shown in figure 4.20. The performance of ODMAC drops, as the network becomes more dense, when the sender and the receiver are fully active. This is due to the linearly increasing probability of collisions. IMR+ is more resilient in this scenario and remains robust. However, even with the problem of scalability, ODMAC completely out performs IMR+ in a sparse network, while in a dense network, it still maintains a faster sensing frequency.

While it was previously observed that ODMAC gracefully handles an increase in packet size, it can now be seen that an increase in packet size actually benefits ODMAC immensely, far out performing IMR+ for large packet sizes.

The network has the worst performance, when the amount of harvested energy is the lowest for both the senders and receiver. Such a scenario is shown in figure 4.21. For smaller packet sizes ODMAC performs worse than IMR+. However, for large packet sizes, ODMAC out performs IMR+, and maintains a higher sensing frequency under all circumstances. Furthermore, like IMR+, ODMAC remains scalable and robust.

Figure 4.22 shows the scenario when the senders are starved of power, while the receiver remains fully active. Although the goodput of the network is higher than in the worst case, the performance of ODMAC and IMR+ show similar characteristics.

The receiver is flooded when the senders are fully active and the receiver is harvesting the lowest amount of power, as shown by figure 4.23. This scenario is similar to the best

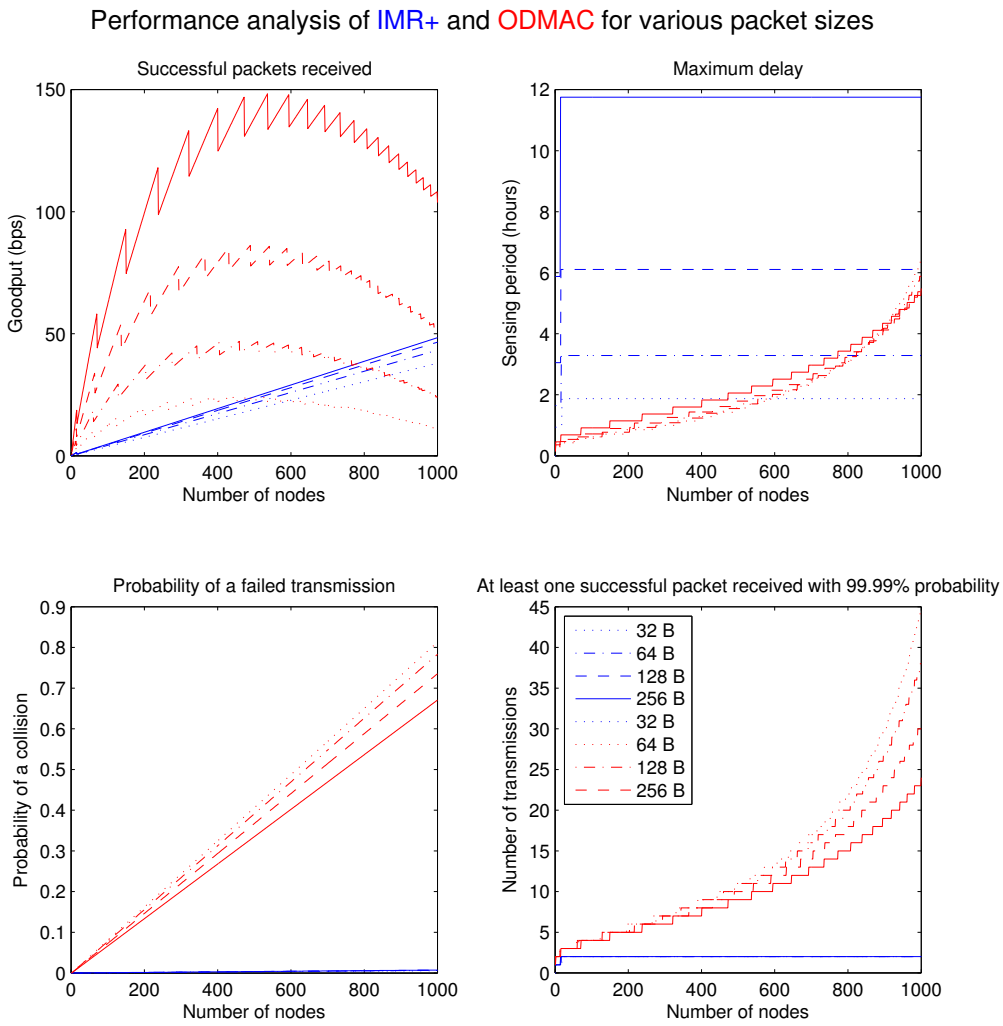

Figure 4.20: Best case: senders and receiver harvest the maximum power

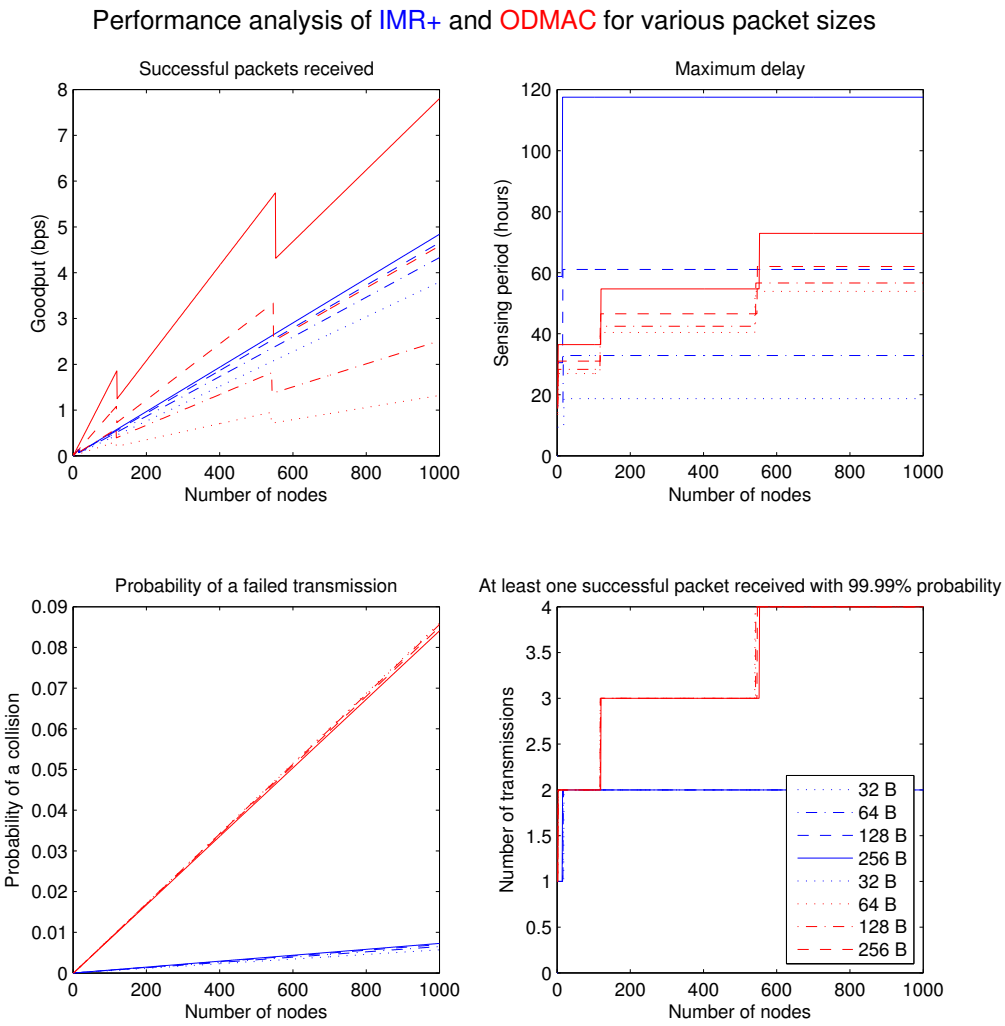

Figure 4.21: Worst case: senders and receiver harvest the minimum power

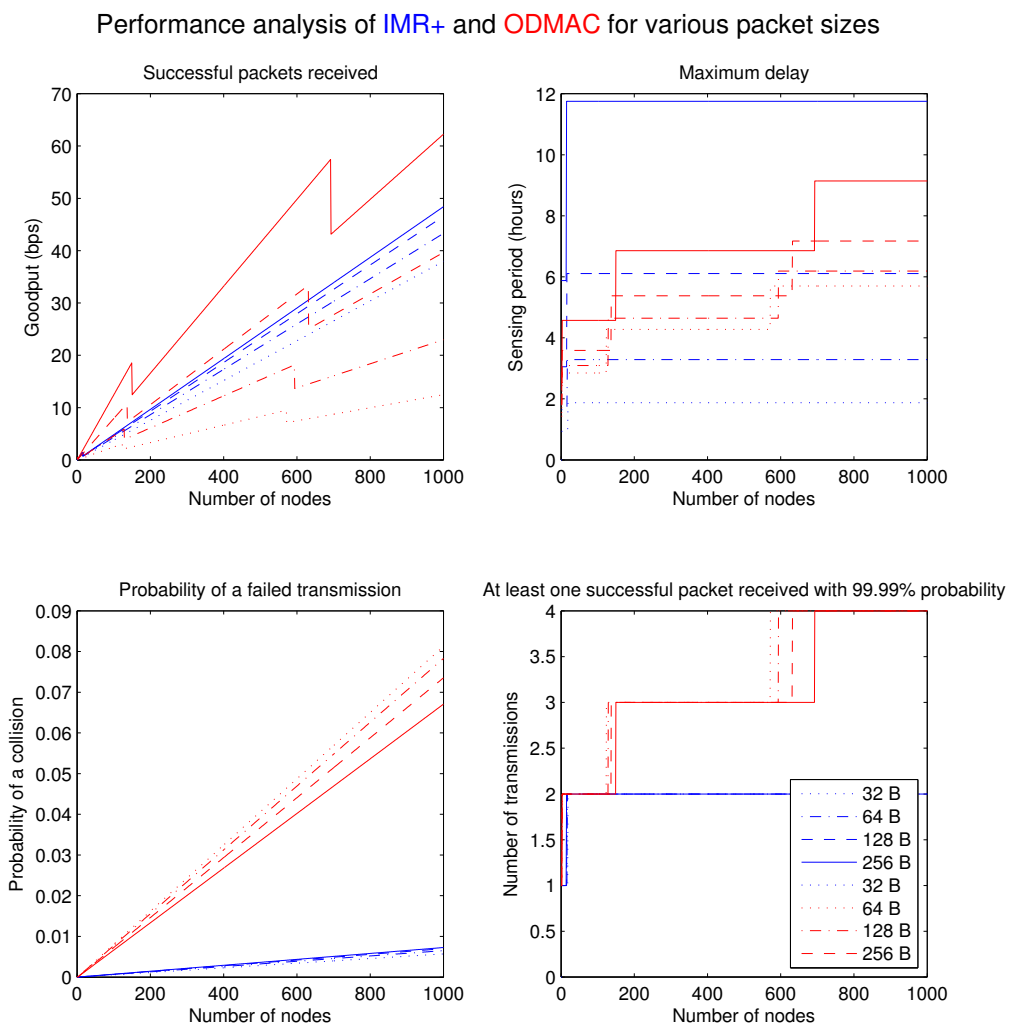

Figure 4.22: Receiver in a drought: senders harvest the minimum power and receiver harvests the maximum power

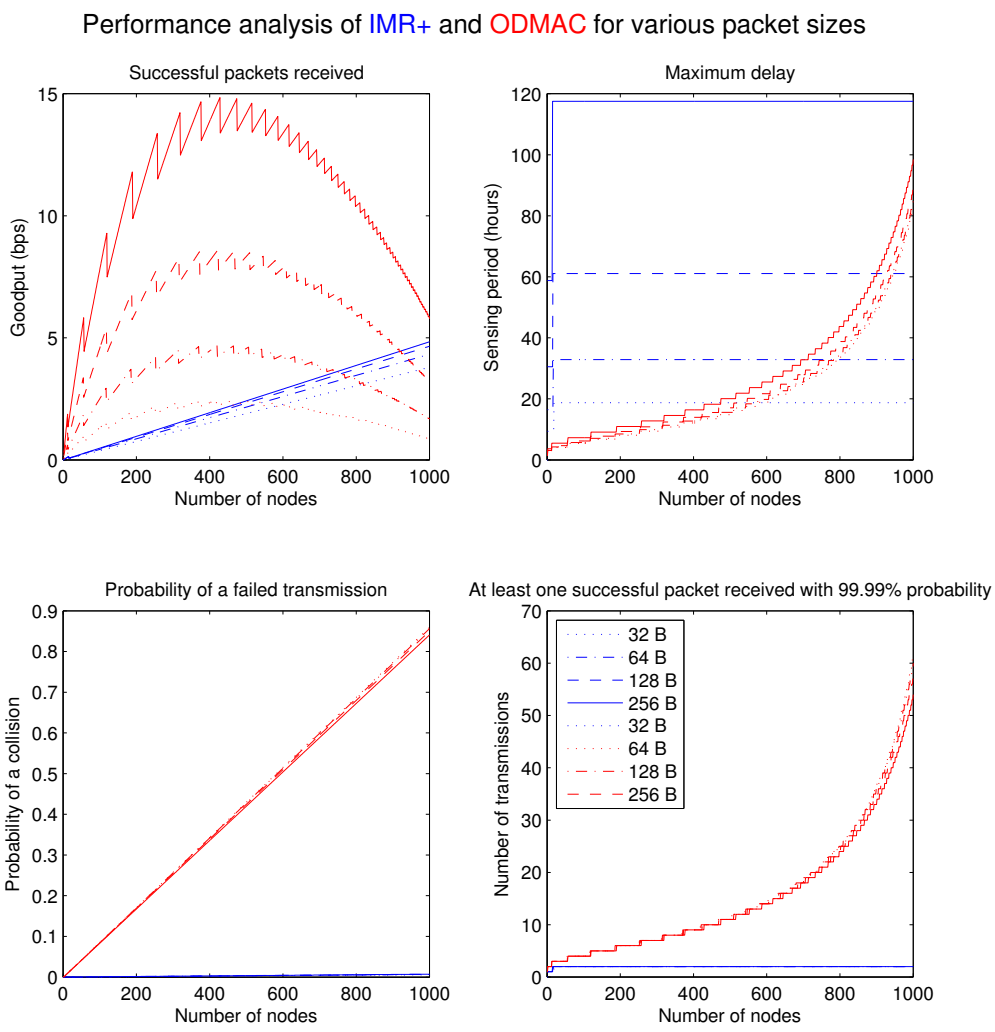

Figure 4.23: Receiver flooded: senders harvest the maximum power and receiver harvests the minimum power

case with a very low goodput, and IMR+ and ODMAC demonstrates the same characteristics.

4.4.3.1 Data Aggregation

Even though the case where nodes only transmit a single packet was considered, an interesting observation from the analysis leads to a more generalized conclusion. Buffering can be introduced into the senders, so that the measuring period could be further reduce. As shown by figure 4.24, senders are able to perform sensing tasks and store the packets in a buffer, while the MAC scheme transmits several aggregated data packets and removes them from the buffer.

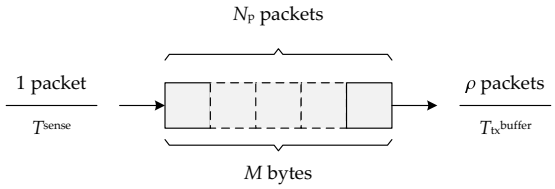

Figure 4.24: Buffering measurement data

M	is the buffer size, in bytes
N_p	is the number of packets that can be stored in the buffer
ρ	is the number of packets exchanged in a single rendezvous
T_{tx}^{buffer}	is the duty cycle period for transmitting ρ packets from the buffer, in seconds

In IMR+, the senders are contending for the receiver when they transmit a packet, during which collisions can occur. In contrast, senders in ODMAC contend for the receiver while listening for a beacon, and collisions can occur in the transmission that follows. This observation is expressed in equations (4.3) and (4.12) respectively.

Due to this difference, IMR+ cannot benefit from buffering, in fact, transmitting more data increases the probability of collisions, suffering from poor performance. Furthermore, due to the lack of MAC level acknowledgements, the large data transmissions, will increase the probability of channel errors. On the other hand, ODMAC is able to utilize the benefits of buffering efficiently, without a large impact from additional collisions or channel errors. As described by equation (4.15), the sensing period could be further reduced according to the amount of memory available for the buffer, essentially, decoupling the sensing period from the transmission period of a sender.

$$N_p = \left\lfloor \frac{M}{D} \right\rfloor \tag{4.14}$$

$$\frac{1\text{packet}}{T^{sense}} \leqslant \frac{\rho \text{ packets}}{T_{tx}^{buffer}} \quad \text{where } \rho \in [1, N_p]$$

$$T^{\text{sense}} \geqslant \frac{T_{\text{tx}}^{\text{buffer}}}{\rho} \tag{4.15}$$

4.4.3.2 Opportunistic Collision Avoidance

The need for a simple collision avoidance mechanism for receiver-initiated MAC schemes is well established in the study performed thus far. Therefore inspired by OC-MAC, a novel collision avoidance mechanism called Collision Avoidance with Opportunistic Data Aggregation (CAODA) is proposed. It is an efficient collision avoidance mechanism which exploits the receiver-initiated paradigm. Since collisions occur at the receiver when two or more senders are contending for the same beacon from a receiver, as in OC-MAC, CAODA exploits the fact that contending senders are in an active listening state. Figure 4.25 provides an overview of the CAODA mechanism.

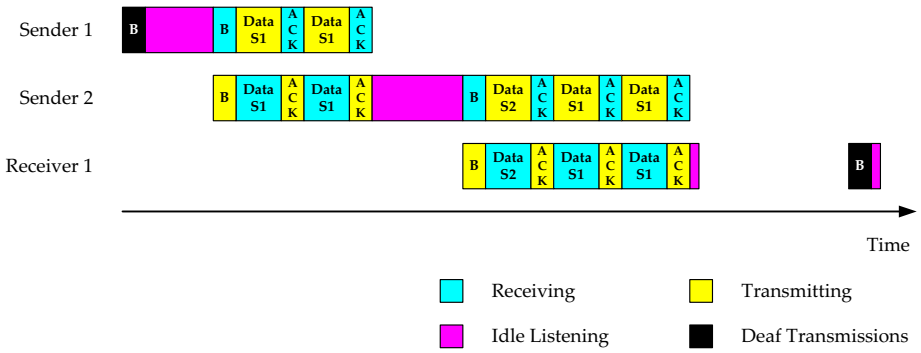

Figure 4.25: Mechanics of CAODA

A sender that has data to exchange with a receiver, begins by transmitting a RTR beacon after a CCA to inform another contending sender of its availability to forward data to a receiver. The address of the receiver that the sender is waiting for is included in the RTR beacon. If another contending sender that coincidentally happens to be awake, receives the RTR beacon, it immediately transmits its data to the sender from which it received the RTR beacon, and enters the sleep state. The sender that receives the data, aggregates it in a transmit buffer, and continues to listen for either the base beacon from the receiver or another RTR beacon from a sender. If it receives the base beacon, the data is passed onto the receiver and the mechanism is complete, or if it receives a RTR beacon, the process continues until the intended receiver wakes up.

This opportunistic mechanism of avoiding collisions ensure that only a single sender is waiting for an individual receiver to wake up at any given time. It also reduces the idle listening time of senders contending for the same receiver, so as the network becomes more dense, less energy is wasted on idle listening. Furthermore, all the data generated by senders are treated fairly, by ensuring delivery to the receiver within a single cycle.

While CAODA is a general collision avoidance scheme for receiver-initiated MAC schemes, it is more efficient when used with an EH receiver-initiated MAC scheme such as ODMAC. This is because all senders in a EH-WSN operates in a energy sustainable state, i.e., they

are less active if a low amount of energy is harvested. Hence, a sender that wakes up to transmit data, can be designed to also carry the burden of forwarding data. In contrast, OC-MAC is designed for a static duty cycling WSN, where the residual energy of the sender should be broadcasted with the RTS beacon.

4.4.4 Summary

The analysis performed, shows that the simplicity of IMR+ makes it very scalable and robust. However, it is highly unsuitable for EH-WSN due to its inability to dynamically manage its resources to improve performance. In contrast, ODMAC far out performs IMR+. Since ODMAC is able to dynamically manage its resources to achieve a maximum performing state for a given amount of energy, it is well suited for a EH-WSN. The main weakness of ODMAC is the high number of collisions in a dense network, making it less scalable. CAODA is proposed as an efficient solution to this problem, while the collision avoidance scheme described in RI-MAC can be also used. Finally, due to the low complexity of receiver-initiated MAC schemes, it can be easily implemented in low-cost low-performance microcontrollers.

4.5 Further Improvements

Since the need for a collision avoidance scheme in ODMAC is established in this study, the advantages and disadvantages of CAODA should be closely examined and analytically compared to other collision avoidance schemes. Then the presented analytical model should be expanded to include a collision avoidance scheme. To reflect the benefits of data aggregation, the model should also be extended to include a senders ability to buffer packets. Furthermore, to analyse the impact of channel errors, such a model should also be considered in the study.

When additional receivers are included in the network, the opportunistic forwarding policy introduced by ODMAC enables the network to gracefully balance the load in a distributed manner. However, the addition of receivers in IMR+ would only create redundancy because of overhearing in the receiver. The model used in this study should be expanded with multiple receivers, to analytically verify this phenomena.

The improvements proposed by OC-MAC and EE-RI-MAC should also be analytically verified, after performing a survey on collision avoidance mechanisms, to determine whether it is more energy efficient than a BEB collision avoidance scheme.

Chapter 5

Discussion

As this study concludes with the results obtained thus far, this chapter presents the next phase of the research, which is currently on going. An overview of the planned application scenario is described, along with a discussion of the implementation of ODMAC. Next, a system overview of a scalable emulation technique for thermal energy harvesting is presented, with a proposed initial experiment setup. Finally, the chapter concludes with a retrospective of this study.

5.1 Application Scenario

The battery powered HCA currently produced by Brunata approximately consumes 15μW of power on average. When a 3V primary Li battery with a capacity of 600mAh is used, the HCA has a service life of around 13 years, before the battery has to be replaced. The electronics of the HCA that do not support very low supply voltages will shut down as the voltage of the battery drops rapidly towards the end of its service life. Therefore, Brunata deploys a battery with a capacity of 900mAh to ensure that the service life of the HCA is at least 11 years including 1 year of reserve power.

5.1.1 Using IMR+

Assuming that thermal energy can be harvested during the 3 months of the winter season, and considering the same power consumption rate by the system of the HCA for an EH-HCA, the battery capacity required to operate the rest of the year is given by equation (5.1).

$$C = \frac{P_{\text{avg}} \cdot t}{V} \qquad \text{where} \begin{cases} C & \text{is in milliampere hours} \\ P_{\text{avg}} & \text{is in watt} \\ t & \text{is in seconds} \end{cases} \tag{5.1}$$

$$C = \frac{15\mu\text{W} \cdot 9 \text{ months}}{3\text{V}} \approx 34\text{mAh}$$

The number of charge cycles a VL-3032 battery with a capacity of 100mAh can with stand is given by equation (2.13), while the permanent capacity loss per charge cycle is given by (2.16).

$$N_{\text{cycles}}^{\max} = \frac{30000}{(\frac{34\text{mAh}}{100\text{mAh}} \cdot 100)^{1.474}} \approx 166 \text{ cycles}$$

$$C_{\text{loss}} = \frac{100\text{mAh}}{166 \text{ cycles}} \approx 0.6\text{mAh}$$

If the battery is charged only during the winter season, it is able to theoretically survive for 166 years. This means that the lifetime of the battery, and in turn the EH-HCA, would not be dictated by the number of charge cycles, but rather by the aging of the device.

Similarly, the battery capacity required for operation during the winter season can be found.

$$C = \frac{15\mu\text{W} \cdot 3 \text{ months}}{3\text{V}} \approx 11\text{mAh}$$

Therefore, the average amount of power that is required to be harvested during the winter season, in order for the EH-HCA to operate and replenish the battery is around 62μW.

$$P_{\text{avg}} = \frac{(34\text{mAh} + 11\text{mAh}) \cdot 3\text{V}}{3 \text{ months}} \approx 62\mu\text{W}$$

This shows that an LST radiator would not be able to provide enough power to operate an EH-HCA with the IMR+ protocol, further motivating the use of ODMAC. If the range of the empirical model given by equation (2.49) is increased by a further 10K to investigate the required temperature difference to sustain the EH-HCA, an average temperature difference of at least 28K between the surface of the radiator and the room is required, before an EH-HCA using Brunata's IMR+ protocol is feasible. This scenario is similar to the case when the surface temperature of the radiator is around 48°C, while the room temperature is around 20°C.

$$P_{\text{out}} = \frac{0.15}{28^{-1.45} - 0.006} - 3 \approx 73\mu\text{W}$$

5.1.2 Using ODMAC

The power consumption of an EH-HCA can be divided into static (quiescent) and dynamic portions. The static power is the amount of power consumed by the system load when all of the components are in a sleep state, while the dynamic power is the amount of power consumed in the active state. Since ODMAC is able to dynamically adjust the duty cycle, it is able to adapt to the varying amount of available power. Nonetheless, ODMAC is not immune to the challenge posed by the static power consumed by the system load. In fact, MAC protocols cannot help reduce the static power consumption, as it is a hardware characteristic of the system load.

While ODMAC is able to operate in a sustainable state when more than about 10μW of power is harvested, at the expense of latency, due to the static power consumed by the system load, the battery would not be fully charged by the end of the winter season. Therefore, the requirement [R2] and the static power consumed by the system load is the main limiting factor for ODMAC.

5.1.2.1 Implementation

The implementation of ODMAC on the ıota platform is currently ongoing, and is not considered as part of this thesis. Nonetheless, the work done thus far is mentioned to clarify how the results from this thesis are adopted. The frame structures shown in figure 5.1 are used to utilize the hardware packet handler on the SX1212 radio transceiver.

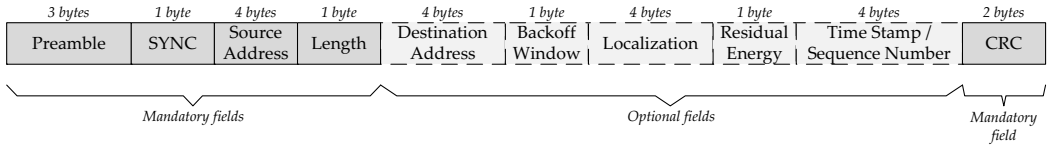

(a) Beacon frame structure

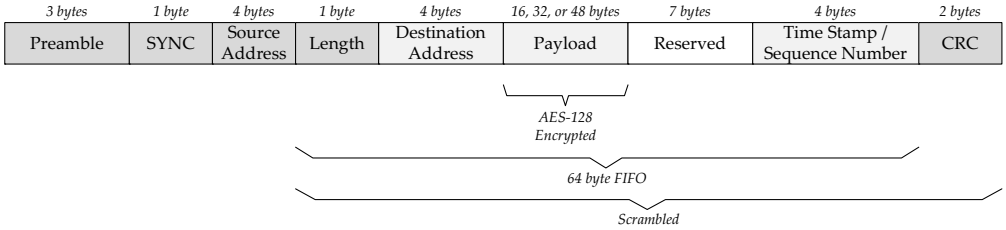

(b) Datagram frame structure

Figure 5.1: ODMAC frame structures

There are two fundamental frames used by ODMAC, a beacon and datagram frame. The beacon frame is used by the receivers as a RTR indicator, while the datagram frame is used to transfer the payload with the measurement data. The mandatory hardware preamble, sync, and the source address is initialized once during the first boot of ıota, while the CRC is automatically calculated and appended by the SX1212 radio transceiver to maintain the integrity of the data. The length field reflects the number of payload or optional bytes included in a single frame.

The beacon frame contains optional fields which can be implemented if required by the application. The destination address and the back off window fields provides functionality similar to RI-MAC. The localisation field is intended to be used by any accompanying routing protocol to broadcast geographical information to localise the node within a network. The residual energy field contains an estimate of the amount of energy present in the energy buffer of the node, while the time stamp field provides the current POSIX time of the node, which can be also used as a sequence number if necessary.

In contrast to the beacon frame, the datagram frame does not contain any optional fields. Instead, a variable length payload is encrypted with AES-128, where discrete lengths of 16, 32, or 48 bytes is used. A reserved field that is not utilised currently, is left for future expansion. The data in the FIFO plus the CRC is scrambled using a LFSR automatically by

the SX1212 radio transceiver.

CCA can be implemented using the RSSI measurements performed by the SX1212 radio transceiver. If the measured RSSI value, which is converted to power, is greater than -80dBm, the channel is assumed to be occupied, while if it is less, the channel is assumed to be clear. The acceptance level of the RSSI value is inspired from the IEEE 802.15.4 standard, and could require further tweaking before it is deployed.

5.1.3 Feasibility Requirements

Several solutions exist for an EH-HCA to be feasible.

- The static power consumption of the system could be is reengineered to be less than 4μW, assuming that 2μW of dynamic power is allowed.
- Radiators other than LST radiators can be considered, to obtain a larger temperature gradient between the surface of the radiator and the room.
- The requirement [R2] could be amended as "Each node shall guarantee delivery of at least one measurement per day to the collector, *when the radiator is in use*".

The last solution would allow the sleep state, which consumes the static power, to be replaced by a stop state, where the power to the entire system is shut down. In such a scenario, the EH-HCA would be active within a EH-WSN when there is heat present on the radiator, which is typically the winter season, while being dormant the rest of the time.

5.2 Experiment Setup

Once the implementation of ODMAC is completed, it should be assessed in a controlled environment to validate the results obtained from the analytical model. Since channel effects were not included in the model, a wired network as shown in figure 5.2 is proposed for the initial experiment.

Attenuator

The nodes are wired together in a star network to reflect the application scenario of Brunata, where *ιota* nodes are configured as multiple senders and a single receiver. Attenuators ensure that the transmission power in the network is within the limits support by the radio receiver in the SX1212. A 10-way RF divider/combiner is used to combine the senders and the receiver. Finally, the receiver connects to a PC over USB, so that statistics from the experiment can be gathered.

5.2.1 Emulation of Thermal Energy Harvesting

Due to the high cost of prototyping the thermo-plastic lid, an alternative technique is required to setup an EH-WSN for the initial experiment. The empirical model of the thermal energy harvesting system described by equation (2.49), can be used to emulate an EH-HCA on *ιota*. Figure 5.3 shows an overview of the proposed emulation system that can be implemented on *ιota*.

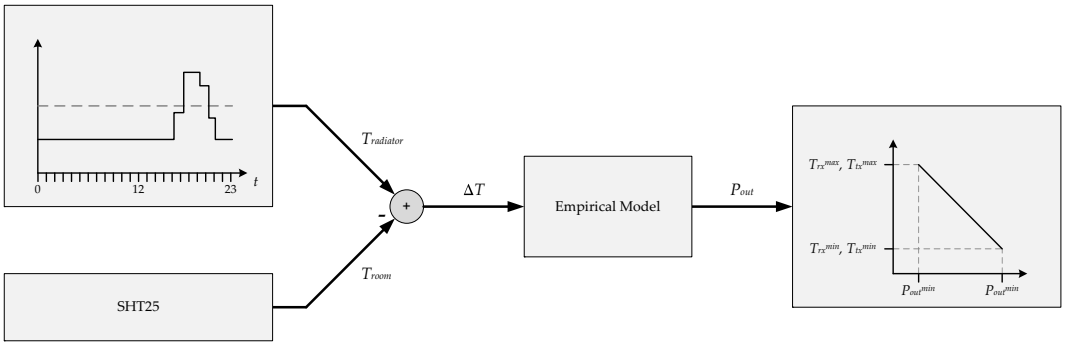

Figure 5.3: System overview of emulator

Two types of LST radiators can be emulated, a radiator with a Thermostatic Radiator Valve (TRV) or a radiator that follows a diurnal cycle. A LST radiator with a TRV typically has a surface temperature that is slowly changing, due to its self-regulating nature. A LST radiator that is manually controlled by the tenant typically follows a pattern that recurs every 24 hours, due to similar behaviour of the inhabitant that recurs every day. The function that describes the surface temperature of a LST radiator, T_{radiator}, can be defined to reflect the two types of LST radiators. The temperature of the room, T_{room}, is measured using the SHT25 temperature sensor. Then the empirical model is used to calculate the amount of power extracted from the thermal energy harvesting system. In the senders, the minimum and maximum power levels, $P_{\text{out}}^{\text{min}}$ and $P_{\text{out}}^{\text{max}}$, are linearly mapped to the duty cycling period, $T_{\text{tx}}^{\text{max}}$ and $T_{\text{tx}}^{\text{min}}$, respectively, while in the receiver, the minimum and maximum power levels, $P_{\text{out}}^{\text{min}}$ and $P_{\text{out}}^{\text{max}}$, are linearly mapped to the duty cycling period, $T_{\text{rx}}^{\text{max}}$ and $T_{\text{rx}}^{\text{min}}$, respectively.

If the execution speed is critical, the functions, T_{radiator} and P_{out}, can be initialised as a look-up table, where the intermediate values are interpolated.

5.2.2 State Of Residual Energy

The VL-3032 rechargeable battery has a large drop in the voltage between a DOD of 0 to 5%, which can be utilised to regulate the duty cycle of a node. Figure 5.4a shows a typical discharge of a battery, while figure 5.4b shows how the voltage of the battery is linearly mapped to the duty cycle period of the node.

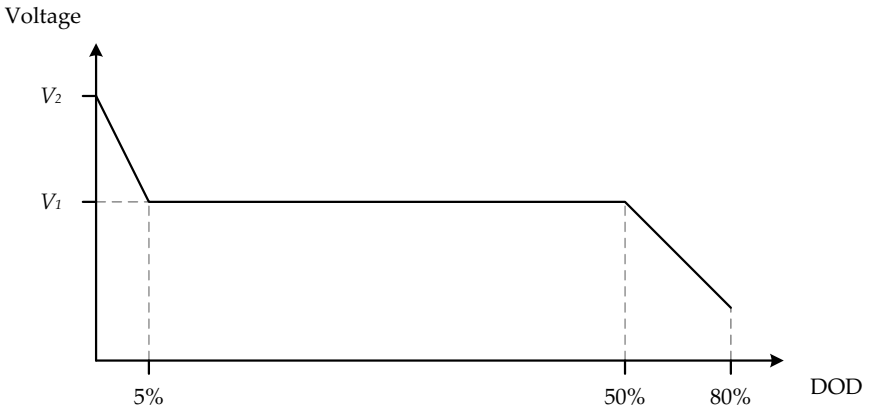

(a) Depth of discharge of the VL-3032 secondary battery

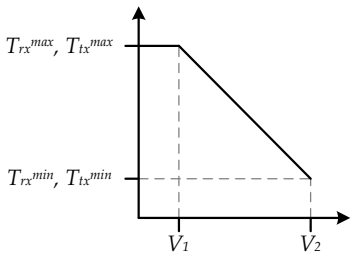

(b) Linear mapping of the battery voltage to the duty cycle period

Figure 5.4

Although, this technique seems trivial, it is indeed a challenge to measure the voltage of a battery accurately while being loaded, due to the current pulses drawn by the system. A thorough examination of possible solutions is considered beyond the scope of this study. Nonetheless, although it is neither an energy friendly or accurate solution, a running average filter can be applied to the measurements to obtain a decent approximation of the battery voltage.

A metric known as the State Of Residual Energy (SORE) is proposed to indicate the amount of energy accumulated in the energy buffer and the harvesting or consuming rate. A discrete time function of the measured battery voltage can be used to define SORE as shown in figure 5.5.

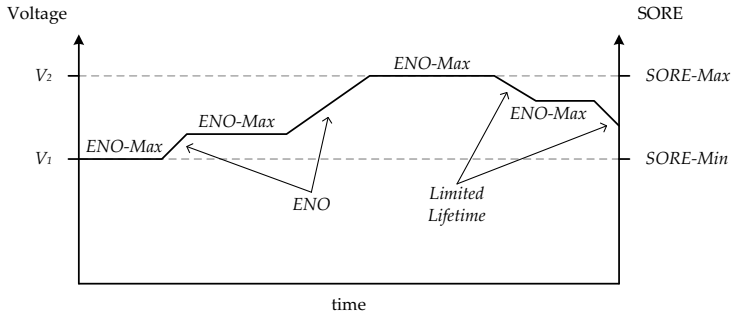

Figure 5.5: Overview of SORE

In contrast to the work presented in [105], the ENO-Max state is not defined as maintaining the initial state of the energy storage device. Here, the ENO-Max state is defined as a state when the battery voltage is constant between V_2 and V_1, where the energy harvested is equal to the energy consumed. A rising slope indicates that the system is in an ENO state, where the energy harvested is greater than the energy consumed, while a falling slope indicates that the lifetime of the system is limited, where the energy harvested is less than the energy consumed. Furthermore, the a measure of the slope can be used to assess the rate of harvesting or consuming energy, while SORE can provide an estimate of the lifetime of the device by considering the residual energy in the system.

A SORE-Max state is defined as the state when a system with a full energy buffer is operating in an ENO-Max state. Then the task of the power management system is to achieve and maintain a SORE-Max state. The SORE metric can be used by the power manager to easily adapt to battery operated systems, where SORE will continuously decrease, energy harvesting systems, where a SORE-Max state can be achieved, or a mains powered system, where a constant SORE-Max state will be maintained.

5.3 Significance Of The Study

The study performed in this thesis researches the foundation of EH systems and MAC schemes. Three vital areas, namely energy harvesting, a wireless sensor node, and MAC schemes, are required to initiate an in-depth study of a novel protocol stack for EH-WSNs. While this study is focused on thermal energy harvesting HCAs in an AMI system, the results obtained provide insight into the challenges that lie ahead. Furthermore, the modelling techniques used can be refined into a more generalised spectrum.

In particular, the results demonstrate that state-of-the-art technology can be used to develop an EH-HCA that can sustain itself with the heat energy scavenged from an LST radiator. The challenge lies in the low surface temperature of modern radiators, as the EH

system is unable to extract enough energy to recharge the battery, and the average static power consumed by the system, since a sensor node spends most of its time in the sleep state. The discontinuity of the heat source poses a challenge due to the requirements set by the application. While this can be solved by modifying the requirements, it is a challenge to motivate such an organisational change. Further research into both reducing the static power consumption of the HCA and finding the optimal mechanical construction for the thermal energy harvester is required, before an EH-HCA can be deployed by Brunata. Out of all the challenges mentioned, the most significant challenge for the industry would be the cost of the thermal energy harvesting system. In other words, the return of investment from the EH system should be greater than from a battery powered system.

Chapter 6

Conclusion

This thesis explores the feasibility of harvesting the heat energy emitted from the surface of low temperature radiators to power the HCA mounted on them. As HCAs are mandatorily mounted on radiators in Denmark and many other countries, an EH-HCA would be able to function as a node within a EH-WSN of an AMI system.

There is presently a lack of state-of-the-art deployments of EH-WSNs in the metering industry. Although a radiator is an attractive source to harvest energy, the large surface of the radiator is a challenging environment to establish proper thermal insulation to obtain a sufficient temperature gradient across the thermal energy harvester. Very few studies carried out by academia focus on practical industrial applications, where the construction and installation of the EH product is considered. Since an increase in the number of deployed EH applications will help reduce the cost of the EH system, it is a requirement of current research to provide some insight into current application challenges and possible solutions, which will help motivate the industry to adopt EH.

The field of EH requires a paradigm shift from the conventional approach in low-power design. In particular, this interdisciplinary study considers the mechanical construction of the thermal energy harvester, design of an EH wireless sensor node, and the MAC scheme required to maintain a sustainable EH-WSN.

A thermal energy harvester using the TGP-751 from Micropelt was designed and its feasibility was verified with a mathematical model. Then the thermal energy harvester was prototyped to test its performance. An experiment was designed in a temperature controlled room, where the temperature on the surface of the radiator and the room was carefully regulated. The power harvested by the TGP-751, which is in the order of tens of millivolts, was converted to a stable power level using the BQ25504 boost converter from Texas Instruments. The thermal EH system is characterised to obtain an empirical model of the power output, to emulate an EH system in future experiments.

The mathematical model was found to sufficiently describe the behaviour of the thermal energy harvester in the EH-HCA within a temperature gradient of 11K to 20K, between the surface of the radiator and the ambient air of the room. The results obtained from the experiments performed demonstrate that approximately 1μW to 20μW of power can be feasibly harvested from the heat energy of the radiator with a temperature difference between 8K to 20K respectively. A particularly interesting observation was the larger amount of power harvested during transient periods that occur when the surface temperature of the radiator changes due the rapid rise in the temperature gradient across the thermal energy harvester.

A wireless sensor node, *ıota*, that closely resembles industrial requirements was designed and manufactured using state-of-the-art components as a research platform for an EH-WSN testbed. Platforms that are currently used by academia are designed for research on WSNs, and do not support the flexibility and performance required for an EH-WSN. In contrast to these wireless sensor nodes, *ıota* supports battery operated systems with a limited power source, mains powered systems with an unlimited power source, power input from an external EH system, as well as a combination of them. The low-power high performance ARM Cortex-M3 core is able to fulfill all the demands of both a node and a gateway node in an EH-WSN. The SX1212 radio transceiver from Semtech that is used in *ıota* offers the industry's lowest power consumption during the receive mode. Application software such as protocol sniffers can easily communicate with *ıota* over the USB virtual serial port. *ıota* offers jumper shunts on the power trace for both the radio and the entire system so that the power consumption can be accurately measured during operation. Furthermore, a right angle SMA connector on the PCB provides easy support for experiments based on both wired and wireless networks.

The state-of-the-art of MAC schemes was established after a literature survey. A MAC scheme, ODMAC, was found to be suitable for EH-WSNs after qualitatively examining the key challenges faced by a MAC scheme in an EH-WSN. The MAC scheme used by Brunata, IMR+, and ODMAC was mathematically modelled to determine the achievable sensing period for a given power budget in the worst case. Both the MAC schemes were analytically compared with respect to the network density, to determine the feasibility of operating in a sustainable EH-WSN with the power levels scavenged using the prototype thermal energy harvester.

Interestingly, the simplicity of IMR+ made it very scalable and robust. However, compared to ODMAC it was inefficient due to its inability to dynamically manage its duty cycle to improve performance. While ODMAC far outperforms IMR+ for a given power budget, the results showed that it is severely affected by collisions as the density of the network increases. As an solution to this problem either a conventional random backoff mechanism, or the proposed novel collision avoidance mechanism, CAODA, could be used.

Bibliography

[1] W. Wang, Y. Xu, and M. Khanna, "A survey on the communication architectures in smart grid," *Computer Networks*, 2011.

[2] D. Tejani, A. M. A. H. Al-Kuwari, and V. Potdar, "Energy Conservation in a Smart Home," in *Proceedings of the 5th IEEE International Conference on Digital Ecosystems and Technologies Conference (DEST)*. IEEE, 2011, pp. 241–246.

[3] B. Kaplan, "The importance of the user behaviour in the design process of energy-renovation projects," Technical University of Denmark, Tech. Rep., 2012.

[4] D. MacKay, "A reality check on renewables," http://www.ted.com/talks/lang/en/david_mackay_a_reality_check_on_renewables.html, 2012.

[5] C. S. Raghavendra, K. M. Sivalingam, and T. Znati, *Wireless Sensor Networks*. Kluwer Academic Publishers, 2004.

[6] G. E. Moore, "Moore's Law," http://en.wikipedia.org/wiki/Moore's_law, 2012.

[7] U. Ahmed, A. Tchounikine, M. Miquel, and S. Servigne, "Real-Time Temporal Data Warehouse Cubing," in *Database and Expert Systems Applications*, vol. 6262. Springer, 2010, pp. 159–167.

[8] R. time Database, "Real-time Database," http://en.wikipedia.org/wiki/Real-time_database, 2012.

[9] H. Karl and A. Willig, *Protocols and Architectures for Wireless Sensor Networks*. John Wiley & Sons, Ltd., 2005.

[10] C4ISTAR, "C4ISTAR," http://en.wikipedia.org/wiki/C4ISTAR, 2012.

[11] I. Akyildiz and X. Wang, *Wireless Mesh Networks*. John Wiley & Sons, Ltd., 2009, vol. 1.

[12] U. D. Black, *OSI: A Model for Computer Communications Standards*. Prentice Hall, 1990.

[13] P. Ferrari and D. Marioli, "IEEE802.11 Sensor Networking," *IEEE Transactions on Instrumentation and Measurement*, vol. 55, no. 2, pp. 615–619, 2006.

[14] IEEE, *Part 11: Wireless LAN Medium Access Control (MAC) and Physical Layer (PHY) Specifications*, IEEE Standards Association Std., 2012.

[15] I. Demirkol, C. Ersoy, and F. Alagöz, "MAC Protocols for Wireless Sensor Networks: A Survey," *Communications Magazine, IEEE*, vol. 44, no. 4, pp. 115–121, 2006.

[16] S. S. Kulkarni and M. U. Arumugam, "TDMA Service for Sensor Networks," in *Proceedings on 24th International Conference on Distributed Computing Systems Workshops.* IEEE, 2004, pp. 604–609.

[17] W. Dargie and C. Poellabauer, *Fundamentals of Wireless Sensor Networks*. John Wiley & Sons Ltd., 2010.

[18] M. A. Labrador and P. M. Wightman, *Topology Control in Wireless Sensor Networks*. Springer Science + Business Media, 2009.

[19] J. I. Capetanakis, "Generalized TDMA: The multi-access tree algorithm," *IEEE International Conference on Communications*, vol. 27, no. 10, pp. 1476–1484, 1979.

[20] T. S. Rappaport, *Wireless Communications: Principles and Practice*, 2nd ed. Prentice Hall, 2002.

[21] K. Sohraby, D. Minoli, and T. Znati, *Wireless Sensor Networks: Technology, Protocols, and Applications*. John Wiley & Sons, Inc., 2007.

[22] L. Kleinrock, "Packet Switching in Radio Channels: Part I-Carrier Sense Multiple-Access Modes and Their Throughput-Delay Characteristics," *IEEE Transactions on Communications*, vol. 23, no. 12, pp. 1400–1416, 1975.

[23] Y. Sun, O. Gurewitz, and D. B. Johnson, "RI-MAC: A Receiver-Initiated Asynchronous Duty Cycle MAC Protocol for Dynamic Traffic Loads in Wireless Sensor Networks," in *Proceedings of the 6th ACM conference on Embedded network sensor systems*. ACM, 2008, pp. 1–14.

[24] Y. K. Tan and S. K. Panda, "Review of Energy Harvesting Technologies for Sustainable Wireless Sensor Network," in *Sustainable Wireless Sensor Network. INTECH.*, 2010.

[25] A. Kansal, J. Hsu, S. Zahedi, , and M. B. Srivastava, "Power Management in Energy Harvesting Sensor Networks," *ACM Transactions on Embedded Computing Systems (TECS)*, vol. 6, no. 4, p. 32, 2007.

[26] V. Raghunathan, A. Kansal, J. Hsu, J. Friedman, and M. Srivastava, "Design Considerations for Solar Energy Harvesting Wireless Embedded Systems," in *Proceedings of the 4th international symposium on Information processing in sensor networks*. IEEE Press, 2005, p. 64.

[27] C. Mathuna, T. O'Donnell, R. V. Martinez-Catala, J. Rohan, and B. O'Flynn, "Energy scavenging for long-term deployable wireless sensor networks," *Talanta*, vol. 75, no. 3, pp. 613–623, 2008.

[28] P. Fiorini, I. Doms, C. V. Hoof, and R. Vullers, "Micropower Energy Scavenging," in *34th European Solid-State Circuits Conference. ESSCIRC.* IEEE, 2008, pp. 4–9.

[29] A. Harb, "Energy harvesting: State-of-the-art," *Renewable Energy*, vol. 36, no. 10, pp. 2641–2654, 2011.

[30] Z. Wan, Y. Tan, , and C. Yuen, "Review on Energy Harvesting and Energy Management for Sustainable Wireless Sensor Networks," in *IEEE 13th International Conference on Communication Technology (ICCT)*. IEEE, 2011, pp. 362–367.

[31] J. H. Pedersen, "Low Frequency Low Voltage Vibration Energy Harvesting Converter," Technical University of Denmark, Tech. Rep., 2011.

[32] X. Fafoutis and N. Dragoni, "ODMAC: An On-Demand MAC Protocol for Energy Harvesting - Wireless Sensor Networks," in *Proceedings of the 8th ACM Symposium on Performance evaluation of wireless ad hoc, sensor, and ubiquitous networks*. ACM, 2011, pp. 49–56.

[33] W. Punt, "Micropelt GmbH," http://www.micropelt.com/, 2012.

[34] B. Habbe and J. Nurnus, "Thin Film Thermoelectrics Today and Tomorrow," in *Electronics Cooling*, 2011.

[35] M. Freunek, M. Muller, T. Ungan, W. Walker, and L. M. Reindl, "New Physical Model for Thermoelectric Generators," *Journal of electronic materials*, vol. 38, pp. 1214–1220, 2009.

[36] J. Davidson, M. Collins, and S. Behrens, "Thermal Energy Harvesting Between the Air/Water Interface for Powering Wireless Sensor Nodes," in *Proceedings of SPIE*, vol. 7288, 2009.

[37] S. Riffat and X. Ma, "Thermoelectrics: a review of present and potential applications," *Applied Thermal Engineering*, vol. 23, no. 8, pp. 913–935, 2003.

[38] P. Bertreau, "Novel thermoelectric materials development, existing and potential applications, and commercialization routes," Ph.D. dissertation, Massachusetts Institute of Technology, Department of Materials Science and Engineering, 2006.

[39] F. Ritz and C. E. Peterson, "Multi-Mission Radioisotope Thermoelectric Generator (MMRTG) Program Overview," in *Proceedings of Aerospace Conference*, vol. 5. IEEE, 2004.

[40] NASA, "Curiosity Rover," http://mars.jpl.nasa.gov/msl/mission/technology/technologiesofbroadbenefit/power/, 2012.

[41] D. Hoang, Y. Tan, H. Chng, and S. Panda, "Thermal Energy Harvesting From Human Warmth For Wireless Body Area Network In Medical Healthcare System," in *International Conference on Power Electronics and Drive Systems, PEDS*. IEEE, 2009, pp. 1277–1282.

[42] V. Leonov, P. Fiorini, T. Torfs, R. J. M. Vullers, and C. V. Hoof, "Thermal matching of a thermoelectric energy harvester with the environmental and its application in wearable self-powered wireless medical sensors," in *15th International Workshop on Thermal Investigations of ICs and Systems, THERMINIC*. IEEE, 2009, pp. 95–100.

[43] C. Knight and J. Davidson, "Thermoelectric Energy Harvesting as a Wireless Sensor Node Power Source," in *Proceedings of SPIE*, vol. 7643, 2010.

[44] D. A. Koester, P. Croccoa, R. Mahadevana, E. Siivolaa, and K. von Guntena, "Thin-Film Thermoelectric Energy Harvesting for Security and Sensing Applications," in *Proceedings of SPIE*, 2011.

[45] V. Leonov, "Thermoelectric energy harvester on the heated human machine," *Journal of Micromechanics and Microengineering*, vol. 21, 2011.

[46] X. Lu and S.-H. Yang, "Thermal Energy Harvesting for WSNs," in *International Conference on Systems Man and Cybernetics (SMC)*. IEEE, 2010, pp. 3045–3052.

[47] S. Dalola, M. Ferrari, V. Ferrari, M. Guizzetti, D. Marioli, and A. Taroni, "Characterization of Thermoelectric Modules for Powering Autonomous Sensors," *IEEE Transactions on Instrumentation and Measurement*, vol. 58, no. 1, pp. 99–107, 2009.

[48] Micropelt, "TGP-751," http://www.micropelt.com/down/thermo_generator_package.pdf, 2012.

[49] T. Instruments, "Highly efficient boost charger IC for nano (ultra-low) power energy harvesting and management applications," http://www.ti.com/lit/gpn/bq25504, 2011.

[50] Micropelt, "MPG-D751," http://www.micropelt.com/down/datasheet_mpg_d651_d751.pdf, 2012.

[51] Micronews, "Micropelt's thin film thermoelectric technology," http://www.i-micronews.com/upload/pdf/Micropelt_Micronews_127.pdf, 2012.

[52] C. B. Vining, "An inconvenient truth about thermoelectrics," *Nature Materials*, vol. 8, no. 2, pp. 83–85, 2009.

[53] F. P. Industries, "SARCOM XR-m Thermal Gap Filler Pad," http://www.fujipoly.com/assets/files/Fujipoly_2012_Catalog.pdf, 2012.

[54] C. Polymers, "CoolPoly D5506 Thermally Conductive Liquid Crystalline Polymer (LCP)," http://www.coolpolymers.com/files/ds/Datasheet_d5506.pdf, 2007.

[55] F. P. Industries, "Sarcon D-Tac 9A Thermally Conductive Double-sided Silicone Tape," http://www.fujipoly.com/announcements/sticky-situation.html, 2012.

[56] S. I. Inc, "Super-Small Package PWM Control, PWM/PFM Control Step-Up Switching Regulator (DC/DC Converter ICs) S-8353/8354 series," http://datasheet.sii-ic.com/en/switching_regulator/S8353_8354_E.pdf, 2010.

[57] L. Technology, "LTC3109 - Auto-Polarity, Ultralow Voltage Step-Up Converter and Power Manager," http://cds.linear.com/docs/Datasheet/3109fa.pdf, 2010.

[58] C. J. Udalagama, "Electrical Energy Generation From Body Heat," in *IEEE International Conference on Sustainable Energy Technologies (ICSET)*, 2010.

[59] C. Corporation, "EnerChip CBC050-M8C Solid-state Battery," http://www.cymbet.com/pdfs/DS-72-01.pdf, 2010.

[60] P. I. Devices, "VL-3032 Vanadium-Pentoxide (VL-type) Rechargeable Lithium Coin Cell," http://industrial.panasonic.com/www-data/pdf/AAD4000/AAD4000PE11.pdf, 2012.

[61] J. Møltoft and L. Rimestad, *Thermal Design*, D. of Measurement and Instrumentation, Eds. Ørsted DTU, 2004.

[62] Y. K. Tan and S. K. Panda, "Energy Harvesting From Hybrid Indoor Ambient Light and Thermal Energy Sources for Enhanced Performance of Wireless Sensor Nodes," in *IEEE Transactions on Industrial Electronics*. IEEE, 2011.

[63] Stelrad, "Low Surface Temperature Radiators," http://www.stelrad.com/uk/radiators/lst_standard, 2012.

[64] T. Instruments, "Evaluation Module for BQ25504 Ultra Low Power Boost Converter with Battery Management," http://www.ti.com/lit/pdf/sluu654, 2011.

[65] A. S. Limited, "Radial, Epoxy-Coated NTC Thermistors," http://www.atcsemitec.co.uk/pdfdocs/ET_thermistor.pdf, 2012.

[66] P. Technology, "ADC-16 High-Resolution Logger," http://www.picotech.com/document/pdf/adc16-2.pdf, 2007.

[67] ——, "PicoLog R5.22.6 Data Acquisition Software for ADC-16," http://downloads.picotech.com/winxp/PicoLog_r5_22_6.exe, 2012.

[68] M. I. Products, "Low-Power Operational Amplifiers," http://datasheets.maxim-ic.com/en/ds/ICL7611-ICL764X.pdf, 2010.

[69] Y. Xu, J. Heidemann, and D. Estrin, "Geography-informed Energy Conservation for Ad Hoc Routing," in *Proceedings of the 7th annual international conference on Mobile computing and networking*. ACM, 2001, pp. 70–84.

[70] T. W. R. G. . E. Zurich, "The Sensor Network Museum," http://www.snm.ethz.ch/, 2012.

[71] G. Sakthidharan and S.Chitra, "A Survey on Wireless Sensor Network : An Application Perspective," in *International Conference on Computer Communication and Informatics (ICCCI)*. IEEE, 2012, pp. 1–5.

[72] P. Baronti, P. Pillai, V. W. Chook, S. Chessa, A. Gotta, and F. Hu, "Wireless sensor networks: A survey on the state of the art and the 802.15. 4 and ZigBee standards," *Computer communications*, vol. 30, no. 7, pp. 1655–1695, 2007.

[73] MEMSIC, "Wireless Modules," http://www.memsic.com/products/wireless-sensor-networks/wireless-modules.html, 2012.

[74] Semtech, "SX1212 Ultra-Low Power Integrated 300-510MHz Transceiver," http://www.semtech.com/apps/filedown/down.php?file=sx1212.pdf, 2009.

[75] F. T. D. I. Ltd., "FT230X USB to Basic UART IC," http://www.ftdichip.com/Support/Documents/DataSheets/ICs/DS_FT230X.pdf, 2012.

[76] STMicroelectronics, "STM32L162RD Ultra Low-Power 32-bit ARM Cortex-M3 MCU," http://www.st.com/internet/com/TECHNICAL_RESOURCES/TECHNICAL_LITERATURE/DATASHEET/DM00039232.pdf, 2012.

[77] E. M. B. Consortium, "CoreMark," http://www.coremark.org/benchmark/index.php?pg=benchmark, 2012.

[78] STMicroelectronics, "STM32Lxx," http://www.emcu.it/STM32/STM32Lxx/STM32Lxx.html, 2012.

[79] Sensirion, "SHT25 Digital Humidity and Temperature Sensor IC," http://www.sensirion.com/fileadmin/user_upload/customers/sensirion/Dokumente/Humidity/Sensirion_Humidity_SHT25_Datasheet_V2.pdf, 2011.

[80] W. Ye, J. Heidemann, and D. Estrin, "An Energy-Efficient MAC Protocol for Wireless Sensor Networks," in *Proceedings on the 21st Annual Joint Conference of the IEEE Computer and Communications Societies. INFOCOM.*, vol. 3. IEEE, 2002, pp. 1567–1576.

[81] T. V. Dam and K. Langendoen, "An Adaptive Energy-Efficient MAC Protocol for Wireless Sensor Networks," in *Proceedings of the 1st international conference on Embedded networked sensor systems*, no. 5-7. ACM, 2003, pp. 171–180.

[82] J. Ai, J. Kong, and D. Turgut, "An Adaptive Coordinated Medium Access Control for Wireless Sensor Networks," in *Proceedings on the 9th International Symposium on Computers and Communications. ISCC.*, vol. 1. IEEE, 2004, pp. 214–219.

[83] P. Lin, C. Qiao, and X. Wang, "Medium Access Control With A Dynamic Duty Cycle For Sensor Networks," in *Wireless Communications and Networking Conference. WCNC.*, vol. 3, 2004, pp. 1534–1539.

[84] H. Cao, K. W. Parker, and A. Arora, "O-MAC: A Receiver Centric Power Management Protocol," in *Proceedings of the 14th IEEE International Conference on Network Protocols. ICNP'06.* IEEE, 2006, pp. 311–320.

[85] W. Ye, F. Silva, and J. Heidemann, "Ultra-Low Duty Cycle MAC with Scheduled Channel Polling," in *Proceedings of the 4th international conference on Embedded networked sensor systems*. ACM, 2006, pp. 321–334.

[86] V. Rajendran, K. Obraczka, and J. Garcia-Luna-Aceves, "Energy-Efficient, Collision-Free Medium Access Control for Wireless Sensor Networks," *Wireless Networks*, vol. 12, no. 1, pp. 63–78, 2006.

[87] S. Du, A. K. Saha, and D. B. Johnson, "RMAC: A Routing-Enhanced Duty-Cycle MAC Protocol for Wireless Sensor Networks," in *26th IEEE International Conference on Computer Communications. INFOCOM.* IEEE, 2007, pp. 1478–1486.

[88] Y. Sun, S. Du, O. Gurewitz, and D. B. Johnson, "DW-MAC: A Low Latency, Energy Efficient Demand-Wakeup MAC Protocol for Wireless Sensor Networks," in *Proceedings of the 9th ACM international symposium on Mobile ad hoc networking and computing*. ACM, 2008, pp. 53–62.

[89] Q. Hu and Z. Tang, "ATPM: An Energy Efficient MAC Protocol with Adaptive Transmit Power Scheme for Wireless Sensor Networks," *Journal of Multimedia*, vol. 6, no. 2, pp. 122–128, 2011.

[90] J. Polastre, J. Hill, and D. Culler, "Versatile Low Power Media Access for Wireless Sensor Networks," in *Proceedings of the 2nd international conference on Embedded networked sensor systems*. ACM, 2004, pp. 95–107.

[91] G. P. Halkes, T. V. Dam, and K. G. Langendoen, "Comparing Energy-Saving MAC Protocols for Wireless Sensor Networks," *Mobile Networks and Applications*, vol. 10, no. 5, pp. 783–791, 2005.

[92] N. Abramson, "THE ALOHA SYSTEM—Another alternative for computer communications," in *Proceedings of the November 17-19, fall joint computer conference*. ACM, 1970, pp. 281–285.

[93] F. Kuo, "The ALOHA System," *ACM SIGCOMM Computer Communication Review*, vol. 25, no. 1, pp. 41–44, 1995.

[94] C. Cano, B. Bellalta, A. Sfairopoulou, and M. Oliver, "Low energy operation in WSNs: A survey of preamble sampling MAC protocols," *Computer Networks*, vol. 55, pp. 3351–3363, 2011.

[95] A. El-Hoiydi, J.-D. Decotignie, C. Enz, and E. L. Roux, "Poster abstract: WiseMAC, an Ultra Low Power MAC Protocol for the WiseNET Wireless Sensor Network," in *Proceedings of the 1st international conference on Embedded networked sensor systems*. ACM, 2003, pp. 302–303.

[96] A. El-Hoiydi and J.-D. Decotignie, "WiseMAC: An Ultra Low Power MAC Protocol for Multi-hop Wireless Sensor Networks," *Algorithmic Aspects of Wireless Sensor Networks*, pp. 18–31, 2004.

[97] M. Buettner, G. V. Yee, E. Anderson, and R. Han, "X-MAC: A Short Preamble MAC Protocol for Duty-Cycled Wireless Sensor Networks," in *Proceedings of the 4th international conference on Embedded networked sensor systems*. ACM, 2006, pp. 307–320.

[98] TinyOS, "TinyOS: An embedded operating system for wireless sensor networks," http://www.tinyos.net/, 2012.

[99] UPMA, "UPMA Package: Unified Power Management Architecture for Wireless Sensor Networks," http://tinyos.cvs.sourceforge.net/tinyos/tinyos-2.x-contrib/wustl/upma/, 2012.

[100] P. Kumar, M. Gunes, Q. Mushtaq, and B. Blywis, "A Real-Time and Energy-Efficient MAC Protocol for Wireless Sensor Networks," *International Journal of Ultra Wideband Communications and Systems*, vol. 1, no. 2, pp. 128–142, 2009.

[101] P. Kumar, M. Gunes, Q. Mushtaq, and J. Schiller, "Performance Evaluation of AREA-MAC : A Cross-Layer Perspective," in *The Fifth International Conference on Mobile Computing and Ubiquitous Networking (ICMU'10), Seattle, USA*, 2010.

[102] X. Wang and Q. Zhang, "Opportunistic Cooperation in Low Duty Cycle Wireless Sensor Networks," in *IEEE International Conference on Communications (ICC)*. IEEE, 2010, pp. 1–5.

[103] D. Yang, Y. Qiu, S. Li, and Z. Li, "RW-MAC: An asynchronous receiver-initiated ultra low power MAC protocol for Wireless Sensor Networks," in *IET International Conference on Wireless Sensor Network. IET-WSN.* IET, 2010, pp. 393–398.

[104] Y.-T. Yong, C.-O. Chow, J. Kanesan, and H. Ishii, "EE-RI-MAC: An energy-efficient receiver-initiated asynchronous duty cycle MAC protocol for dynamic traffic loads in wireless sensor networks," *International Journal of Physical Sciences*, vol. 6, no. 11, pp. 2633–2643, 2011.

[105] C. M. Vigorito, D. Ganesan, and A. G. Barto, "Adaptive Control of Duty Cycling in Energy-Harvesting Wireless Sensor Networks," in *4th Annual IEEE Communications Society Conference on Sensor, Mesh and Ad Hoc Communications and Networks. SECON'07.* IEEE, 2007, pp. 21–30.

[106] H. Yoo, M. Shim, and D. Kim, "Dynamic Duty-Cycle Scheduling Schemes for Energy-Harvesting Wireless Sensor Networks," *IEEE Communications Letters*, vol. 16, no. 2, pp. 1–3, 2012.

[107] X. Fafoutis and N. Dragoni, "Analytical Comparison of MAC Schemes for Energy Harvesting-Wireless Sensor Networks," in *The International Workshop on Algorithms and Concepts for Networked Sensing Systems Powered by Energy Harvesters (EnHaNSS'12)*, 2012.

[108] L. Tang, Y. Sun, O. Gurewitz, and D. B. Johnson, "PW-MAC: An Energy-Efficient Predictive-Wakeup MAC Protocol for Wireless Sensor Networks," in *Proceedings of IEEE INFOCOM*. IEEE, 2011, pp. 1305–1313.

[109] IEEE, *Part 15.4: Wireless Medium Access Control (MAC) and Physical Layer (PHY) Specifications for Low-Rate Wireless Personal Area Networks (WPANs)*, IEEE Standard for Information technology - Telecommunications and information exchange between systems - Local and metropolitan area networks Std., 2006.

[110] K. Whitehouse, A. Woo, F. Jiang, J. Polastre, and D. Culler, "Exploiting The Capture Effect For Collision Detection And Recovery," in *The Second IEEE Workshop on Embedded Networked Sensors. EmNetS-II.* IEEE, 2005, pp. 45–52.

[111] Y. Sun, O. Gurewitz, S. Du, L. Tang, and D. B. Johnson, "ADB: An Efficient Multihop Broadcast Protocol based on Asynchronous Duty-cycling in Wireless Sensor Networks," in *Proceedings of the 7th ACM Conference on Embedded Networked Sensor Systems*. ACM, 2009, pp. 43–56.

Appendix A

EH-HCA Technical Drawings

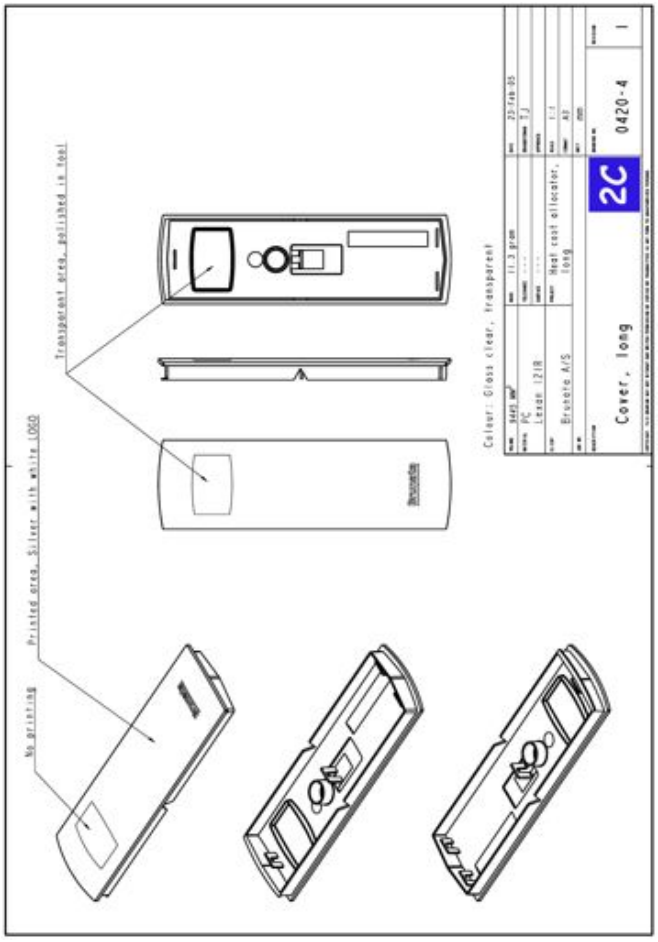

Figure A.1: Existing plastic lid

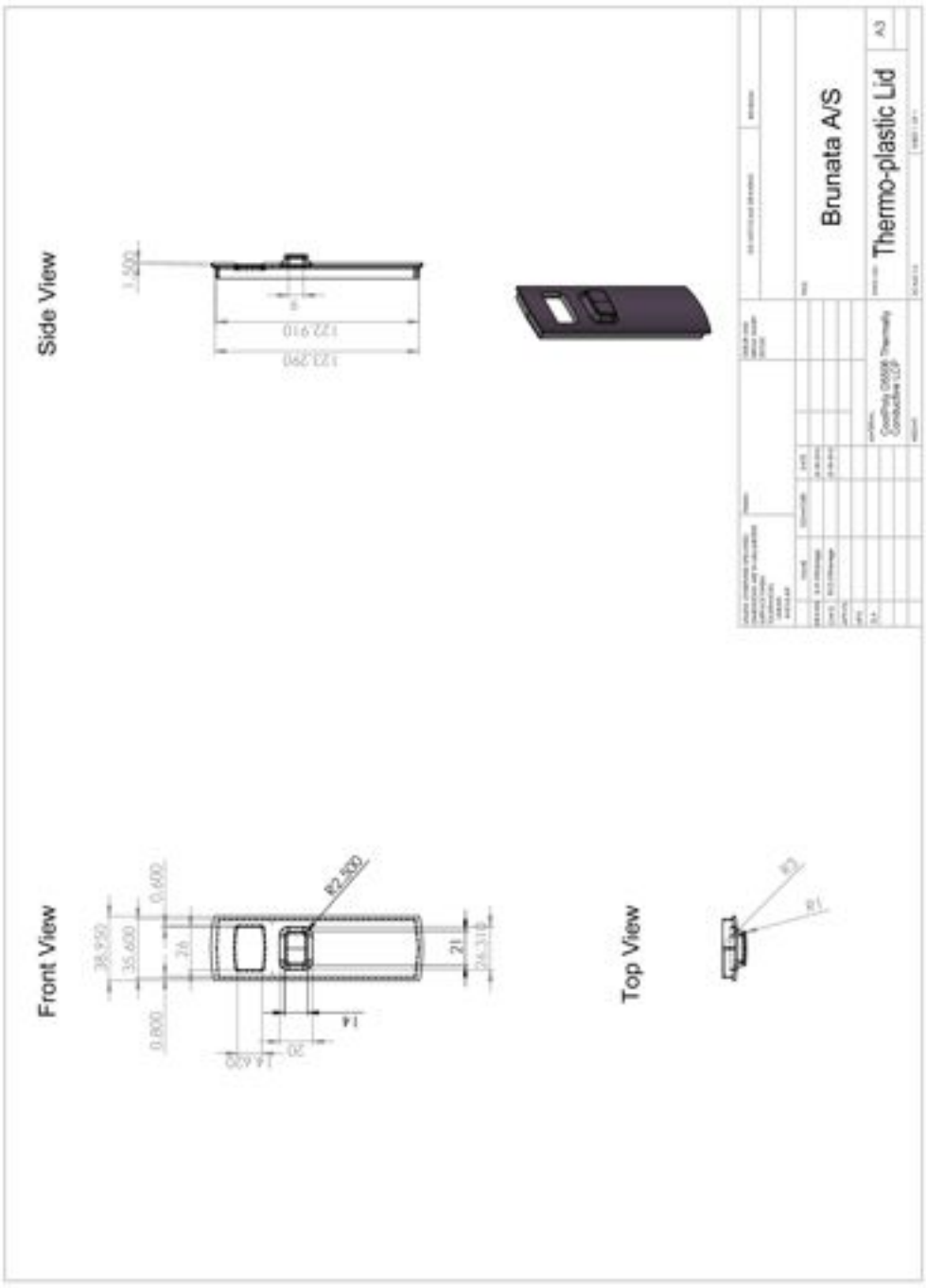

Figure A.2: New thermo-plastic lid

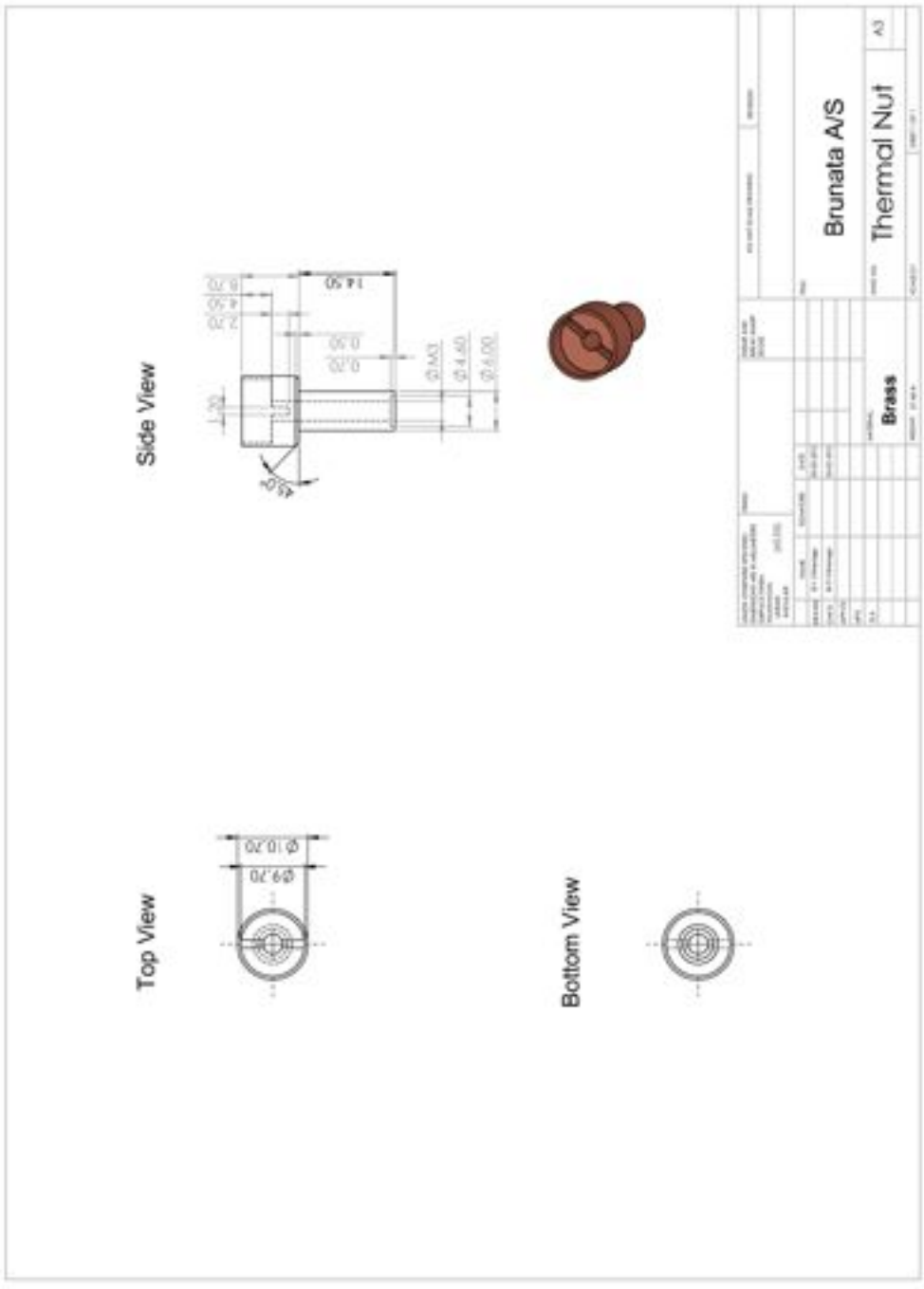

Figure A.3: New brass nut

Appendix B

IOTA Fabrication Data

Table B.1: Bill of materials

Designator	Quantity	Part No. / Value	Package	Description	Manufacturer
BT1	1		AA	2460 - Battery Holder	Keystone
C1, C4, C5, C6, C7, C8, C13, C14, C21, C22, C24, C27	12	100nF	0402	Capacitor X5R (±15%), Decoupling	
C2, C3, C11, C12	4	1μF	0402	Capacitor X7R (±10%), Decouple and Filter	
C9, C10	4	6.8pF	0402	Capacitor NP0 (±5%), Crystal	
C15	1	10pF	0402	Capacitor NP0 (±5%), DC Block and L4 Adjust	
C16	1	3.3pF	0402	Capacitor NP0 (±0.25pF), Matching	
C17	1	8.2pF	0402	Capacitor NP0 (±5%), Matching	
C18, C28, C29	3	47pF	0402	Capacitor X7R (±10%), Decoupling	
C19	1	1nF	0402	Capacitor X7R (±10%), Decoupling	
C20	1	680pF	0402	Capacitor NP0 (±5%), Loop Filter	
C23	1	10nF	0402	Capacitor NP0 (±5%), Loop Filter	
C25, C26	2	4.7μF	0402	Capacitor X7R (±10%), Decouple and Filter	

C30	1		AA	2460 - Battery Holder + 3300μF Polarised Electrolytic Capacitor, 10V, 20mΩ, Axial Leaded	Keystone, Vishay
CON1	1	1981584-1	Micro-AB	Surface Mounted USB Female Receptacle	TE Connectivity
D1	1	Green	0402	Light Emitting Diode, Iv = 50mcd @ If = 4mA	
D2	1		0603	Schottky Diode, Vf = 0.5V Max @ If = 200mA, Ir = 1μA Max @ Vr = 5V	
D3	1		0603	Schottky Diode, Vf = 0.35V MAX @ If = 30mA, Ir = 1μA MAX @ Vr = 5V	
L1	1	7427927161	0402	Z = 1.3 kΩ @ 300MHz, R(DC) = 60mΩ Max, Ferrite Bead	Würth Elektronik
L2, L3	2	19nH	0402	Wire Wound Inductor ($\pm$0.2nH), VCO Tank	
L4	1	27nH	0402	Multilayer Chip Inductor ($\pm$5%), Matching	
L5	1	18nH	0402	Wire Wound Inductor ($\pm$5%), PA Choke	
L6	1	7427927261	0402	Z = 600Ω @ 100MHz, R(DC) = 600mΩ Max, Ferrite Bead	Würth Elektronik
L7	1	742792664	0603	Z = 1.1kΩ @ 120MHz, R(DC) = 600mΩ Max, Ferrite Bead	Würth Elektronik
LCD1	1		18-Pin	Brunata Liquid Crystal Display with Five 7-Segments, Two Radix, 8 Icons	
P1	1	90130-1X20	20-Pin	2.54mm Pitch, Male, Dual Row, Straight, Shrouded Header	Molex
P2	1		4-Pin	2.54mm Pitch, Male, Single Row, Straight, Header	3M
P3	1		4-Pin	2.54mm Pitch, Male, Single Row, Straight, Header	3M
P4	1	19-49-2-TGG	SMA	RF SMA Connector, Right-Angle Surface Mount Socket, 50Ω Impedance	Multicomp
P5	1	CTB5000/2	2-Pin	5mm Pitch, Low Profile Straight, Screw Terminal Block	Camden Electronics
R1, R2, R3, R4, R5, R6	6	100kΩ	0402	Resistor ($\pm$1%), CRG (Thick Film)	
R7, R8	2	10kΩ	0402	Resistor ($\pm$1%), CRG	
R9	1	1Ω	0402	Resistor ($\pm$1%), CRG	

R10	1	6.8kΩ	0402	Resistor (±1%), CRG	
R11	1	1.27kΩ	0402	Resistor (±1%), CRG	
R12, R13	2	27Ω	0402	Resistor (±1%), CRG	
S1	1	1301.9314	6.0 x 6.0mm	Switch, Push Button, Normally Open	Schurter
S2	1	PCM12SMTR	6.7 x 2.6mm	SPDT Ultra-miniature Surface Mount Slide Switch, 10000 Cycles, 70 mΩ Contact Resistance	C & K
U1	1	STM32L152RB	LQFP64	Low-power 32-bit ARM Cortex-M3	ST Micro-elec-tronics
U2	1	SX1212	TQFN32	Ultra-Lower Power Integrated 300 - 510MHz Transceiver	Semtech
U3	1	B3710 TMX CT04	3.0 x 3.0mm	433.92MHz SAW Filter	Epcos Temex
U4	1	SHT25	DFN6	Digital Temperature & Humidity Sensor	Sensirion
U5	1	FT230X	QFN16	USB Virtual COM Port to BASIC UART IC	FTDI Chip
W1	1		2-Pin	2.54mm Pitch, Male, Single Row, Straight, Header + Jumper	3M
W2	1		2-Pin	2.54mm Pitch, Male, Single Row, Straight, Header + Jumper	3M
Y1	1	MC-306	8.0 x 3.8mm	32.768kHz Crystal, CL = 6pF, Tolerance ±20ppm @ 25°C, Stability ±20ppm over -40°C to +85°C, Ageing $\pm 3 \frac{\text{ppm}}{\text{year}}$	Epson Toy-ocom
Y2	1	12.288MHz	5.0 x 3.2mm	Crystal, CL = 15pF, Tolerance ±15ppm @ 25°C, Stability ±20ppm over -40°C to +85°C, Ageing $\pm 2 \frac{\text{ppm}}{\text{year}}$	Siward / MtronPTI

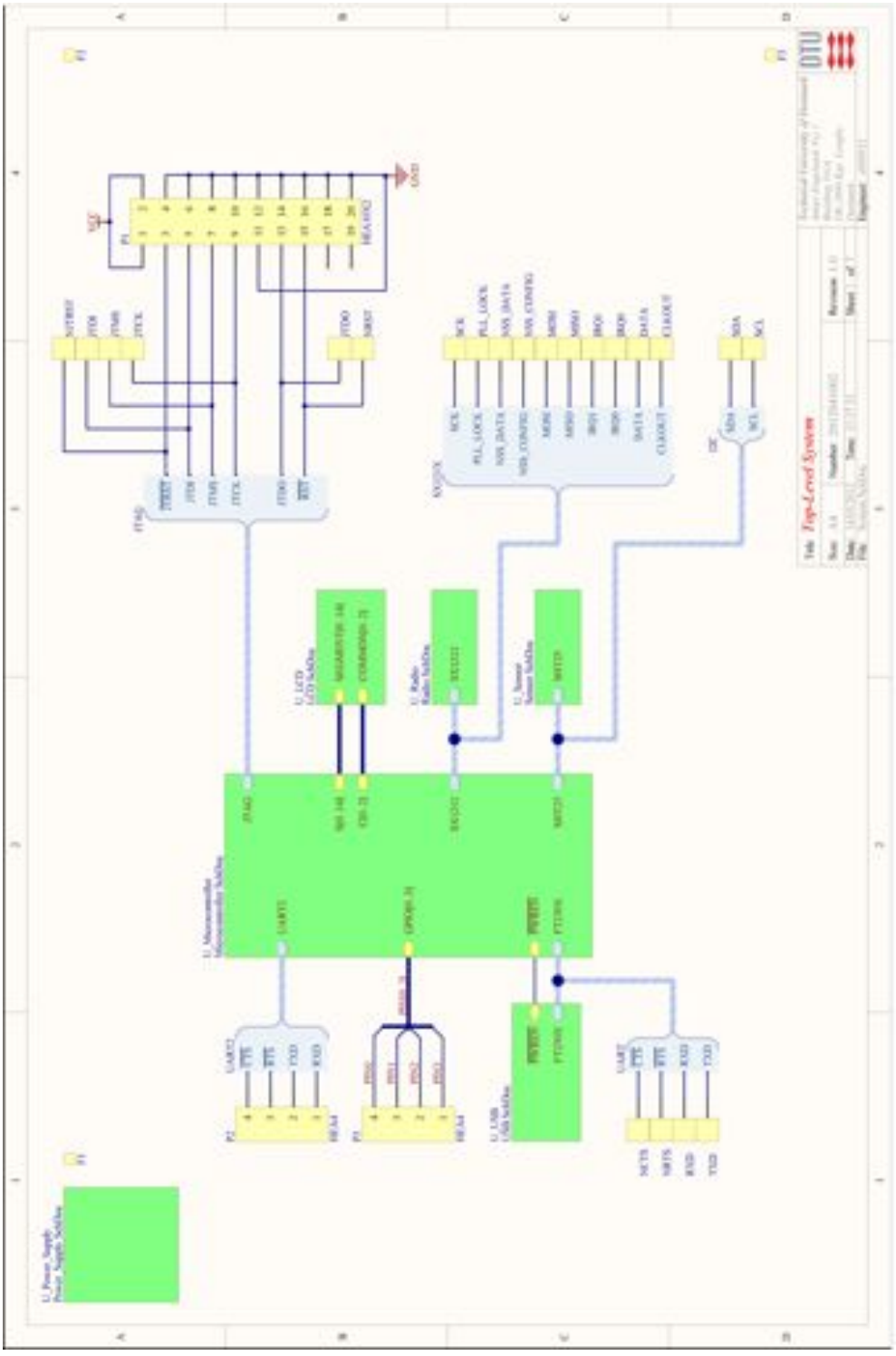

Figure B.1: Top-level system

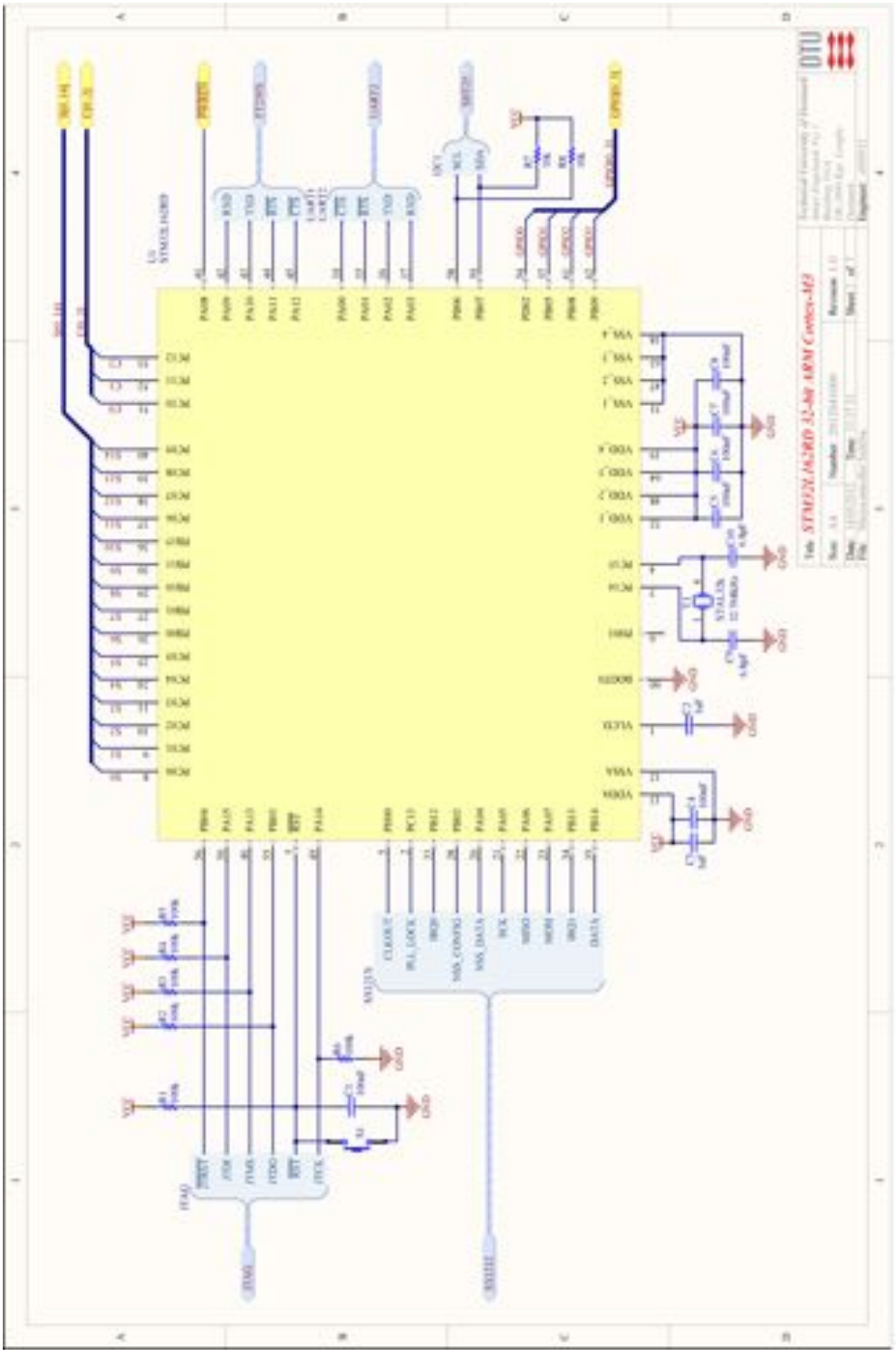

Figure B.2: Microcontroller unit

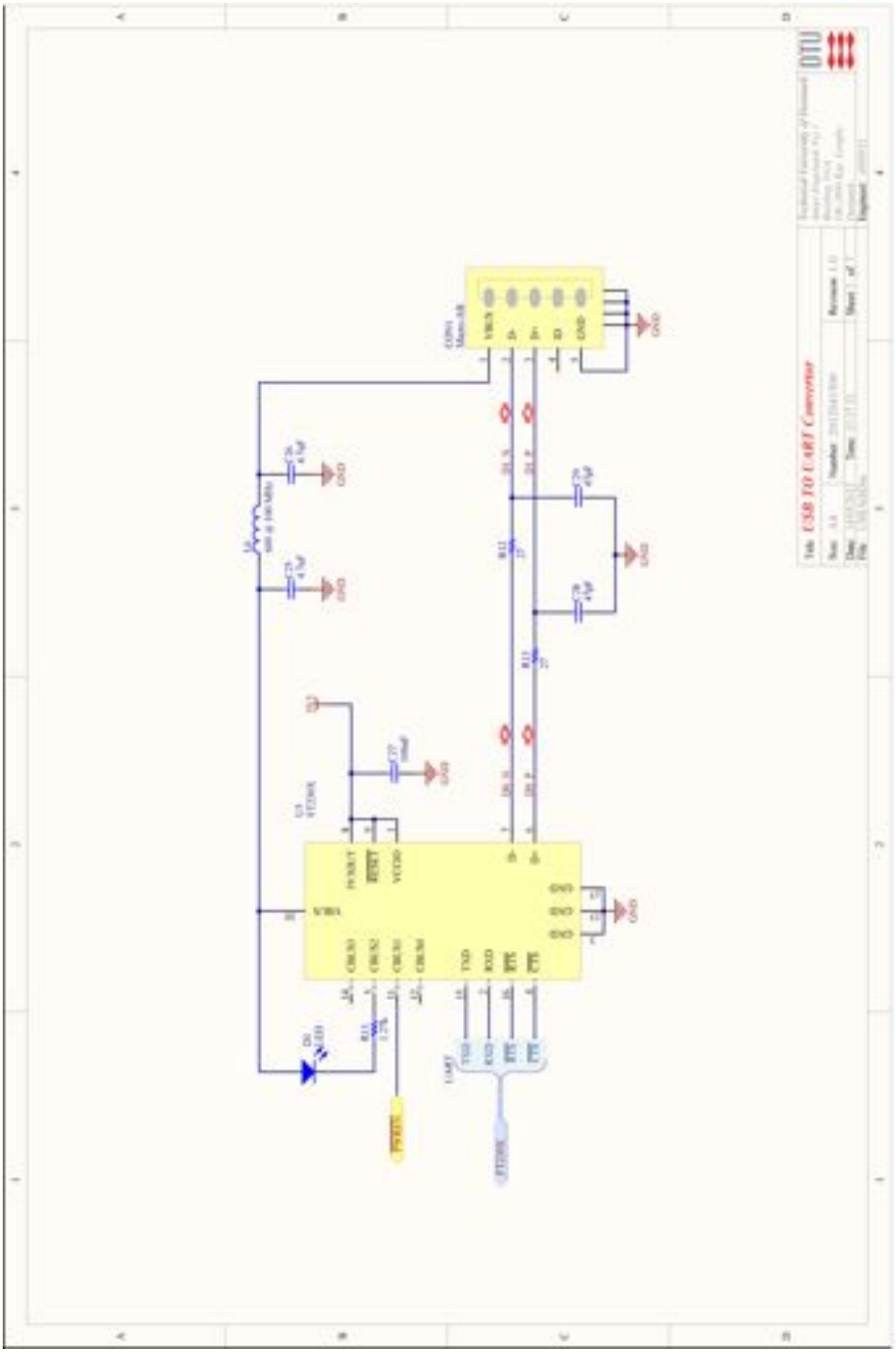

Figure B.3: USB virtual COM port

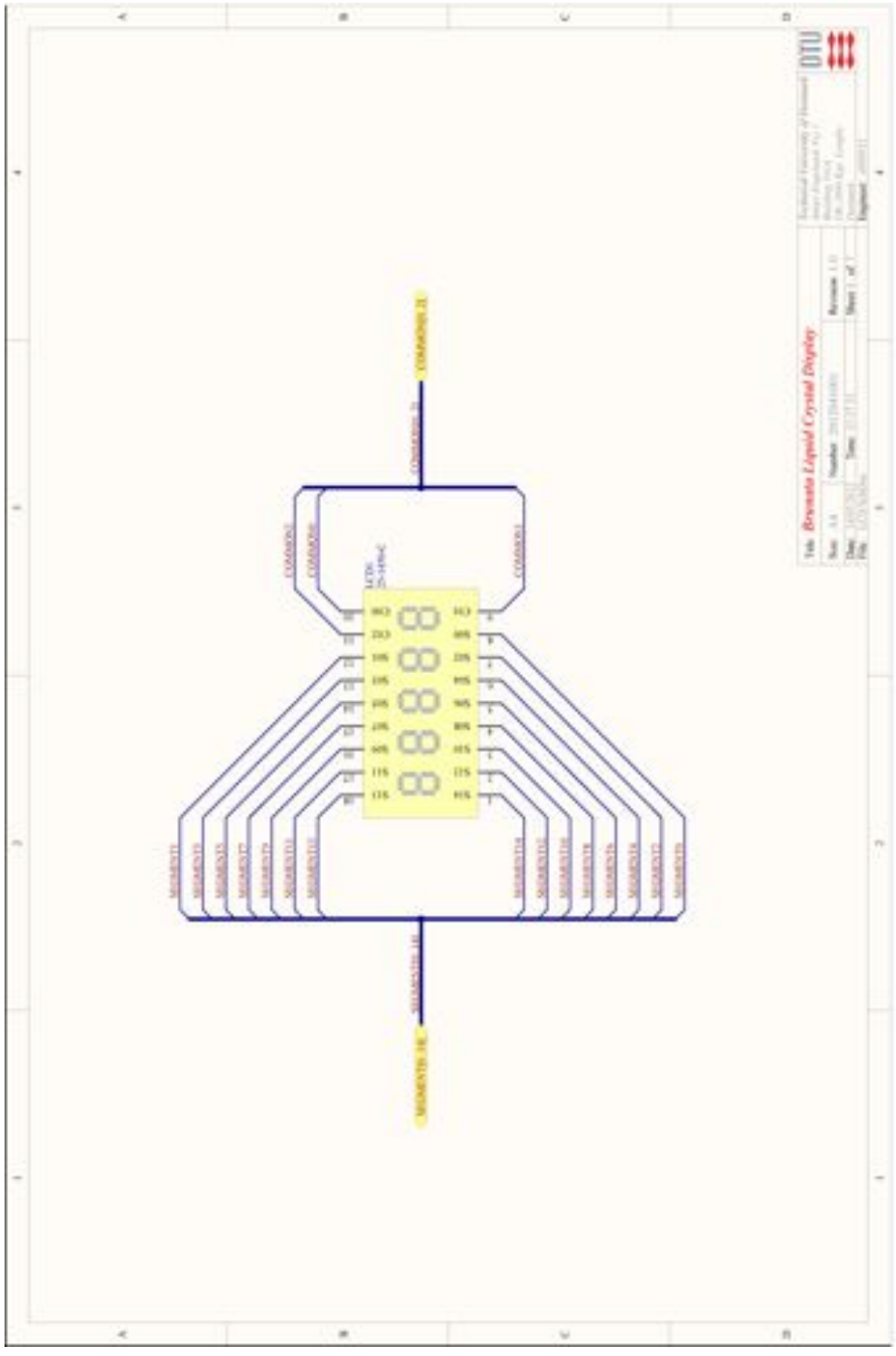

Figure B.4: Display

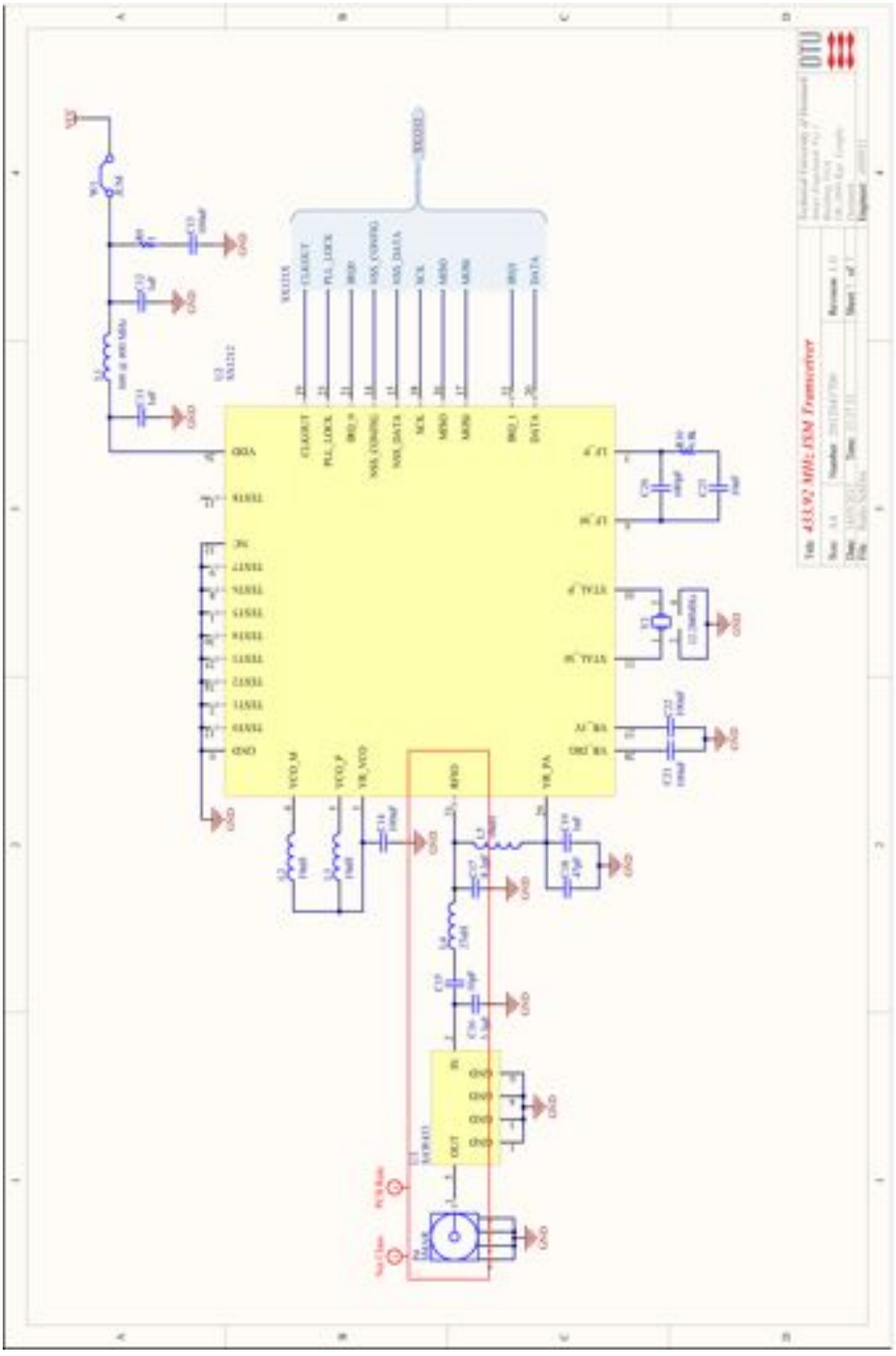

Figure B.5: Radio transceiver

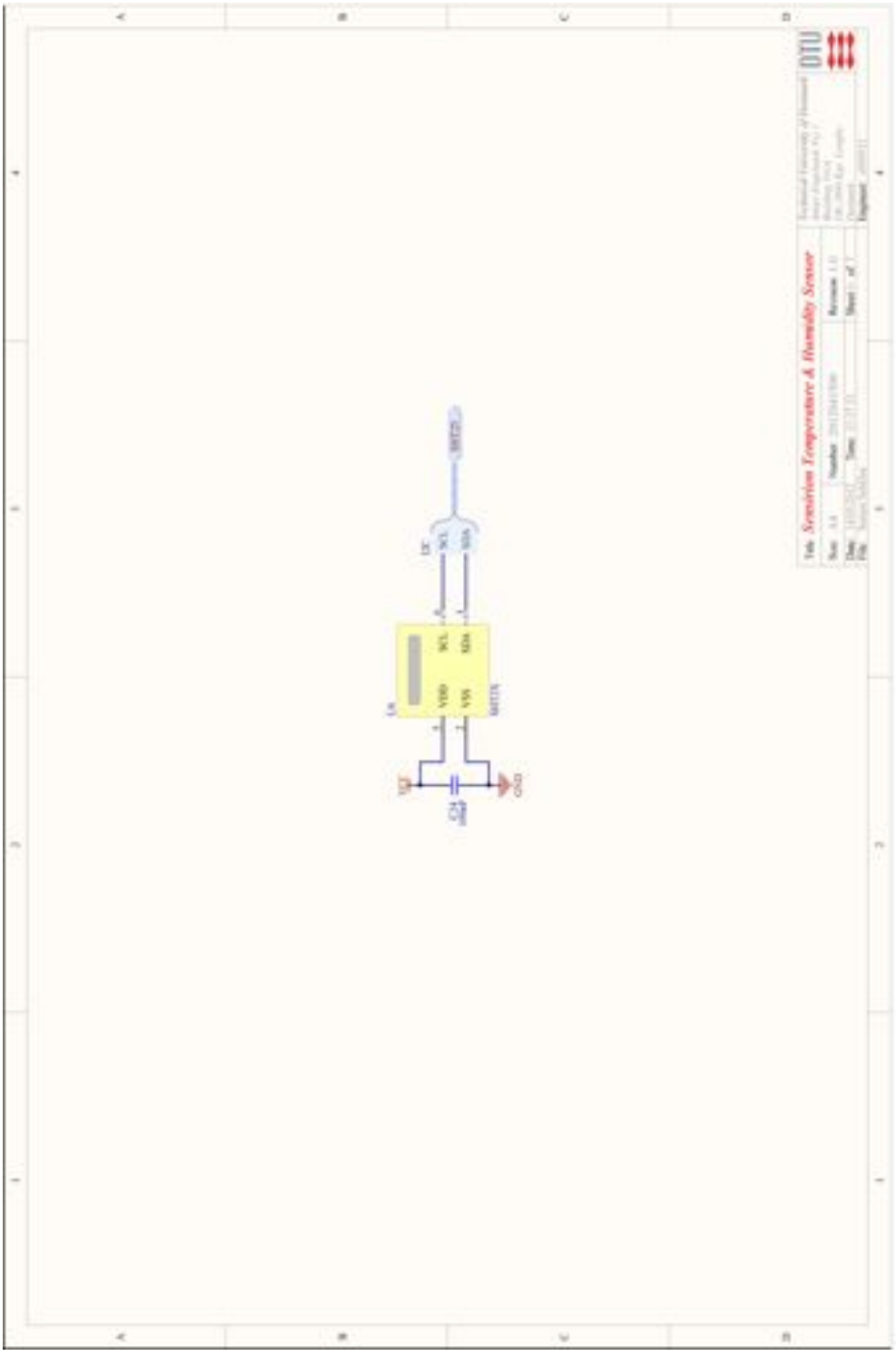

Figure B.6: Humidity and temperature sensor

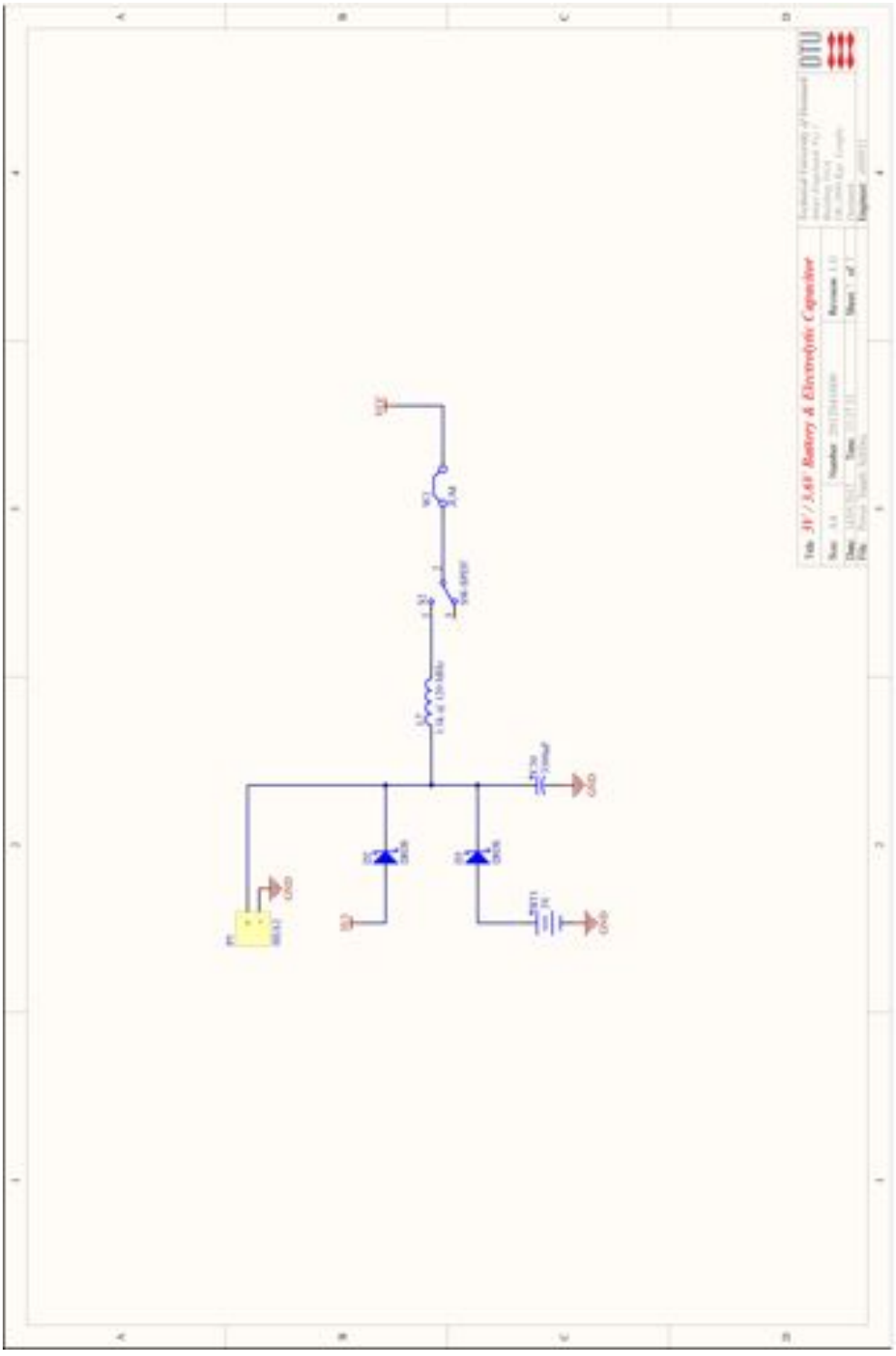

Figure B.7: Power supply

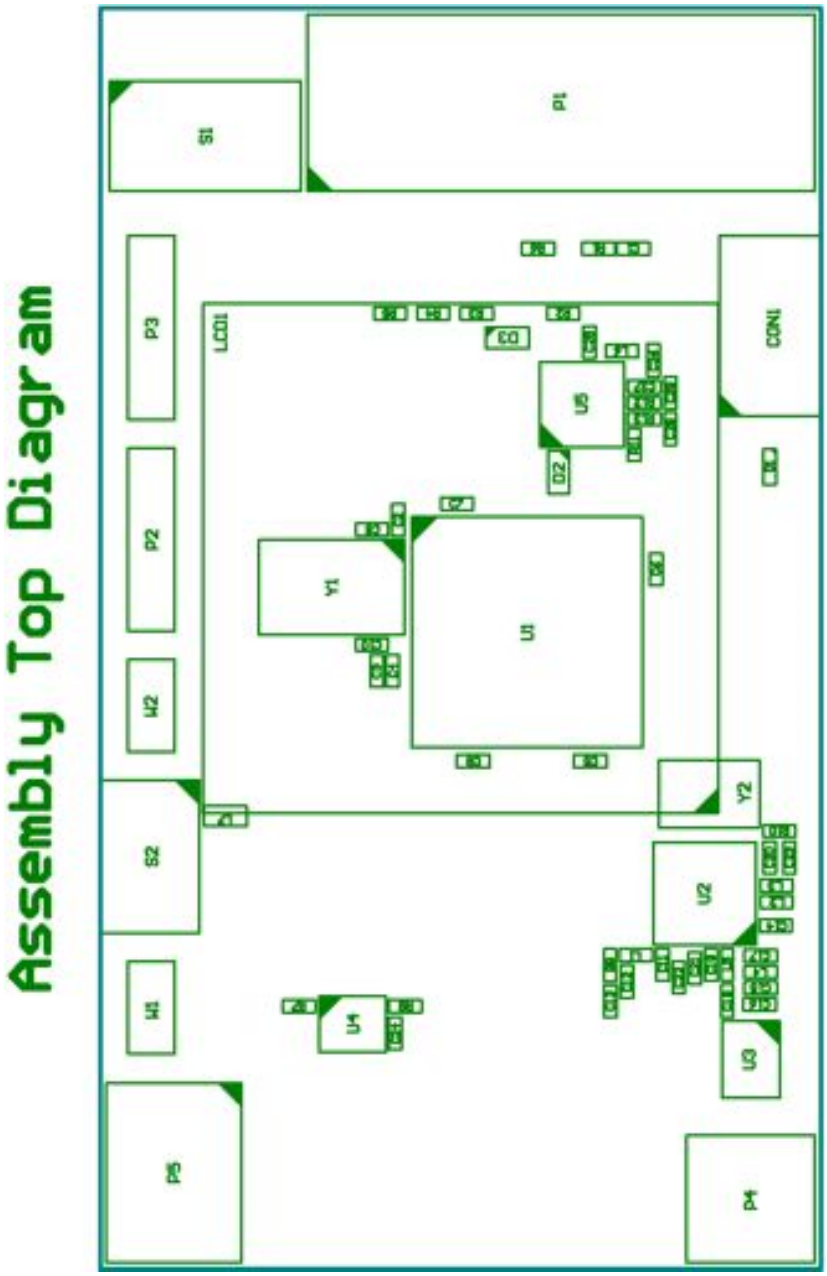

Figure B.8: Assembly top

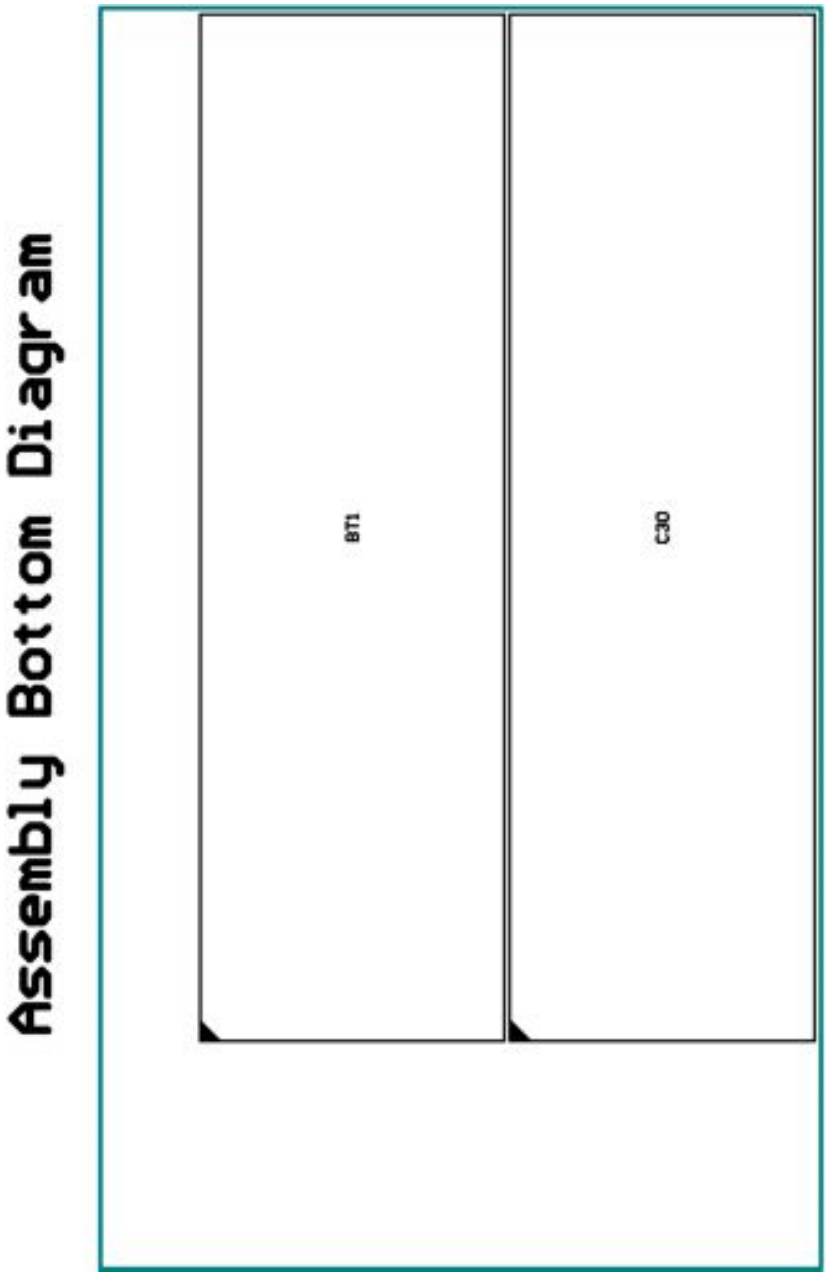

Figure B.9: Assembly bottom

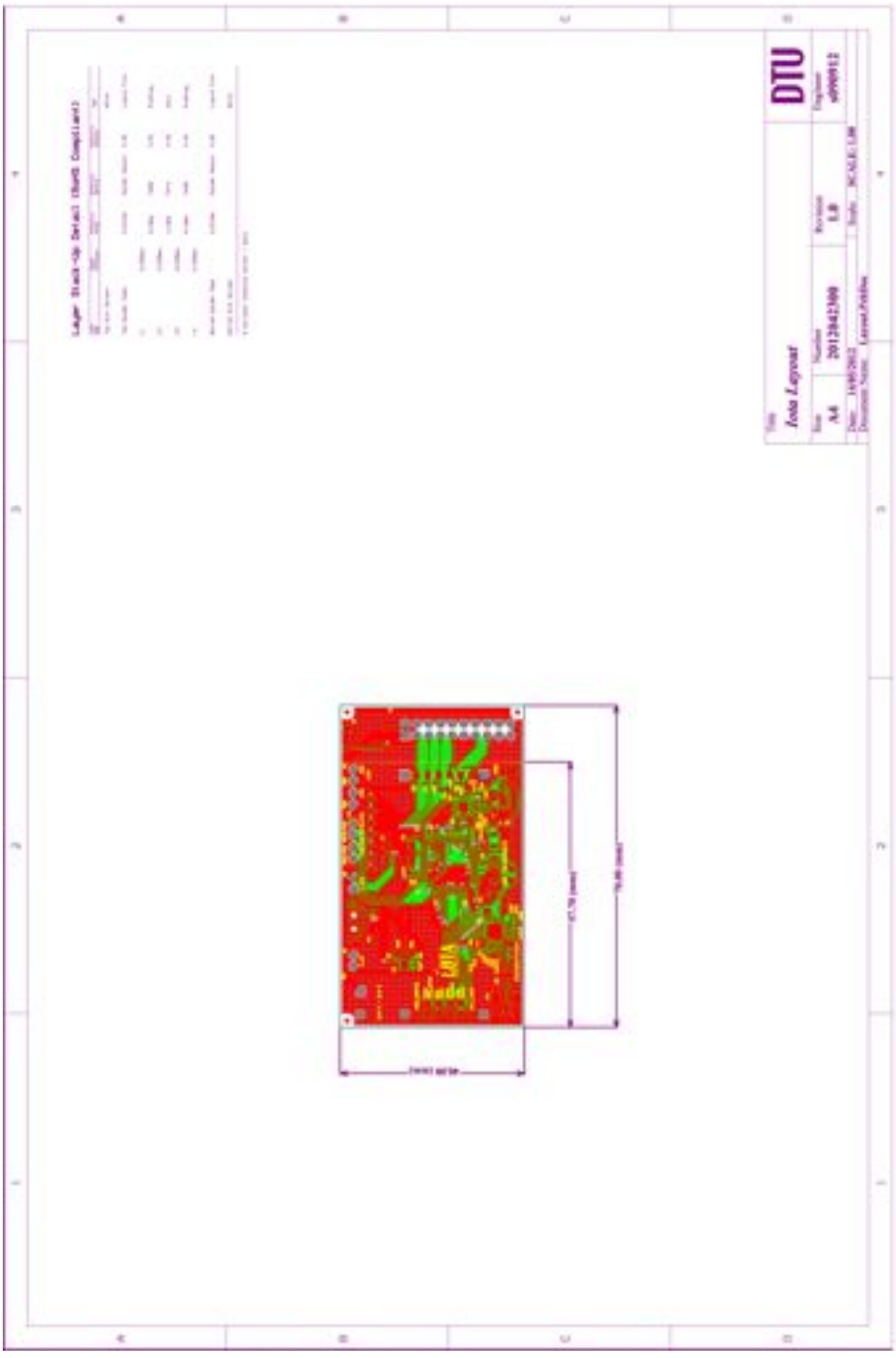

Figure B.10: PCB layout

Appendix C

Contents of the CD-ROM

The reference material used in this study is presented in an accompanying CD-ROM. This appendix provides an overview of the folders contained in the CD-ROM.

C.1 Raw Data from the Experiments

C.2 Altium Designer Project

C.3 Literature Survey

C.4 MATLAB Code

C.5 Firmware Library and Project Template for ıota

www.imm.dtu.dk

DTU Informatics
Department of Informatics and Mathematical Modelling
Technical University of Denmark
Richard Petersens Plads, Building 321,
DK-2800 Kgs. Lyngby
Denmark
Tel: (+45) 4525 3351
Fax: (+45) 4588 2673
E-mail: reception@imm.dtu.dk

IMM-MSC-96